



---

## **X-Ray Pebble Recirculation Experiment (X-PREX) Design and Initial Experimental Results**

Michael Laufer, Project Manager  
Grant Buster, Graduate Student Researcher

UCBTH-15-002

January 20, 2015  
Department of Nuclear Engineering  
University of California, Berkeley

This research is being performed using funding received from the U.S. Department of Energy  
Office of Nuclear Energy's Nuclear Energy University Programs.



## Executive Summary

This report documents the work completed on the X-PREX facility under NEUP Project 11-3172. This project seeks to demonstrate the viability of pebble fuel handling and reactivity control for fluoride salt-cooled high-temperature reactors (FHRs). The research results also improve the understanding of pebble motion in helium-cooled reactors, as well as the general, fundamental understanding of low-velocity granular flows. Successful use of pebble fuels in with salt coolants would bring major benefits for high-temperature reactor technology. Pebble fuels enable on-line refueling and operation with low excess reactivity, and thus simpler reactivity control and improved fuel utilization. If fixed fuel designs are used, the power density of salt-cooled reactors is limited to 10 MW/m<sup>3</sup> to obtain adequate duration between refueling, but pebble fuels allow power densities in the range of 20 to 30 MW/m<sup>3</sup>. This can be compared to the typical modular helium reactor power density of 5 MW/m<sup>3</sup>. Pebble fuels also permit radial zoning in annular cores and use of thorium or graphite pebble blankets to reduce neutron fluences to outer radial reflectors and increase total power production.

Combined with high power conversion efficiency, compact low-pressure primary and containment systems, and unique safety characteristics including very large thermal margins (>500°C) to fuel damage during transients and accidents, salt-cooled pebble fuel cores offer the potential to meet the major goals of the Advanced Reactor Concepts Development program to provide electricity at lower cost than light water reactors with improved safety and system performance.

This report presents the facility description, experimental results, and supporting simulation methods of the new X-Ray Pebble Recirculation Experiment (X-PREX), which is now operational and being used to collect data on the behavior of slow dense granular flows relevant to pebble bed reactor core designs. The X-PREX facility uses novel digital x-ray tomography methods to track both the translational and rotational motion of spherical pebbles, which provides unique experimental results that can be used to validate discrete element method (DEM) simulations of pebble motion. The validation effort supported by the X-PREX facility provides a means to build confidence in analysis of pebble bed configuration and residence time distributions that impact the neutronics, thermal hydraulics, and safety analysis of pebble bed reactor cores. Experimental and DEM simulation results are reported for silo drainage, a classical problem in the granular flow literature, at several hopper angles. These studies include conventional converging and novel diverging geometries that provide additional flexibility in the design of pebble bed reactor cores. Excellent agreement is found between the X-PREX experimental and DEM simulation results. This report also includes results for additional studies relevant to the design and analysis of pebble bed reactor cores including the study of forces on shut down blades inserted directly into a packed bed and pebble flow in a cylindrical hopper that is representative of a small test reactor.

# Contents

<b>X-Ray Pebble Recirculation Experiment (X-PREX) Design and Initial Experimental Results .....</b>	<b>1</b>
<b>Contents .....</b>	<b>3</b>
<b>List of Figures.....</b>	<b>5</b>
<b>List of Tables .....</b>	<b>12</b>
<b>Acronyms and Abbreviations .....</b>	<b>13</b>
<b>1 Facility Description .....</b>	<b>14</b>
<b>1.1 X-Ray Imaging System.....</b>	<b>17</b>
1.1.1 System Description.....	17
1.1.2 Shielding Enclosure.....	19
1.1.3 Remote Operator Workstation.....	21
1.1.4 System Geometry Verification .....	23
<b>1.2 Modular Test Bay .....</b>	<b>24</b>
1.2.1 Modular Test Base Structure .....	24
1.2.2 Actuation and Sensor Capabilities.....	27
1.2.3 Test Configurations .....	34
<b>1.3 Pebble Modification.....</b>	<b>35</b>
1.3.1 Instrumented Pebble Design .....	35
1.3.2 Instrumented Pebble Physical Properties.....	40
<b>1.4 Image Processing Methods.....</b>	<b>44</b>
1.4.1 Module 1: Pin Image Detection.....	46
1.4.2 Module 2: Packed Bed Reconstruction.....	54
1.4.3 Module 3: Pebble Motion Tracking.....	59
1.4.4 Code Verification .....	61
<b>1.5 Quality Assurance.....</b>	<b>68</b>
1.5.1 Facility Safety and Records Requirements.....	68
1.5.2 Data Processing Management.....	71
<b>2 Experimental Program.....</b>	<b>73</b>
<b>2.1 Quasi Two-Dimensional (2D) Silo Experiment.....</b>	<b>73</b>
2.1.1 Experimental Methods and Setup.....	74
2.1.2 Results .....	81
2.1.3 Conclusions .....	97
<b>2.2 Control Blade Insertion Experiment (CoBIE) .....</b>	<b>98</b>
2.2.1 Experimental Methods and Setup.....	98
2.2.2 Results .....	104
2.2.3 Conclusions .....	113
<b>2.3 Cylindrical Silo Experiment .....</b>	<b>114</b>
2.3.1 Experimental Methods and Setup.....	115
2.3.2 Results .....	120
2.3.3 Conclusions .....	124

<b>3</b>	<b>Simulation and Validation .....</b>	<b>125</b>
3.1	Discrete Element Method Simulations.....	125
3.2	Quasi-2D Silo Validation Study.....	128
3.3	Simulation Results for Quasi-2D Diverging Geometry .....	132
3.4	Simulation Results for Cylindrical Silo .....	135
3.5	Conclusions.....	138
<b>4</b>	<b>References.....</b>	<b>139</b>

## List of Figures

Figure 1-1. View of the X-Ray Pebble Recirculation Experiment (X-PREX) Facility at U.C. Berkeley.....	15
Figure 1-2. X-ray mass attenuation coefficients for tungsten, polyethylene, bone, and soft tissue. ....	15
Figure 1-3. Sample x-ray image of 4,500 instrumented pebbles in a packed bed with a depth of eight pebble diameters. The cropped area shows a detailed view where the pin images are resolved. ....	16
Figure 1-4. Quasi-2D Silo (left), Control Blade Insertion Experiment (middle), and Cylindrical Silo (right) installed on the modular test base in the X-PREX facility. ....	17
Figure 1-5. CAD model of the layout of the X-PREX x-ray imaging system. The x-ray detector is on the left side and the x-ray tube is on the right. The green region represents the volume used for data collection. The test section region is mounted on the modular test base and turntable. ....	18
Figure 1-6. View of the x-ray tube and the remote visual camera mounted in line with the focal point.....	19
Figure 1-7. CAD model for the X-PREX facility shielding enclosure, including the wood structural framing and x-ray system (left) and the lead-lined drywall around the four walls (right). The enclosure also includes a lead-lined door (not shown). ....	20
Figure 1-8. External view of the X-PREX shielding enclosure.....	20
Figure 1-9. View of the X-PREX facility remote operator station at U.C. Berkeley. ....	22
Figure 1-10. Precision-machined disk for X-PREX geometry measurements (top), sample calibration image (bottom left) and top view geometry sketch (bottom right). ....	23
Figure 1-11. X-PREX Facility at U.C. Berkeley. ....	24
Figure 1-12. Standard 80/20 <sup>®</sup> aluminum beam and connection piece.....	25
Figure 1-13. LinearX Systems LT360EX Precision Turntable. ....	25
Figure 1-14. CAD model for the stabilized turntable base in the X-PREX Modular Test Bay....	26
Figure 1-15. Modular Test Bay upper frame and rotary bearing that can be used to stabilize tall test sections in the facility. Additional features can be added to the rails above the bearing. ....	26
Figure 1-16. National Instruments USB-6009 DAQ. ....	27
Figure 1-17. LT360 graphical user interface on the X-PREX remote operator computer. The step size can be set for the desired rotation between each x-ray imaging orientation... ..	28
Figure 1-18. Precision turntable acceleration (top) and resulting smooth velocity (below) profiles can be used to minimize peak accelerations and reduce the potential for pebbles to shift positions during rotation between each x-ray imaging orientation. ....	29
Figure 1-19. Modular Test Bay CAD design (left) and installed system (right) configured with the linear actuator, lower support frame structure, and the precision turntable base. ....	30
Figure 1-20. LabVIEW Graphical User Interface (GUI) for the linear actuator controller.....	31
Figure 1-21. CAD model (left) and manufactured parts (right) of modular interface for continuous discharge device. Pebbles are fed in through adapters at the top of the hopper and discharged in a small diameter tube. ....	32

Figure 1-22. Front view from shielding enclosure camera showing the number of discharged pebbles on the counting scale. The readings can be read by the operator and recorded on study log records. ....	33
Figure 1-23. Modular Test Bay configured with the linear actuator for downward piston motion in the Quasi-2D Silo Test Section (left) and upward blade motion in CoBIE (middle) and the pebble hopper in the Cylindrical Silo (right). ....	34
Figure 1-24. Prototype 12.5 mm diameter polyethylene pebble with tapered stainless steel pin insert. ....	35
Figure 1-25. X-ray image of 500 prototype pebbles in a container with a depth of eight pebble diameters. ....	36
Figure 1-26. Crops of predicted pebble images for pin widths of 10 (left), 5 (center), and 3 (right) pixels. ....	37
Figure 1-27. Signal contrast ratio for several plastic and pin combinations. The contrast ratio is defined as the expected detector signal through plastic divided by the signal through plastic and metal. PE-Fe curve is for the prototype pebbles and other curves are for the pin diameters given in Table 1-1 to match the HDPE density. Plastic thickness used in calculations is 20 cm. ....	38
Figure 1-28. Detail view of a single instrumented pebble. The small end of the tungsten wire can be seen at the upper right side of the pebble. The wire ends are finished with a grind wheel to ensure a smooth pebble surface. ....	39
Figure 1-29. X-ray image of sample 12.57 mm diameter pebbles with 0.13 mm tungsten wire insert. ....	39
Figure 1-30. X-ray image of 1,000 instrumented pebbles packed in a cylinder with diameter of about 15 cm and height of about 10 cm. ....	40
Figure 1-31. Pebble cart used in static friction ramp tests to ensure pure sliding motion. ....	43
Figure 1-32. Sample x-ray images from the X-PREX facility from $-45.0^\circ$ to $+45.0^\circ$ in $22.5^\circ$ increments. ....	44
Figure 1-33. Block diagram of X-PREX image processing code structure and data flow. ....	45
Figure 1-34. Sample results of the X-PREX image processing code for an arranged “X” pattern of pebbles with one pebble located above the “X” in the center. The thin red lines represent the equators of the pebbles based on the pin axis. ....	45
Figure 1-35. Block flow diagram for Module 1 image processing algorithms and data pathways. ....	46
Figure 1-36. Sample crop of original x-ray image (left) and contrast levels (right). Each image has dimensions of 600 x 600 pixels. The pin images are clearly established by the contrast data, though the contrast levels drop around pin intersections. ....	47
Figure 1-37. Sample results of the ScanRing function for a pin endpoint (left) and middle section (right). The length of the arrows is proportional to the magnitude of the gradient. The direction of the minimum gradient magnitude is used as the initial guess for the pin direction. ....	48
Figure 1-38. Quiver plot of the local luminosity gradient vectors around a pin image and the local gradient ring located at one endpoint. The lengths of the arrows are proportional to the magnitude of the local gradient. Axis units are in pixels. Note that this pin image is relatively short compared to typical pin images due to the angle of view. The location of the pin endpoint is accurately determined with sub-pixel resolution. ....	48

Figure 1-39. Pin images that are successfully detected by Image Processing Module 1, including (A) a single pin with intersections, (B) a very short pin, (C)-(D) bent pins, and (E)-(F) long pins with many intersections. ....	50
Figure 1-40. Challenging pin configurations for Image Processing Module 1 including (A) intersecting pins with close alignment and (B) two nearly perfectly overlapping pins. These represent false negatives and false positives that must be corrected in Module 2.....	51
Figure 1-41. Sample results for the pin tracking algorithm. The short green sections are the initial region of pin detection that meet the tight requirements of the pin verification algorithm. The red and blue sections extending from both sides are the resulting pin image from tracking in both directions. ....	52
Figure 1-42. Sample results from Module 1. The red '+' marks indicate the location of the detected pin endpoints. Approximately 10% more pin images are detected than are present in the image, which represent a significant number of false positives. ....	53
Figure 1-43. Block diagram showing the Module 2 functions and data pathways. ....	54
Figure 1-44. Results from the four Module 2 phases. 3D solutions are projected as blue lines onto the original x-ray images. Top left: phase 1 output. Top right: phase 2 output. Bottom left: phase 3 output. Bottom right: phase 4 output (final results). ....	55
Figure 1-45. Place3D results for five different images (0, 22.5, 45, 67.5 and 90 degrees). ....	56
Figure 1-46. Plot of the triangle intersection function. ....	57
Figure 1-47. Plot of Phase 2 outsiders elimination algorithm. ....	58
Figure 1-48. Block flow diagram for Module 3 image processing algorithms and data pathways. ....	59
Figure 1-49. Sample result from image processing Module 3 that tracks pebble motion between time steps. In this example, the pebbles are moving down and the thick lines show the pebble displacement between the two time steps. The red "+" indicates the predicted position. ....	60
Figure 1-50. Continuous discharge device set up for testing and verification of the X-PREX image processing modules. The upper section within the x-ray imaging area contains 470 pebbles. ....	61
Figure 1-51. Front (left) and side (right) x-ray images of the discharge hopper. ....	62
Figure 1-52. Module 1 results for discharge hopper test. The detected pin endpoints are marker in red. Module 1 detected 697 pin images in this time step with approximately 50% false positives. ....	63
Figure 1-53. Packed bed from Module 2 results for the initial configuration of the hopper discharge test. 430 of 470 pebbles were located, indicating a detection rate above 90%.....	64
Figure 1-54. Top view of pebble center positions (red circles) and orientations (blue lines) from the Module 2 results for the initial configuration of the hopper discharge test. Ordered packing is clearly visible throughout the narrow cylindrical channel with an inner diameter of 5.5 pebble diameters. ....	65
Figure 1-55. Side view of Module 3 results for the first motion step of the hopper discharge test. 410 of 430 pebbles were tracked, indicating a tracking rate above 95%. The vertical displacement is $0.533 \pm 0.084$ pebble diameters and the horizontal displacement is $0.078 \pm 0.066$ pebble diameters. ....	66

Figure 1-56. Average vertical (left) and horizontal (right) displacement for each motion step against the number of discharged pebbles. Displacements are given in pebble diameters. ....	67
Figure 1-57. The measured average vertical displacement compared to the predicted vertical displacement based on the column packing fraction (0.58) and the number of discharged pebbles. The best-fit line is within 3% of the predicted values. ....	67
Figure 1-58. Sample completed x-ray data collection study log. ....	70
Figure 1-59. Screenshot example of the image management system for the X-PREX facility. Each study includes folders for the x-ray and visual images and subfolders for each rotational position. In the sample shown, each column includes one rotational position for the 00-degree Converging Quasi-2D Silo test section from -45.0 to +45.0 degrees.....	72
Figure 2-1. Quasi-2D Silo test section in the X-PREX facility. For the test show here, 3,000 pebbles were initially loaded into the test section then downward motion of the pebbles occurs as a piston plate in the orifice chute moves in incremental steps of $d$ . ....	73
Figure 2-2. Isometric (left) and front (right) view of Quasi-2D Silo test section design. The green region is the imaging zone where pebbles are tracked with the digital x-ray tomography.....	74
Figure 2-3. Detail views of the 60-degree wedge installed on the test section (left) and the 45 and 30-degree wedges (right). ....	75
Figure 2-4. Images of the Quasi-2D Silo Test Section in the modular test bay during data collection for the 0-degree (left), 30-degree (center), and 60-degree (right) converging configurations. The white pebbles in the images are instrumented with tungsten wires, while the green pebbles are unmodified HDPE pebbles. ....	75
Figure 2-5. Converging (left) and diverging (right) configurations of the Quasi-2D Silo test section with a 45-degree hopper angle. ....	76
Figure 2-6. Flat piston plates to enforce plug flow boundary conditions for the quasi-2D test section for diverging and converging geometries. ....	77
Figure 2-7. Random packing configuration from DEM simulation (left), CAD model (center), and FDM-manufactured random pebble packing piston plate (right). ....	77
Figure 2-8. Comparison of pebble packing configurations for the 60-degree Diverging Quasi-2D Silo with the flat (left) and random packing (right) piston plate.....	77
Figure 2-9. Initial and final bed configurations for the converging Quasi-2D Silo in the zero degree hopper configuration. The left images are for an initial be height of $24d$ (30.5 cm) and the right images are for an initial bed height of $36d$ (45.7 cm).....	79
Figure 2-10. Initial and final bed configurations for the diverging Quasi-2D Silo in the 45-degree (left) and 60-degree (right) hopper configuration. These data runs were completed without pebble addition. ....	79
Figure 2-11. Rotational image sequences for the Quasi-2D silo for initial and final packing configurations of the 45-degree hopper loaded to an initial height of $24d$ . For each position step, the upper row includes the visual images of the surface and the lower row are the x-ray images. From left to right, each sequence gives the views for -45.0, -22.5, 0.0, +22.5, and +45.0 rotational positions.....	80
Figure 2-12-A. Pebble flow visualization run for zero-degree converging silo. ....	82
Figure 2-13-A. Pebble flow visualization run for 30-degree converging silo. ....	88

Figure 2-14-A. Pebble flow visualization run for 60-degree converging silo. ....	91
Figure 2-15. Comparison of the front view for the x-ray image (left), and photograph image (right) for the step drainage of the Quasi-2D Silo test section without wedges for piston displacements of 0, 16, and 32 d. ....	94
Figure 2-16. Comparison of the front view for the x-ray image (left), and photograph image (right) for the step drainage of the Quasi-2D Silo test section with 30-degree angle for piston displacements of 0, 16, and 32 d. ....	95
Figure 2-17. Comparison of the front view for the x-ray image (left), and photograph image (right) for the step drainage of the Quasi-2D Silo test section with 60-degree angle for piston displacements of 0, 16, and 32 d. ....	96
Figure 2-18. CoBIE test silo physical arrangement without a packed pebble bed. Left: acrylic test silo with 45-degree wedge insert, control blade, and instrumented pebbles. Right: acrylic test silo mounted on the X-PREX assembly with linear actuator partially extended and x-ray detector in-view. ....	99
Figure 2-19. Detailed view of the modular inserts that feature Teflon sleeves for low friction blade insertion. Left: the 45-degree wedge. Right: the 0-degree wedge. ....	100
Figure 2-20. Primary control blade design. Left: cruciform cross section (dimensions in centimeters). Right: Actual blade compared to the 1.257 cm diameter pebbles. .	100
Figure 2-21. Two blade geometries with annotations showing the unconstrained angles in the tip. Left: 30-degree two-angle blade. Right: 30-degree three-angle blade. ....	101
Figure 2-22. Wiring schematic for the force sensors. Voltage probe is representative of the DAQ-6009. ....	101
Figure 2-23. Seven-point calibration of a Tekscan FlexiForce A401 Sensor with resulting fit function. The fit function does not have a Y-axis reference because that value is “zeroed” during the actual experiment. ....	102
Figure 2-24. Detailed view of force sensor setup during an experiment. ....	102
Figure 2-25. Insertion force vs. blade position for four different 3-angle tips with the 0-degree wedge insert and a pebble bed height of 24 pebble diameters above the entry location. ....	105
Figure 2-26. Insertion force vs. blade position for three different 2-angle tips with the 45-degree wedge insert and a pebble bed height of 36 pebble diameters above the entry location. ....	106
Figure 2-27. Insertion force vs. blade position for the 45-degree two-angle blade into four different pebble bed heights with the 45-degree wedge insert. ....	107
Figure 2-28. Maximum insertion force vs. bed height for the 45-degree two-angle blade with the 45-degree wedge insert. ....	108
Figure 2-29. Insertion force vs. blade position for 60-degree 2-angle and 3-angle tip blades with the 45-degree wedge insert and a pebble bed height of 36 pebble diameters above the point of entry. ....	109
Figure 2-30. Insertion force vs. blade position for five consecutive blade insertions without emptying or refilling the silo with pebbles. Configuration consists of 45-degree two-angle tip blade with 45-degree wedge insert and a pebble bed height of 49 pebble diameters above the point of entry. ....	110
Figure 2-31. Insertion force vs. blade position for two different pebble bed heights and two different insertion methods. Configuration consists of 45-degree two-angle tip blade with 45-degree wedge insert. ....	111

Figure 2-32. 0-degree x-ray images showing the blade fully retracted (left) and fully extended (right).....	112
Figure 2-33. 90-degree x-ray images showing the blade fully retracted (left) and fully extended (right).....	112
Figure 2-34. Cylindrical silo test section installed in the X-PREX facility.....	114
Figure 2-35. Neutronics schematic (left) and CAD design model (right) for the random packed TMSR-SF1 reactor currently being considered by SINAP. The design uses 6 cm diameter pebbles and has a pebble to core diameter ratio of 22.5, which is within the imaging capabilities of the X-PREX facility.....	115
Figure 2-36. CAD design (left) and installed test section (right) of the Cylindrical Silo test section mounted on the modular test base. The conical region is machined from a billet of acetal resin. ....	117
Figure 2-37. Side cross-sectional views for the 30 (left), 45 (center), and 60-degree (right) configurations of the Cylindrical Silo test section. ....	117
Figure 2-38. Machined cones with 30 (left) and 60-degree (right) hopper angles. ....	118
Figure 2-39. Random packing piston plate for use in the Cylindrical Silo test section.....	118
Figure 2-40. X-ray image of the Cylindrical Silo Test Section with a 45-degree cone angle loaded with 8,000 pebbles instrumented with tungsten wire inserts.....	119
Figure 2-41. Cylindrical Silo Test Section loaded with alternating layers of instrumented (white) and unmodified (yellow and green) pebbles used for flow visualization tests. Each layer contains 1,000 pebbles and there are 8,000 pebbles in the test section.....	120
Figure 2-42. Initial configuration of the cylindrical silo flow visualization data run.....	121
Figure 2-43. Cylindrical silo flow visualization run after the discharge of 2,000 pebbles (one quarter of the pebbles in the original packed bed). ....	122
Figure 2-44. Cylindrical silo flow visualization run after the discharge of 4,000 pebbles (half the pebbles in the original packed bed). ....	123
Figure 3-1. Comparison of X-PREX front view (left) to DEM front view (right) for the step drainage of the Quasi-2D Silo test section at the initial and final time step. ....	127
Figure 3-2. Comparison of the front view for the x-ray image (left), photograph (center), and DEM simulation (right) for the step drainage of the Quasi-2D Silo test section without wedges for piston displacements of 0, 16, and 32 d.....	129
Figure 3-3. Comparison of the front view for the x-ray image (left), photograph (center), and DEM simulation (right) for the step drainage of the Quasi-2D Silo test section with 30-degree angle for piston displacements of 0, 16, and 32 d. ....	130
Figure 3-4. Comparison of the front view for the x-ray image (left), photograph (center), and DEM simulation (right) for the step drainage of the Quasi-2D Silo test section with 60-degree angle for piston displacements of 0, 16, and 32 d. ....	131
Figure 3-5. Selected front view images from DEM simulations of the Quasi-2D Silo test section with 30 and 60-degree diverging hoppers. ....	133
Figure 3-6. Average vertical (left) and horizontal (right) velocity components below the orifice for the 45-degree diverging Quasi-2D Silo. The velocities are normalized by the displacement of pebbles in the narrow loading chute above the orifice. ....	134
Figure 3-7. Average vertical (left) and horizontal (right) velocity components below the orifice for the 60-degree diverging Quasi-2D Silo. The velocities are normalized by the displacement of pebbles in the narrow loading chute above the orifice. ....	134

Figure 3-8. Average velocity vectors below the orifice for the 45-degree diverging Quasi-2D Silo. The length of the arrows are proportional to the local velocity magnitude. 135

Figure 3-9. DEM simulation screenshots with 8,000 pebbles in the 45-Degree Converging Cylindrical Silo test section geometry under gravity drainage with no pebble recirculation. The three steps show the initial configuration (left) and the packing after  $5 \times 10^6$  (center) and  $1 \times 10^7$  (right) time-steps. .... 136

Figure 3-10. DEM simulation screenshots with 9,000 pebbles in the 45-Degree Converging Cylindrical Silo test section geometry under gravity drainage with no pebble recirculation. The three steps show the initial configuration (left) and the packing after  $5 \times 10^6$  (center) and  $1 \times 10^7$  (right) time-steps. .... 136

Figure 3-11. DEM simulation screenshots with 6,500 pebbles in the 45-Degree Converging Cylindrical Silo test section geometry under gravity drainage with no pebble recirculation. The three steps show the initial configuration (left) and the packing after  $4 \times 10^6$  (center) and  $8 \times 10^6$  (right) time-steps. .... 137

Figure 3-12. DEM simulation screenshots for DEM runs under free gravity drainage in the Converging Cylindrical Silo test section with cone angles of 30 (left), 45 (middle), and 60-degrees (right). Each snapshot of the packed configuration is taken after  $5 \times 10^6$  time-steps. .... 137

## List of Tables

Table 1-1. X-PREX pebble design options with different metals and pin diameters to match the density of unmodified polyethylene pebbles.....	38
Table 1-2. Bounce height and evaluated coefficients of restitution for instrumented pebbles on several plastic materials used in the X-PREX facility. The initial height for the drop tests was 57.5cm. ....	42
Table 1-3. Static friction coefficients derived from a ramp test for instrumented pebbles on several plastic materials used in the X-PREX facility. ....	43
Table 1-4. Selection of X-PREX procedures, records, and templates.....	69
Table 2-1. CoBIE test matrix.....	104
Table 2-2. Key scaling parameters for TMSR-SF1 and the Cylindrical Silo Test Section in X-PREX.....	115

## Acronyms and Abbreviations

CAD – Computer Aided Design  
CNC – Computer Numerically Controlled  
CoBIE – Control Blade Insertion Experiment  
DAQ – Data Acquisition Device  
DEM – Discrete Element Method  
FDM – Fused Deposition Modeling  
FHR – Fluoride Salt-Cooled High-Temperature Reactor  
GUI – Graphical User Interface  
HDPE – High Density Polyethylene  
HTR – High-Temperature Reactor  
PB-FHR – Pebble-Bed Fluoride Salt-Cooled, High-Temperature Reactor  
SINAP – Shanghai Institute of Applied Physics  
THTR – Thorium High Temperature Reactor  
TMSR-SF – Thorium Molten Salt Reactor – Solid Fuel  
UCB – University of California, Berkeley  
USNRC – U.S. Nuclear Regulatory Commission  
X-PREX – X-Ray Pebble Recirculation Experiment

# 1 Facility Description

The X-Ray Pebble Recirculation Experiment (X-PREX), shown in Figure 1-1, is a new facility currently in operation at U.C. Berkeley that uses novel digital x-ray tomography methods to study granular flow in beds of packed spheres. X-PREX is the first experimental facility that has the capability to track both three-dimensional translational and rotational motion of all pebbles in a packed bed. The primary goal of the X-PREX facility is to provide experimental data that can be used to validate friction models in discrete element method (DEM) simulations to support their use in large-scale simulations in reactor core design and analysis. The capability to track the rotational motion of all pebbles gives the X-PREX facility unique potential to achieve this model validation goal.

The key innovation of the X-PREX facility is the use of plastic spheres with thin tungsten wires inserted through one central axis that can be easily resolved through x-ray imaging due to the large difference in attenuation coefficients between the two materials (Figure 1-2). The images of the pin can be correlated between images from multiple rotational views to determine motion in three translational directions and two of the three rotational axes. The rotational motion around the pin axis cannot be resolved, but can be treated statistically as an unknown displacement component that is not significant for the average behavior because the pebbles in the packed bed are randomly oriented. Figure 1-3 shows a sample x-ray image of 4,500 instrumented pebbles in a packed bed with a depth of eight pebble diameters.

The report is divided into three sections. Section 1 details the X-PREX facility design and capabilities, including a description of the novel image processing methods developed. Section 2 covers initial results for the three experiments studied to date in the X-PREX facility. These test sections include the study of granular flow in Quasi-2D and Cylindrical Silos and the forces on a shutdown blade inserted directly into a packed bed (Figure 1-4). Finally, Section 3 describes the supporting simulation and validation efforts completed to date.



**Figure 1-1. View of the X-Ray Pebble Recirculation Experiment (X-PREX) Facility at U.C. Berkeley.**

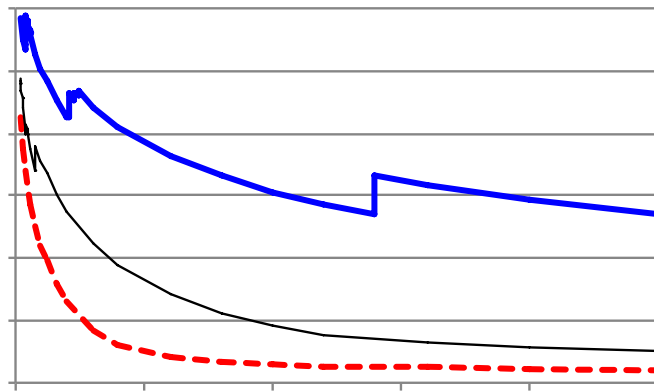


**Figure 1-2. X-ray mass attenuation coefficients for tungsten, polyethylene, bone, and soft tissue.**

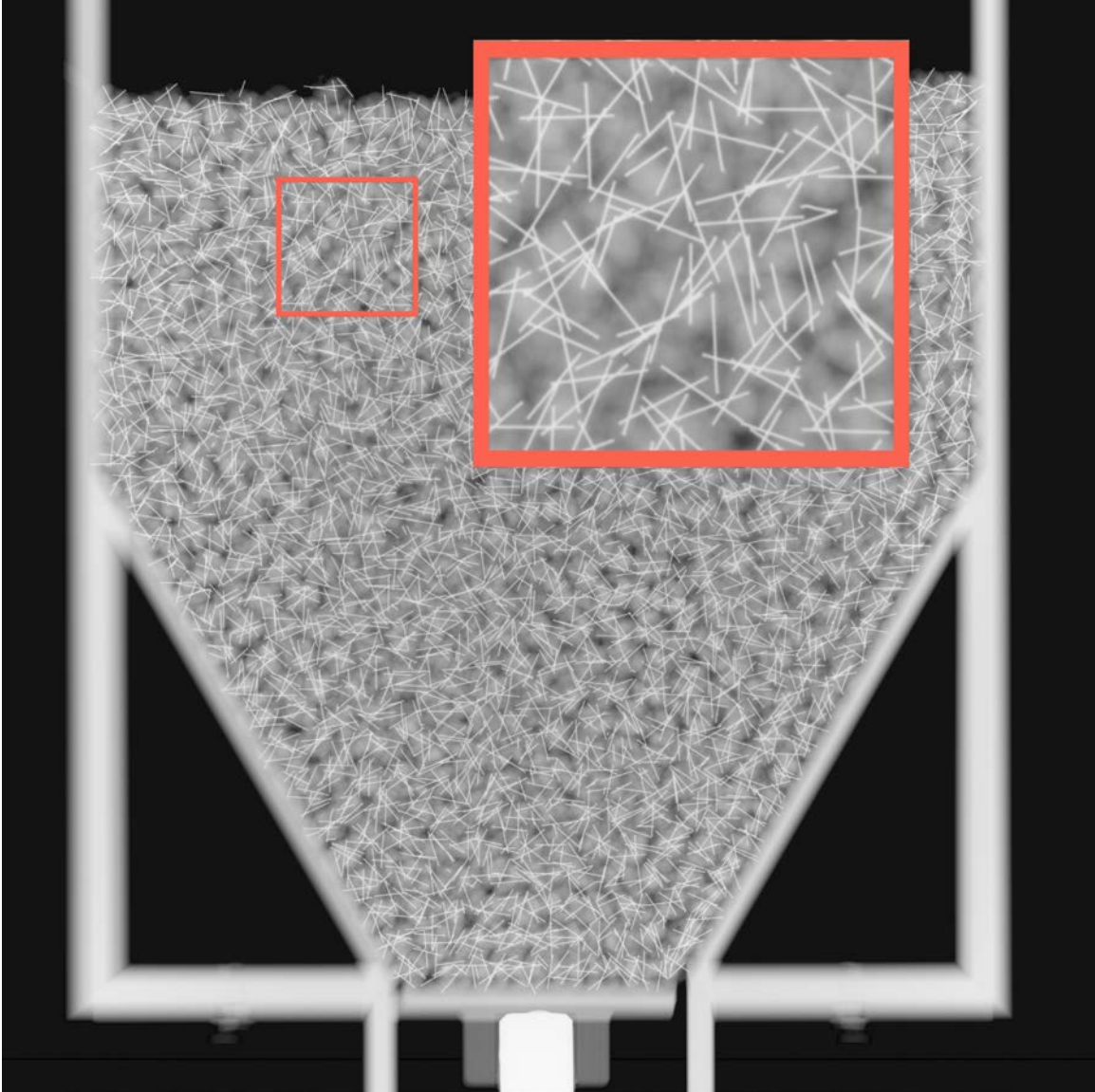


**Figure 1-3. Sample x-ray image of 4,500 instrumented pebbles in a packed bed with a depth of eight pebble diameters. The cropped area shows a detailed view where the pin images are resolved.**

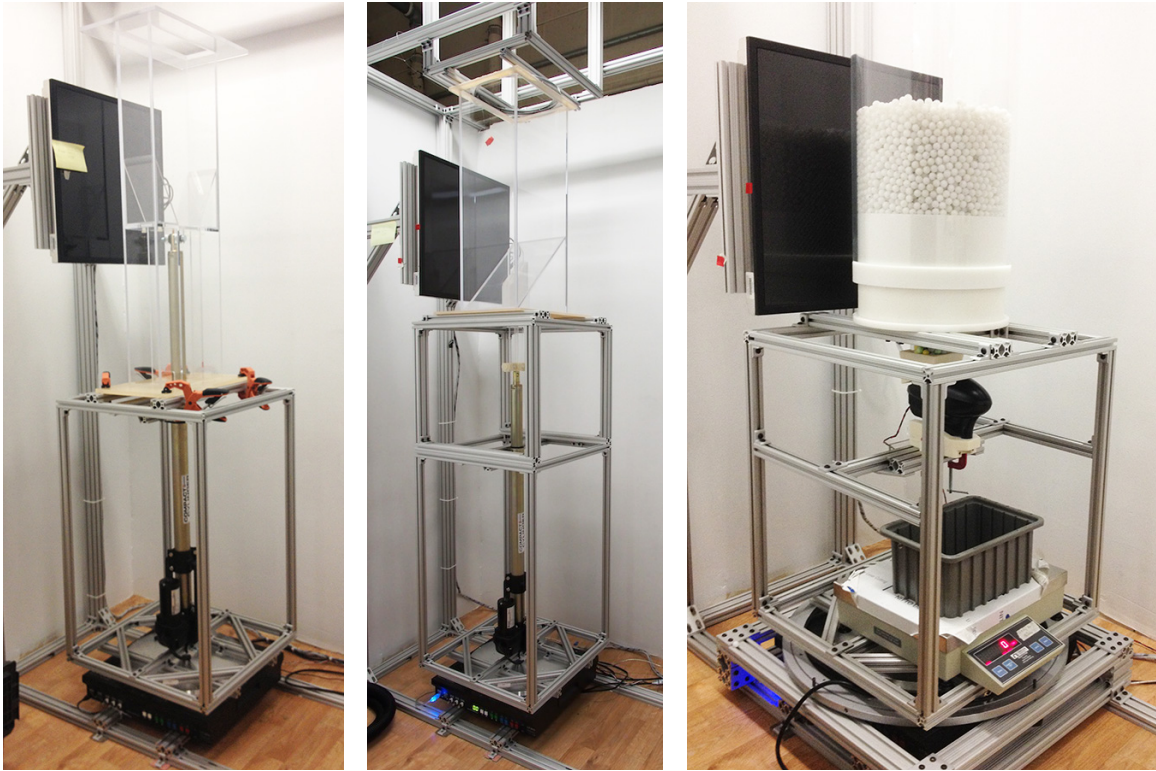


**Figure 1-4. Quasi-2D Silo (left), Control Blade Insertion Experiment (middle), and Cylindrical Silo (right) installed on the modular test base in the X-PREX facility.**

## 1.1 X-Ray Imaging System

### 1.1.1 System Description

The X-PREX facility includes a commercial x-ray imaging system that is comparable to those used for diagnostic medical radiography. The x-ray tube has a maximum shot capacity of 125 kVp and 400 mAs, though typical settings for data collection are in the 80 kVp and 20 mAs range. The tube has a small focal point setting of 0.3 mm, which is assumed to be approximately a point source. The digital CsI-TI x-ray detector has an effective imaging area of 42.9 by 42.9 cm with an effective image array of 3,000 x 3,000 pixels. The pixel resolution of the detector is 143  $\mu\text{m}$ .

The components of the x-ray imaging system are installed in rigid frame assembled from slotted square aluminum tubing. Figure 1-5 shows the design layout of the X-PREX imaging system with the detector located at the left side and the x-ray tube located at the right side. The distance between the x-ray focal point and the detector plane is 209 cm. The vertical position of the x-ray detector and tube may be adjusted to accommodate test sections of different heights or to image different regions of taller geometries. The x-ray focal point is roughly centered on the detector plate, but test section-specific procedures have been developed to precisely determine the precise position of the focal point relative to the test section.

The green region in Figure 1-5 represents the 30x30x30 cm cubic volume used for data collection. The regions above and below the data collection zone may also be used for test sections, but will project images outside of the detector area. The data collection region is shown on top of the modular test base. The rotation axis in the test section is located 24.6 cm from the detector plane and test sections must be designed with appropriate clearance to avoid contact during rotation.

The framing for the x-ray image system may be adapted to include additional pieces of equipment if needed due to the flexible slotted framing. Figure 1-6 shows the x-ray tube with a remote camera positioned below that allows facility operators to observe the test section from the remote operator station during data collection and to record visual images that can be used to verify the test section orientation in an x-ray image.

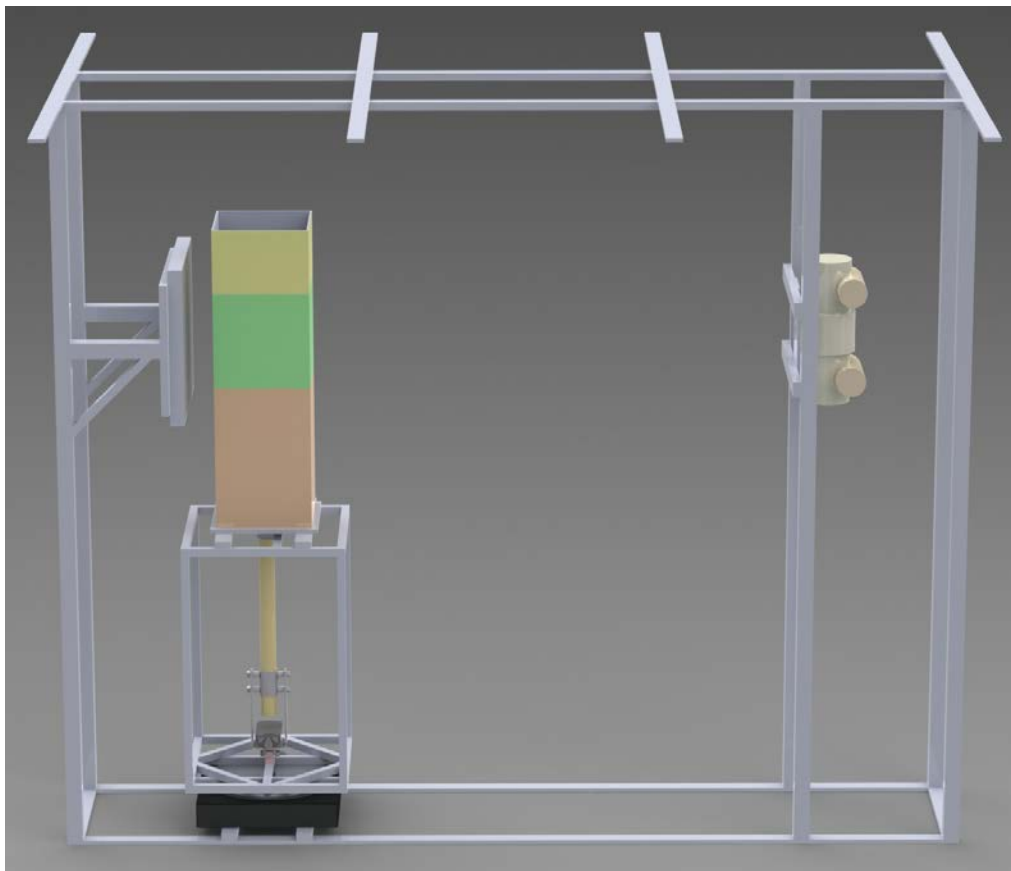


**Figure 1-5. CAD model of the layout of the X-PREX x-ray imaging system. The x-ray detector is on the left side and the x-ray tube is on the right. The green region represents the volume used for data collection. The test section region is mounted on the modular test base and turntable.**



**Figure 1-6. View of the x-ray tube and the remote visual camera mounted in line with the focal point.**

### **1.1.2 Shielding Enclosure**

In accordance with the U.C. Berkeley safety requirements to operate a radiation producing machine, the X-PREX x-ray imaging system is contained within a shielded enclosure located in the Thermal Hydraulics Laboratory in the Department of Nuclear Engineering. Figure 1-7 shows the CAD model design for the shielding enclosure that includes a wood subfloor and structural frame bounded by four walls of lead-lined drywall. The primary shielding wall is behind the detector and includes 1/16" (4 lb/ft<sup>2</sup>) sheet lead. The other secondary walls include 1/32" (2 lb/ft<sup>2</sup>) sheet lead. The enclosure also includes a lead-lined door with a shielded window, shown in Figure 1-8. The X-PREX shielding enclosure does not include a roof structure. The approved system geometry prevents the collimated x-ray beam from extending beyond the primary shielding wall. Interlocks are present in the shielding enclosure to prevent the generation of x-rays while the enclosure door is open or the Emergency Shutdown Switch is pressed while people are working within the facility and the generator is on.

Initial dose verification measurements were completed for maximum possible x-ray shots (125 kVp, 400 mAs) during the facility commissioning under the supervision of U.C. Berkeley Office of Environmental Health and Safety. No measurable cumulative dose was measured in several important locations around the shielding enclosure, including the operator station, the location in the laboratory with the maximum ceiling beam reflection, and the offices located on the floor above the facility. Regular dose verification measurements are completed and recorded on a monthly basis according to the X-PREX Quality Assurance Program.

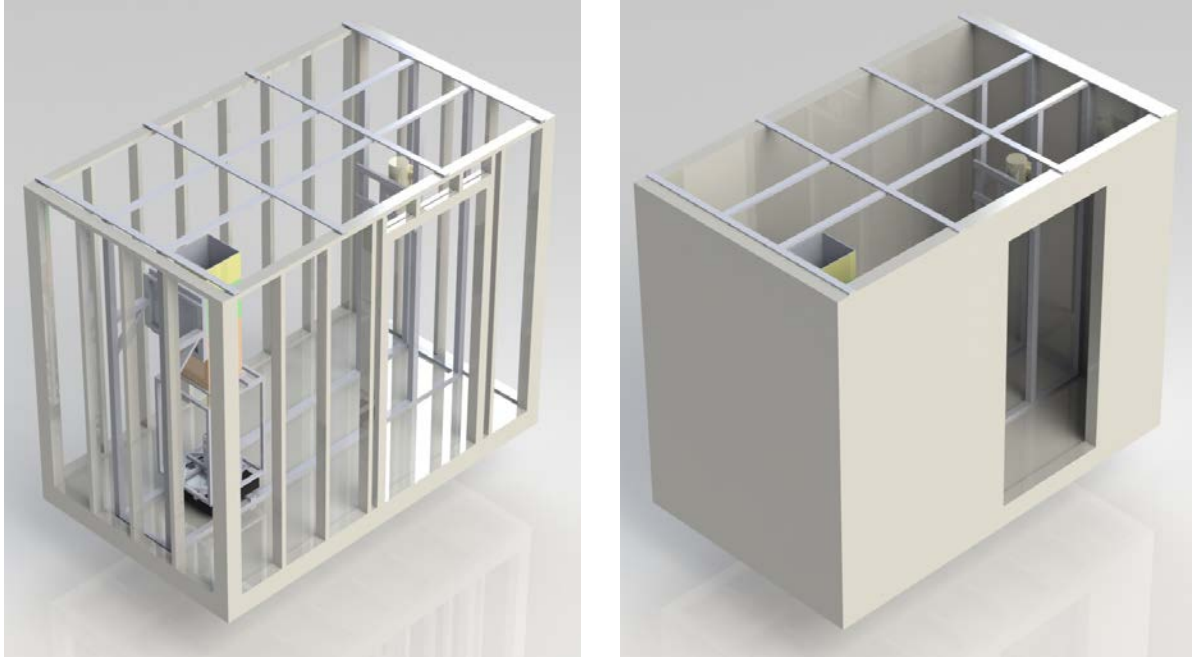


**Figure 1-7. CAD model for the X-PREX facility shielding enclosure, including the wood structural framing and x-ray system (left) and the lead-lined drywall around the four walls (right). The enclosure also includes a lead-lined door (not shown).**



**Figure 1-8. External view of the X-PREX shielding enclosure.**

### 1.1.3 Remote Operator Workstation

The X-PREX facility at U.C. Berkeley includes a remote operator workstation (Figure 1-9) so that all x-ray imaging and data collection operations may be performed outside of the shielding enclosure. Under normal data collection procedures, the capability to do all operations remotely greatly increases the efficiency of an imaging session. The operator workstation includes the X-PREX Logbook, the x-ray generator control panel, and the data collection computer with all relevant software installed. The X-PREX logbook is a legal record that includes all use of the radiation-producing machine in the facility and must be used during every imaging session. The x-ray generator control panel is used to fire each x-ray shot and must be independently controlled under guidelines from the U.C. Berkeley Office of Environmental Health and Safety.

The X-PREX data collection computer is used to upload x-ray images from the detector after each shot and perform a variety of other functions during test runs. The following software is used during data collection:

- Rayence Xmaru Non-Destructive Testing (NDT) X-Ray Imaging Software: Used to upload x-ray images from the detector and review x-ray images during data collection to verify exposure. (Note: Vistek Opal Rad software was originally used for some initial data collection, but included several logistical challenges associated with the Food and Drug Administration requirements for medical software.)
- Precision Turntable Control Interface: Used to control and verify the rotational position of the test section. The step size between images may be set so that the angle does not need to be entered for each rotational motion step.
- LabVIEW Modular Test Bay Control Interfaces: Graphical User Interfaces (GUIs) were developed by U.C. Berkeley to control the linear actuator position and the continuous discharge devices in the modular test bay. These programs may be configured as needed to control and record the motion boundary conditions imposed on the packed pebble bed in the test section.
- Remote Camera Live View Software: The remote camera located in the shielding enclosure is used to create a continuous visual feed to the operator workstation to monitor the position of the test section. Visual images are recorded before each x-ray image to resolve any uncertainties in the system configuration during post-processing. The remote camera may also be used to read digital scales in the modular test bay in order to track pebble inventories.

In addition to the software listed above, the operator workstation is connected to the secure Thermal Hydraulics Laboratory Server to back up all data recorded using the X-PREX facility, in accordance with the X-PREX Quality Assurance Program.



**Figure 1-9. View of the X-PREX facility remote operator station at U.C. Berkeley.**

### 1.1.4 System Geometry Verification

In order to complete the computed tomography algorithms for the packed pebble bed, the geometry of the system must be determined with a sufficient degree of precision. Based on this need, U.C. Berkeley has developed a set of procedures to measure and verify the system geometry when the x-ray detector and tube are moved to accommodate different test sections. The procedures include the leveling of the x-ray detector to within  $0.01^\circ$  and a calibration method to determine the distances from the rotation axis to the detector plan and x-ray tube focal point as well as the height of the x-ray tube focal point.

The X-PREX facility geometry verification procedure uses a precision-machined calibration disk with sharp points that can be marked in the x-ray images for a complete rotation sequence in  $22.5^\circ$  steps and used to extract the geometry data. In the standard configuration, the detector plane and the tube focal point are 24.64 cm and 184.53 cm from the vertical rotation axis. The height can be adjusted to suit the imaging region for each test section. This level of precision is sufficient for the tomography code. Figure 1-10 shows the precision-machined calibration disk, a sample calibration image, and a geometry sketch of the system configuration.

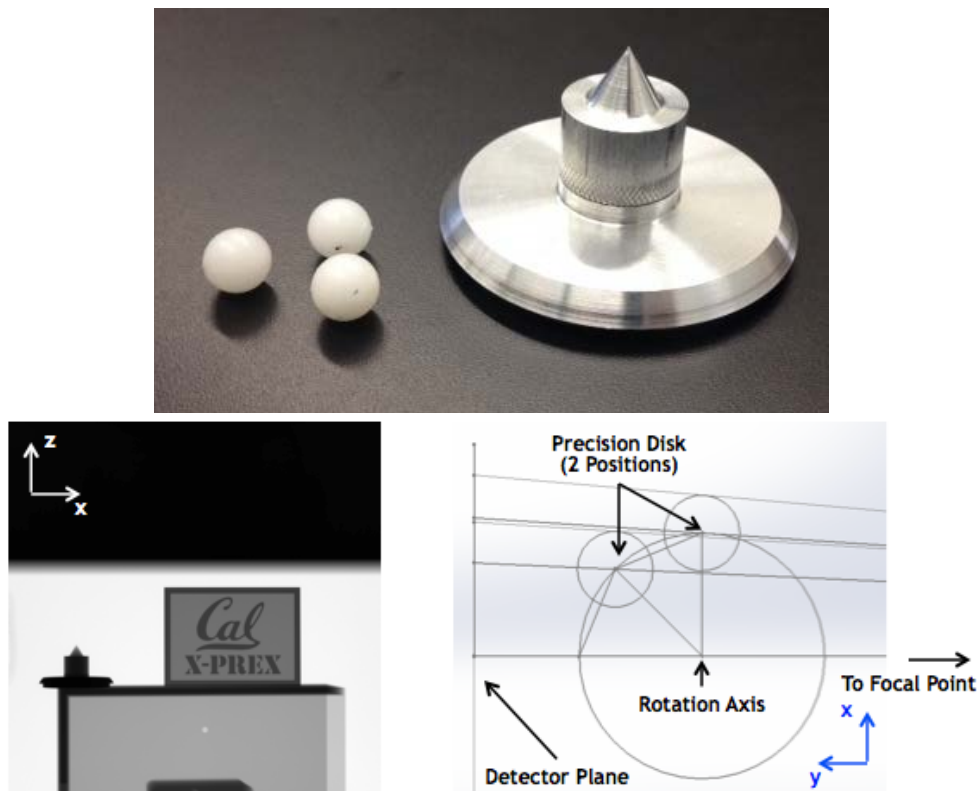


**Figure 1-10. Precision-machined disk for X-PREX geometry measurements (top), sample calibration image (bottom left) and top view geometry sketch (bottom right).**

## 1.2 Modular Test Bay

The x-ray pebble recirculation experiment (X-PREX) facility (Figure 1-11) includes a Modular Test Bay that can accommodate a wide variety of test section geometries and provide precise actuation to move the test section to perform the x-ray tomography imaging. This chapter describes the design and functional modes for the test that demonstrate its flexibility to accommodate different types of granular flow experiments in the X-PREX facility. The contents of this chapter cover the design of the structural framing and stabilized bearing system, the integrated equipment in the test bay, and several configurations used in preliminary studies completed to date.



**Figure 1-11. X-PREX Facility at U.C. Berkeley.**

### 1.2.1 Modular Test Base Structure

The Modular Test Bay base structure consists of structural framing, stabilizer rotational bearings that reduce the possible tilt in the system rotation axis, and a precision turntable. Details of these structures are covered in the following sections.

#### 1.2.1.1 Structural Framing Design

The X-PREX modular test base is able to accommodate a wide variety of test section configurations due to the use of slotted aluminum. This frame structure allows for maximum customization and adjustability for any test setup. 80/20<sup>®</sup> aluminum is designed around standardized cross section aluminum beams that accept a variety of connection pieces. Figure 1-12 shows a standard example of a corner connection.



**Figure 1-12. Standard 80/20<sup>®</sup> aluminum beam and connection piece.**

#### *1.2.1.2 Precision Turntable*

At the bottom of the modular test bay is a LinearX Systems LT360EX Precision Turntable (Figure 1-13) with a rotational resolution of 0.1° and maximum vertical loading of 450 kg. The turntable is used to set the rotational positions of the test sections that are required for the computed tomography image processing algorithms.



**Figure 1-13. LinearX Systems LT360EX Precision Turntable.**

Because the precision of the rotation is one of the most important variables in the pebble tomography, two custom stabilization bearings were added to ensure a highly stable system. One stabilization bearing resides on the same plane as the LinearX turntable platter at the bottom of the assembly (Figure 1-14), while the other bearing is lowered onto the top of the test section from the ceiling 80/20<sup>®</sup> aluminum frame (Figure 1-15). Both bearings work to eliminate any rotational wobble in the system, which can be of significant concern in tall test silos.

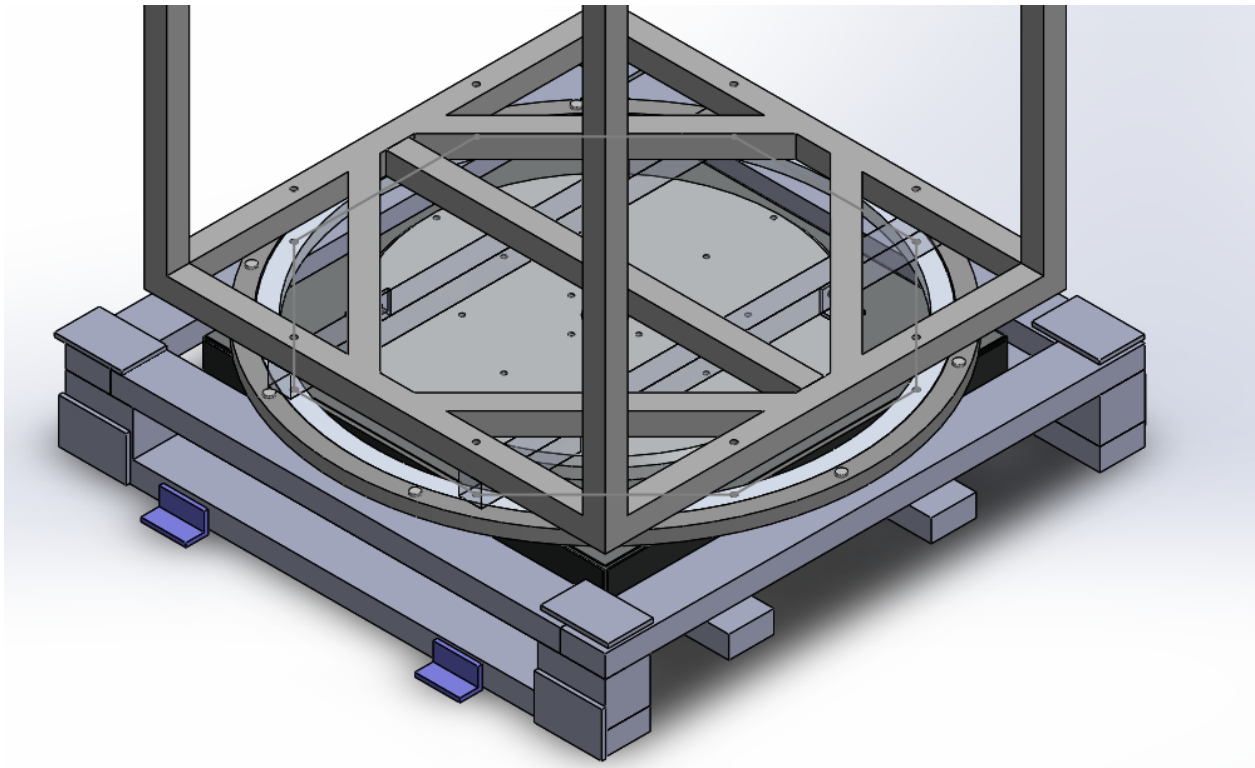


**Figure 1-14. CAD model for the stabilized turntable base in the X-PREX Modular Test Bay.**

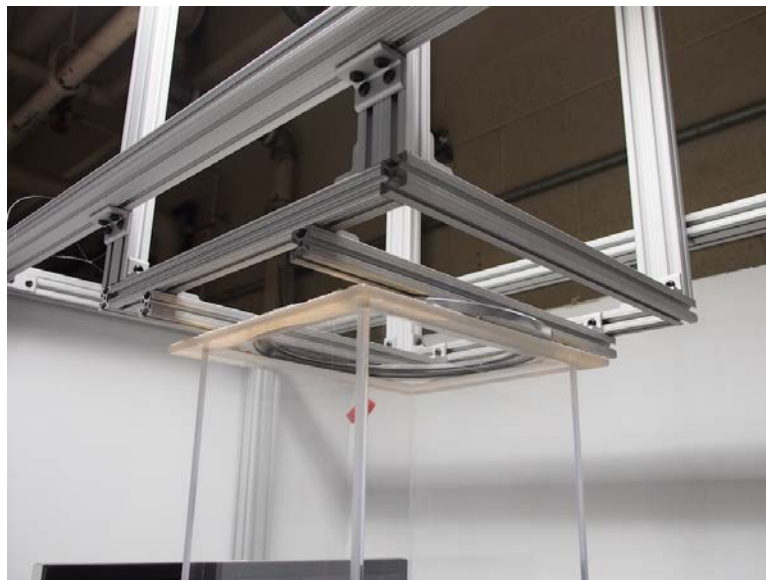


**Figure 1-15. Modular Test Bay upper frame and rotary bearing that can be used to stabilize tall test sections in the facility. Additional features can be added to the rails above the bearing.**

The square frame above the rotation bearing (seen in Figure 1-14) has a side dimension of 52.1 cm and can be precisely leveled. All base structures for X-PREX test sections will mount above this square frame on the base.

## 1.2.2 Actuation and Sensor Capabilities

In addition to x-ray image and digital camera image capture capabilities, the X-PREX facility is outfitted with a variety of digital controls and sensors. Everything is controlled from the X-PREX control computer located outside of the x-ray shielding enclosure. This allows operators to fully control experiments without having to go inside the x-ray shielding enclosure during operation of experiments.

### 1.2.2.1 Data Acquisition and Control Devices

The X-PREX facility utilizes the LabVIEW software suite complemented with various custom LabVIEW Virtual Instruments (VIs) as well as vendor software. The X-PREX facility currently uses two National Instruments USB-6009 Data Acquisition (DAQ) devices (Figure 1-16) to collect sensor data and to actuate experiments.



**Figure 1-16. National Instruments USB-6009 DAQ.**

Each 14-bit DAQ device is capable of recording 48,000 samples per second between 8 analog inputs. Each device additionally has 2 analog outputs, 12 bidirectional digital IO channels and a 5 volt source.

The DAQ devices are used to control the linear actuator, pebble hopper systems, and to record data from force sensors in the Control Blade Insertion Experiment (CoBIE). The DAQ devices can also easily interface with additional sensors or actuators, if necessary.

### 1.2.2.2 Rotation Actuation Motion

The LinearX Systems LT360EX Precision Turntable (Figure 1-13) is controlled using a LinearX vendor software. The graphical user interface (GUI) can be seen in Figure 1-17:

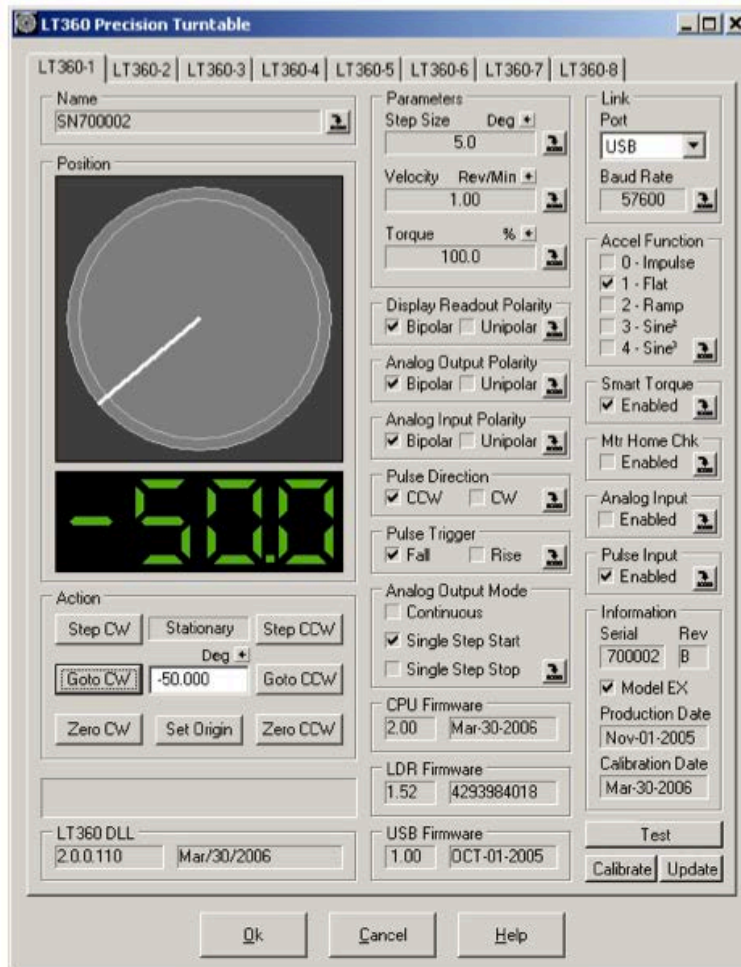


**Figure 1-17. LT360 graphical user interface on the X-PREX remote operator computer. The step size can be set for the desired rotation between each x-ray imaging orientation.**

The LinearX vendor software provides sufficient control options for smooth rotational motion that will not shift pebbles during actuation. For example, the software allows for the user to set various velocity profiles for the rotation, as seen in Figure 1-18:

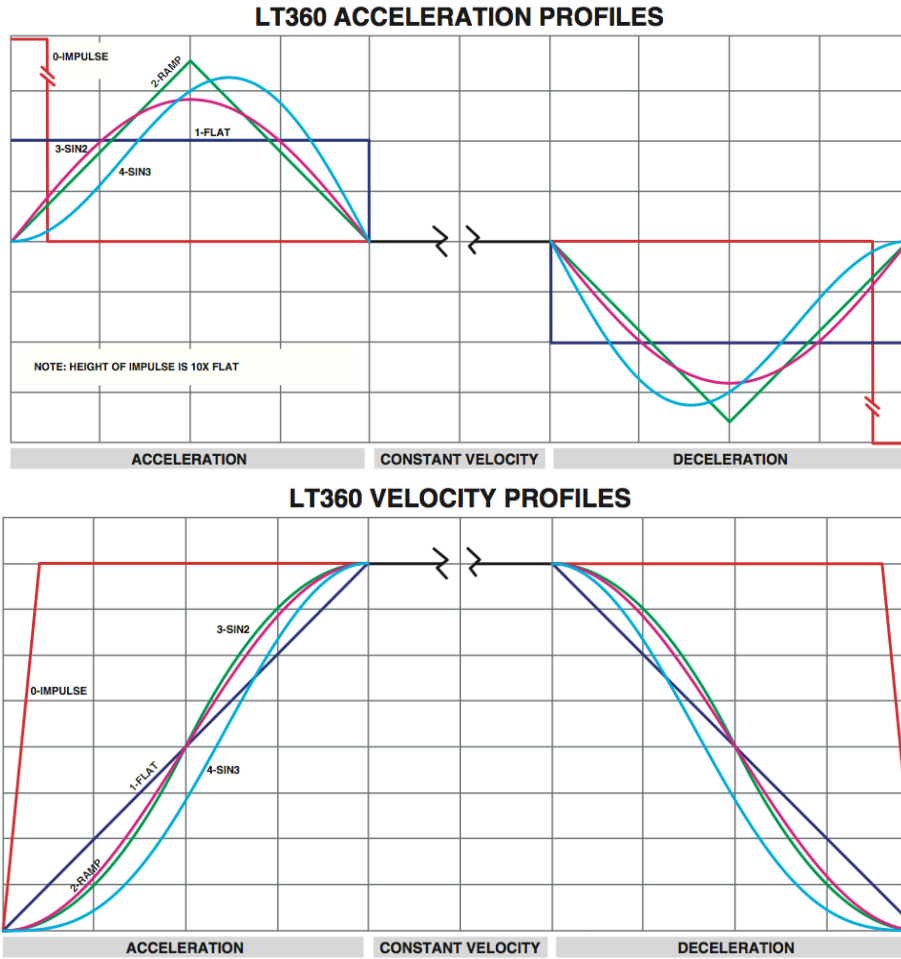


**Figure 1-18. Precision turntable acceleration (top) and resulting smooth velocity (below) profiles can be used to minimize peak accelerations and reduce the potential for pebbles to shift positions during rotation between each x-ray imaging orientation.**

### 1.2.2.3 Linear Actuation Motion

The X-PREX modular base structure includes a linear actuator with 45.7 cm throw distance that is used to control the position of a piston plate during controlled step-wise data collection procedures. The actuator is a Nook Industries CC-18-HD E linear rod style actuator. The actuator can be seen mounted on the test base frame in Figure 1-19.

The linear actuator position is measured using a potentiometer built into the actuator by the manufacturer. The control circuit for the linear actuator includes engineered controls in the form of double pole double throw (DPDT) switch to prevent the operation in the reverse direction during data collection that could degrade results and, due to pebble binding, damage the test sections. The linear actuator is controlled using a LabVIEW control VI (Figure 1-20) which was made specifically for this application.

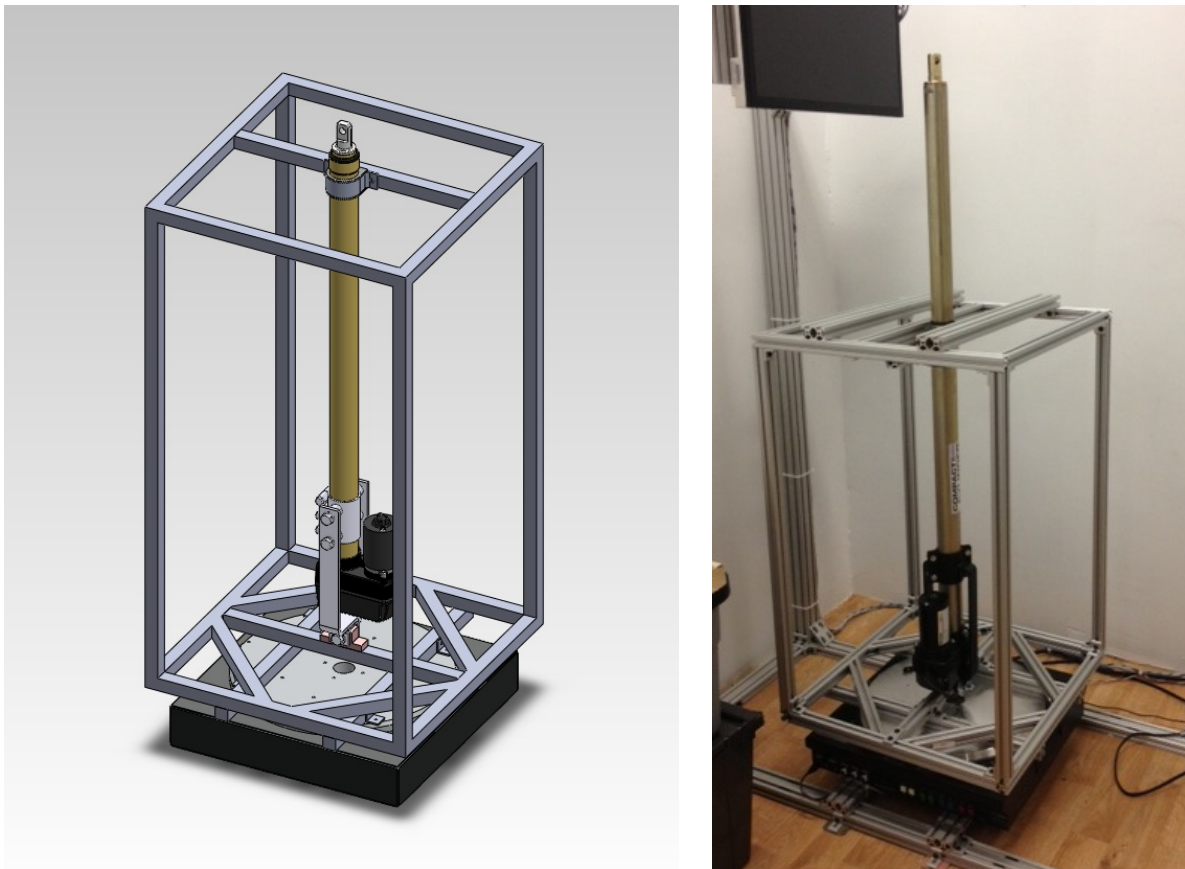


**Figure 1-19. Modular Test Bay CAD design (left) and installed system (right) configured with the linear actuator, lower support frame structure, and the precision turntable base.**

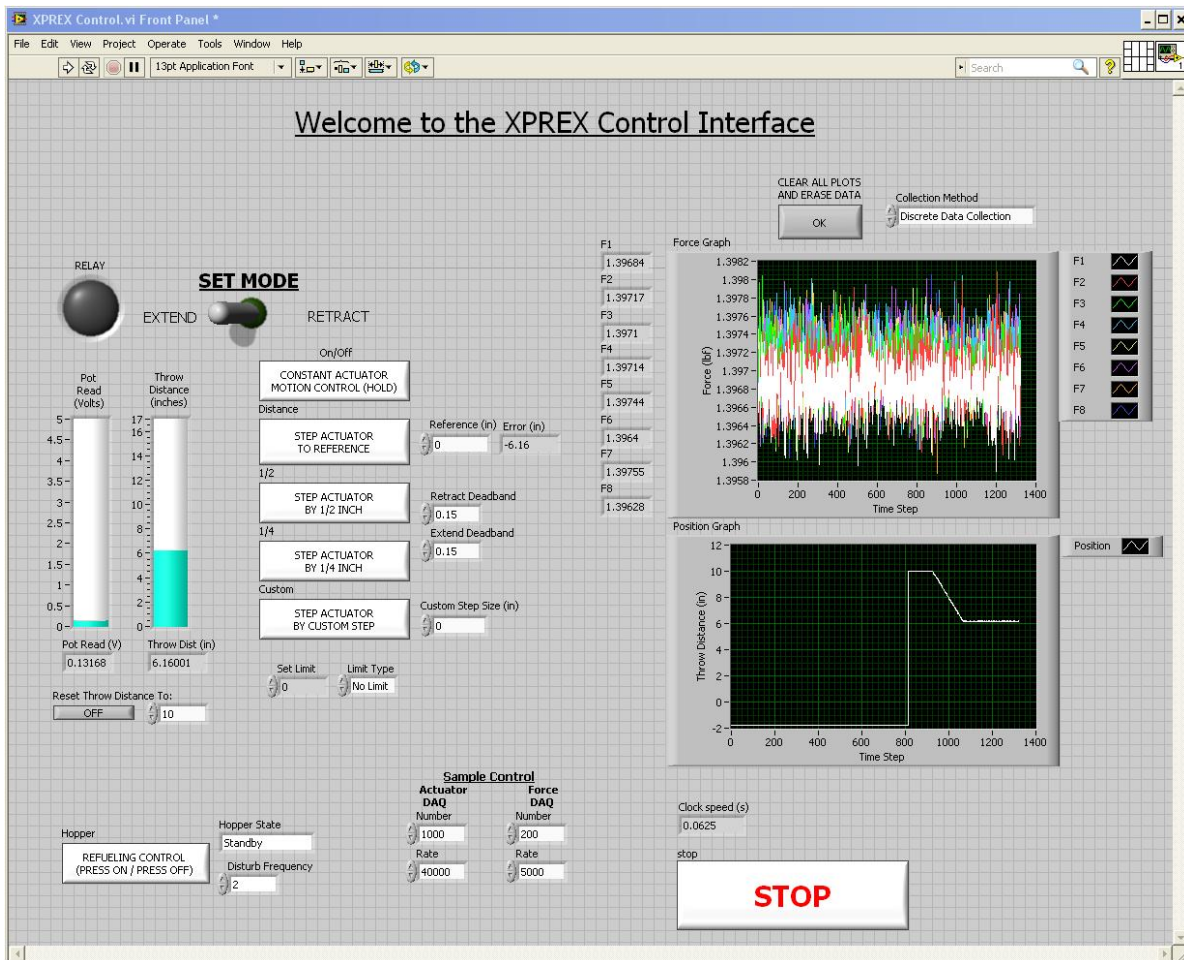


**Figure 1-20. LabVIEW Graphical User Interface (GUI) for the linear actuator controller.**

The VI is a custom piece of software serving as a GUI that controls the DAQ devices. Using the National Instruments DAQ devices, the VI applies voltage to the actuator, and also reads the actuator position using the potentiometer. The VI can control the linear actuator with sub millimeter precision, while simultaneously collecting sensor data. Initial data collection used a small step size of 0.635 cm (half a pebble diameter) to establish confidence in the mapping of pebbles between two time steps. The control VI is capable of adjusting the step size to determine the sensitivity of the granular flow profile to the dynamics of the motion steps. Features of the interface include control over the actuator position, user-specified step motion intervals, user-specified limits on actuator position, and data recording for input signals (e.g. force sensors) and actuator position. The data recording can be done in continuous or discrete modes and allows for user-specified sampling periods. The control VI can also be used to actuate the pebble hopper unloading system detailed in section 1.2.2.4.

#### 1.2.2.4 Pebble Hopper Unloading System

A modular interface for a commercial hopper was designed to transfer pebbles from containers of several pebble diameters to a single pebble diameter tube. This interface can be used to load an exact number of pebbles from a large container into the top of a test silo, or to drain an exact number of pebbles from the bottom of a large test section. Commercially available hoppers were identified as useful devices capable of actuating pebble flow. Modular parts were designed to mount the commercially available hoppers on the 80/20<sup>®</sup> aluminum frame, and to interface variably sized pebble beds on top of the hopper. The modular parts were 3D printed using an FDM machine and can be seen with the hopper in Figure 1-21.

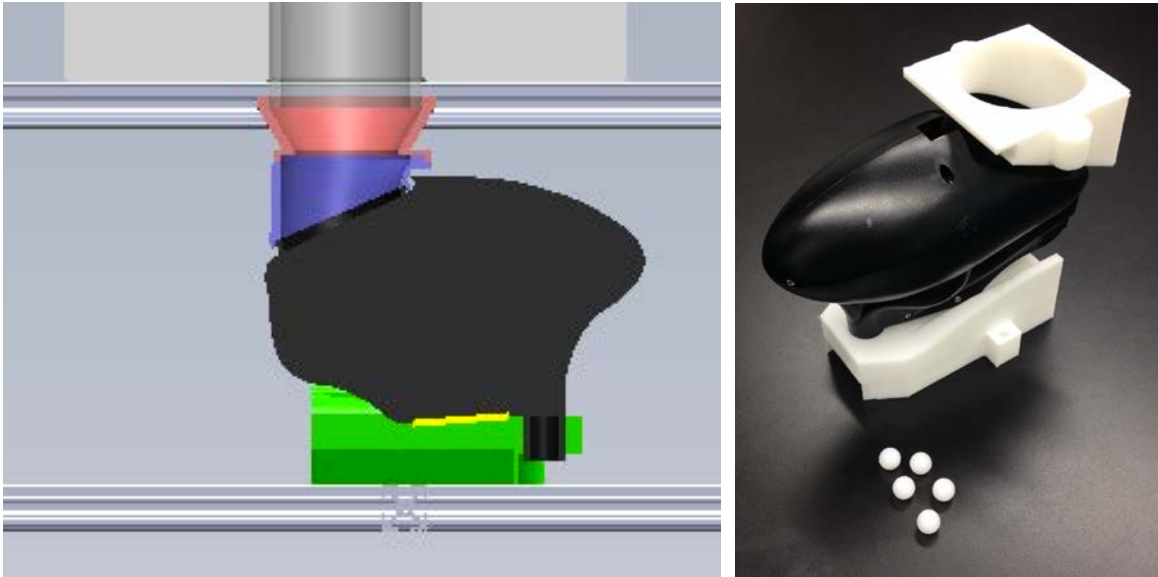


**Figure 1-21. CAD model (left) and manufactured parts (right) of modular interface for continuous discharge device. Pebbles are fed in through adapters at the top of the hopper and discharged in a small diameter tube.**

Control of the hopper was achieved by stripping the hopper of all microprocessors and other control elements, and interfacing the hopper motor directly to an H-Bridge and the National Instruments DAQ devices. By doing so, the hopper is easily controlled using the LabVIEW control VI.

#### 1.2.2.5 Counting Scale

Two counting scales with counting resolution of a single pebble (<1 gram) were sourced in order to have accurate pebble accounting during the continuous discharge mode. One scale is currently installed in the modular test base (Figure 1-22). This system allows for accurate tracking of pebble inventories in the test section that can be used to set up discrete element method (DEM) simulations with matched pebble recirculation conditions. Additionally, the scale placed on the test base can be read using the digital camera images (Figure 1-22).



**Figure 1-22. Front view from shielding enclosure camera showing the number of discharged pebbles on the counting scale. The readings can be read by the operator and recorded on study log records.**

### 1.2.3 Test Configurations

Three main configurations (Figure 1-23) of test sections and actuators have been used to date. For pebble flow experiments, such as the Quasi-2D Silo, the actuator is used in retract mode to allow for downward pebble flow. For blade insertion experiments such as CoBIE, the actuator is used in extend mode to drive the control blade into a packed pebble bed. For the Cylindrical Silo experiment, large quantities of pebbles must be removed from the test silo, so the pebble hopper and counting scale are used on the test base. These configurations demonstrate the flexibility of the modular test base systems. Additional functionality, such as pebble reloading from the top of the test bay, may certainly be added in the future as demanded by test requirements.

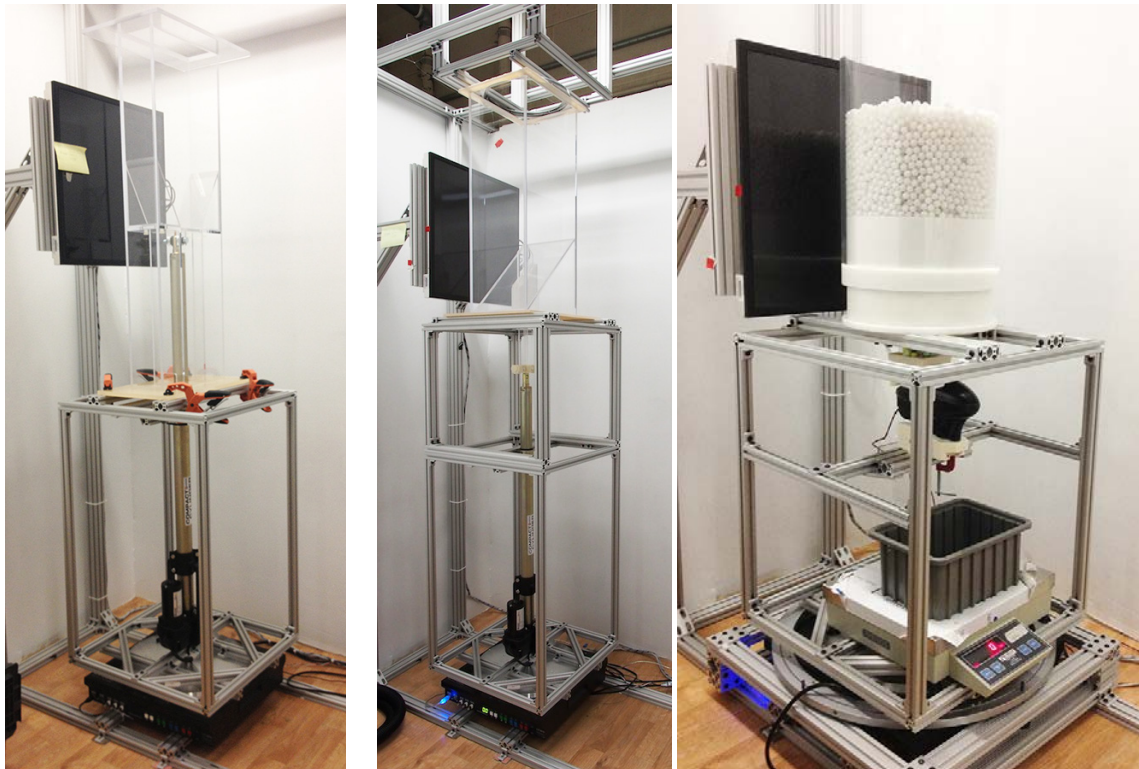


**Figure 1-23. Modular Test Bay configured with the linear actuator for downward piston motion in the Quasi-2D Silo Test Section (left) and upward blade motion in CoBIE (middle) and the pebble hopper in the Cylindrical Silo (right).**

## 1.3 Pebble Modification

This chapter describes the design process and final specifications for the pebbles used in the X-Ray Pebble Recirculation Experiment (X-PREX) at U.C. Berkeley. The X-PREX facility is used to produce high fidelity data on granular flow using instrumented pebbles and x-ray tomography methods. The key innovation in the X-PREX facility is the use of plastic pebbles instrumented with a thin tungsten wire through one axis that generates sufficient contrast to locate the pin image in an x-ray image. The experimental results from the facility include both translational and rotational motion for all the pebbles. Therefore, the results are uniquely suited for the validation of discrete element methods (DEM) simulations that track the motion of all pebbles in a granular system.

### 1.3.1 Instrumented Pebble Design

The X-PREX facility uses plastic spheres with metal wire inserts that are used to track pebble motion in a sequence of x-ray images. The following sections describe the initial prototype development, design process, and final pebble specifications.

#### 1.3.1.1 Prototype Pebble Viability Demonstration

The instrumented pebbles in the X-PREX facility are the key component in the system needed in order to track the translational and rotational motion for the pebbles in the packed bed. Therefore, U.C. Berkeley completed an initial prototype development effort using polyethylene spheres and stainless steel pin inserts to demonstrate the viability of the proposed experimental method and to gain insights for the final pebble design specifications. A set of 500 pebbles was fabricated for initial testing with a pebble diameter of 12.5mm and pin diameter of 1.46mm. Figure 1-24 shows one prototype pebble and the metal pin insert and Figure 1-25 shows an x-ray image of 500 instrumented pebbles packed in a rectangular plastic silo with a depth of eight pebble diameters. These results confirmed the potential to generate clear images of the metal wire inserts in the packed bed.



**Figure 1-24. Prototype 12.5 mm diameter polyethylene pebble with tapered stainless steel pin insert.**

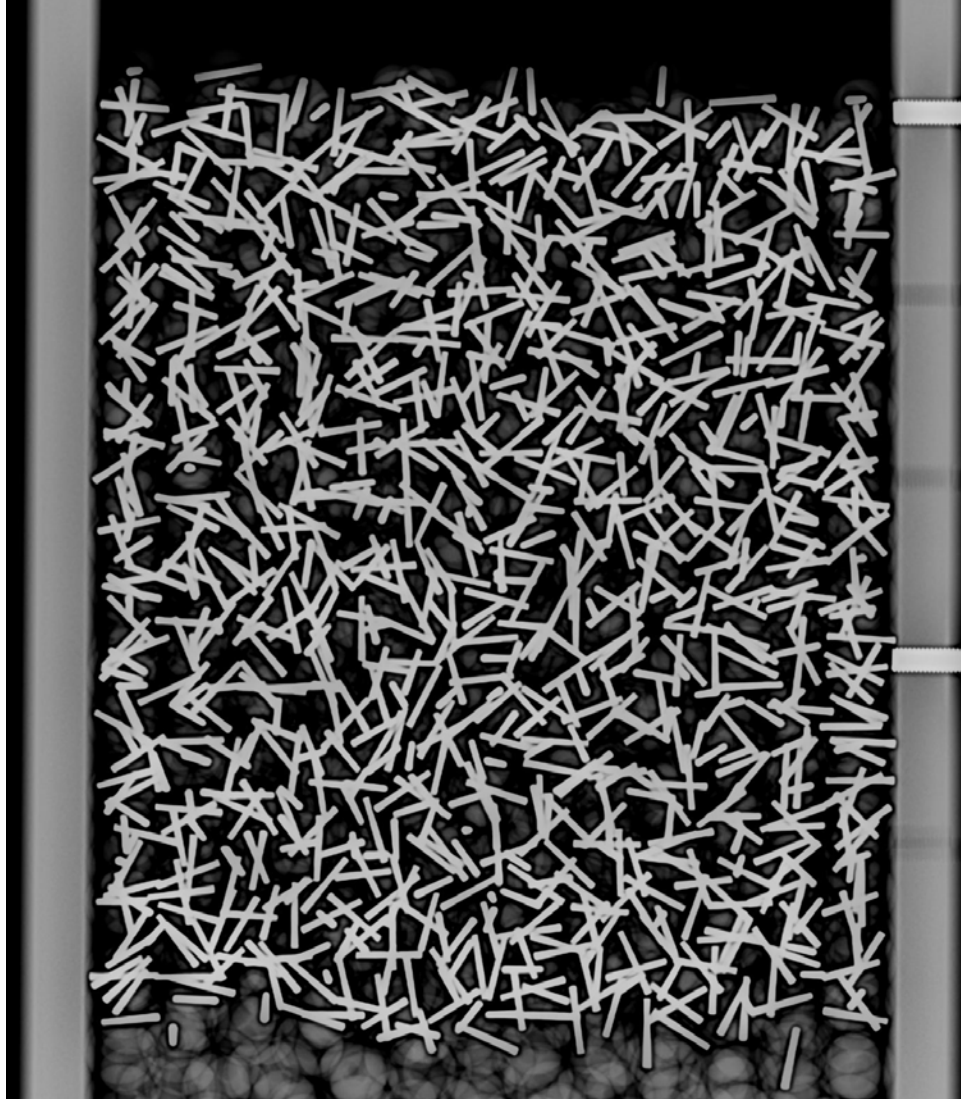


**Figure 1-25. X-ray image of 500 prototype pebbles in a container with a depth of eight pebble diameters.**

### 1.3.1.2 Instrumented Pebble Design Study

Based on the results with the prototype pebbles, U.C. Berkeley completed a thorough design study to select the final instrumented pebble specifications for the X-PREX facility. The key requirements for the pebbles included a high contrast in the x-ray images, a resolvable pin image width, and matched density to unmodified high-density polyethylene pebbles ( $\rho = 0.96 \text{ g/cm}^3$ ) in order to match buoyancy forces in scaled experiments using water in the future.<sup>1</sup>

The prototype pebbles with the stainless steel pins had a density of  $1.06 \text{ g/cm}^3$  and were therefore would have negative buoyancy in water and were not suitable to use in any wet scaled experiments. In addition, the image width of the steel pins was approximately 10 pixels, which would make it difficult to resolve individual pin images in packed beds with a significantly larger number of pebbles. Figure 1-26 shows predicted images for pin image widths of 10, 5, and 3 pixels. From this result, it is clear that smaller pin diameters, using material with a high x-ray attenuation, would be preferred to resolve images in densely packed beds.

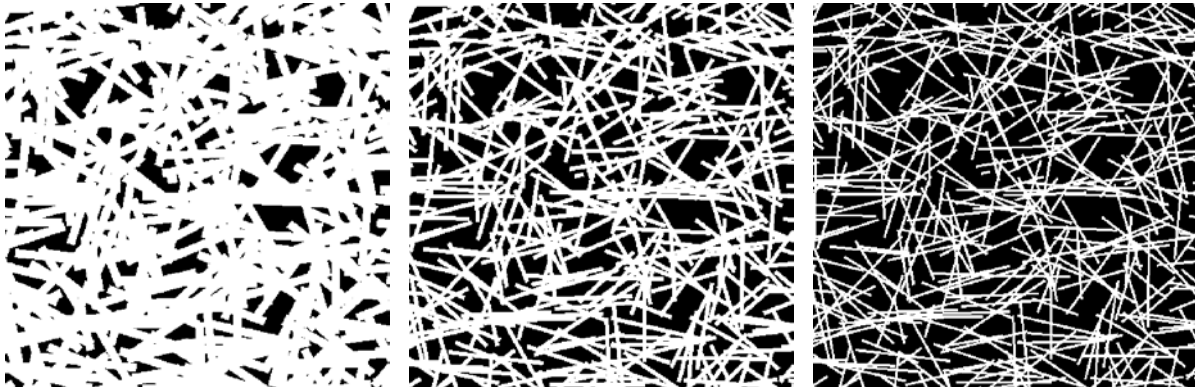


**Figure 1-26. Crops of predicted pebble images for pin widths of 10 (left), 5 (center), and 3 (right) pixels.**

Based on the density requirements, polypropylene was selected as one of the few lighter plastics that could be used to match the positive buoyancy of the unmodified polyethylene pebbles. Several different metals were considered and Table 1-1 shows a summary of the different pin dimensions required to match the density of unmodified pebbles and Figure 1-27 shows the predicted signal contrast ratio for each pebble design based on the different dimensions and x-ray attenuation coefficients. The signal contrast ratio is defined here as the ratio between the predicted detector signal through 30 cm of polyethylene plastic compared to the predicted detector signal through the plastic and the thickness of the metal pin. From these results, it is clear that a 0.13 mm diameter tungsten pin is the most desirable design specification to produce a high contrast ratio and narrow pin image. This is the result of tungsten's combined high density and high x-ray attenuation.

---

<sup>1</sup> U.C. Berkeley has performed a series of scaled experiments with positively buoyant pebbles based on the design parameters for the Pebble-Bed Fluoride Salt-Cooled High-Temperature Reactor (PB-FHR).

**Table 1-1. X-PREX pebble design options with different metals and pin diameters to match the density of unmodified polyethylene pebbles.**

	Unmodified	Prototype	PP-Al	PP-Fe	PP-Cu	PP-W
Pebble Material	Polyethylene	Polyethylene	Polypropylene	Polypropylene	Polypropylene	Polypropylene
Plastic Density [g/cm <sup>3</sup> ]	0.96	0.96	0.9	0.9	0.9	0.9
Pebble Diameter [cm]	1.257	1.257	1.257	1.257	1.257	1.257
Pin Material	-	SS316	Aluminum	SS304	Copper	Tungsten
Metal Density [g/cm <sup>3</sup> ]	-	7.99	2.7	7.99	8.96	19.25
Pin Diameter [cm]	-	0.146	0.041	0.021	0.02	0.013
Pebble Density [g/cm <sup>3</sup> ]	0.96	1.061	0.959	0.961	0.963	0.96
Image Width [Pixels]	-	10	8	5	5	3

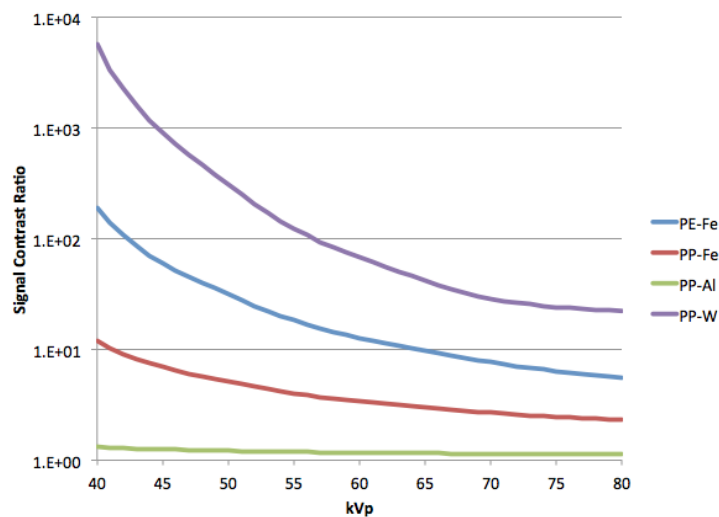


**Figure 1-27. Signal contrast ratio for several plastic and pin combinations. The contrast ratio is defined as the expected detector signal through plastic divided by the signal through plastic and metal. PE-Fe curve is for the prototype pebbles and other curves are for the pin diameters given in Table 1-1 to match the HDPE density. Plastic thickness used in calculations is 20 cm.**

Based on the pebble design specifications, U.C. Berkeley completed a competitive bidding process to procure a set of 20,000 instrumented pebbles through a custom insert injection molding process for use in the X-PREX facility. Figure 1-28 shows one of the resulting pebbles as received from the vendor, with a small length of tungsten wire protruding from the plastic. Tungsten is a very hard material and therefore it was difficult to cut the wire flush with the surface with normal tools. Therefore a machine tool grinding wheel (designed for tungsten-carbide tools) was procured and used to manually grind down the wire protrusions to produce a smooth surface on all the pebbles. Figure 1-29 shows an x-ray image of a small set of finished instrumented pebbles with the metal wire inserts clearly visible. Small defects in the pebbles are also visible and are a common result from the injection molding process. Figure 1-30 shows a sample set of 1,000 instrumented pebbles in a cylinder with a diameter of approximately 15 cm, which confirms the capability to resolve pin images in a thicker packed bed.



**Figure 1-28. Detail view of a single instrumented pebble. The small end of the tungsten wire can be seen at the upper right side of the pebble. The wire ends are finished with a grind wheel to ensure a smooth pebble surface.**

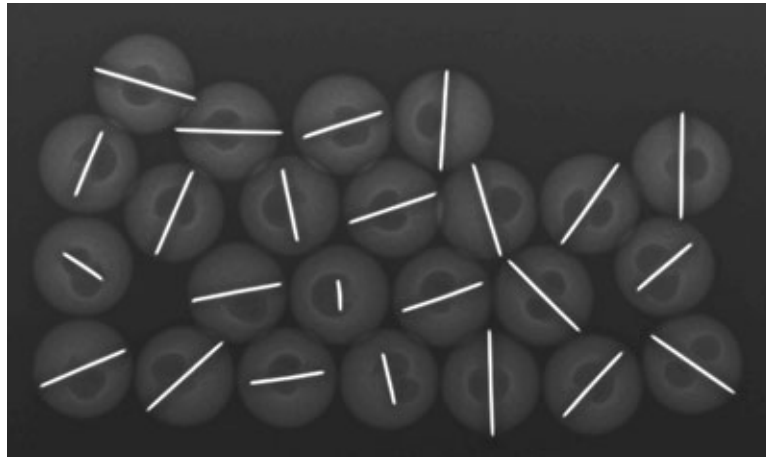


**Figure 1-29. X-ray image of sample 12.57 mm diameter pebbles with 0.13 mm tungsten wire insert.**

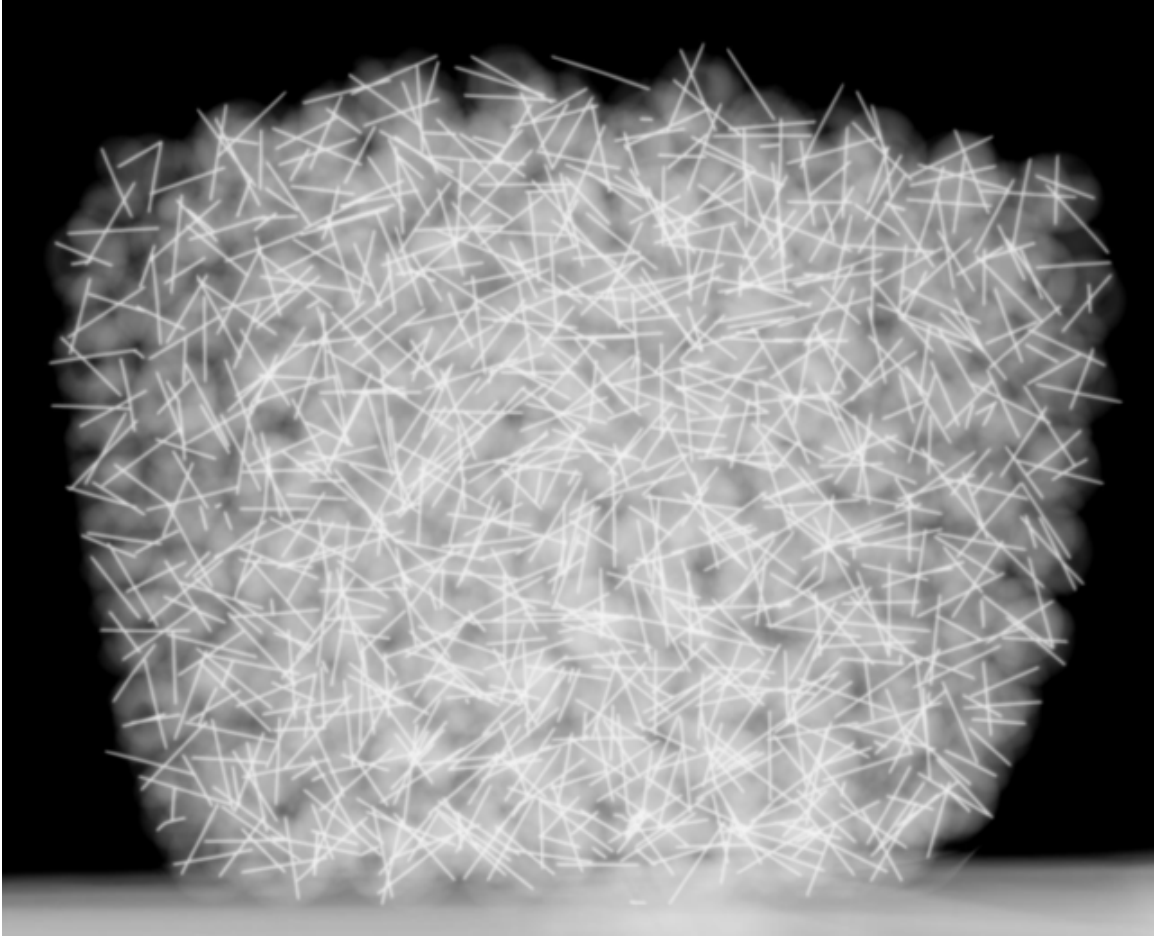


**Figure 1-30. X-ray image of 1,000 instrumented pebbles packed in a cylinder with diameter of about 15 cm and height of about 10 cm.**

### **1.3.2 Instrumented Pebble Physical Properties**

The following sections describe the measured physical properties for the 20,000 instrumented pebbles used in the X-PREX facility. These properties include the pebble diameter, mass, density, coefficient of restitution, and coefficient of friction. These parameters are important for DEM simulations that may be validated with results from the X-PREX facility.

#### **1.3.2.1 Pebble Diameter**

Pebble diameter measurements were performed using calibrated digital calipers with precision of 0.025 mm. A random sample of 100 pebbles was selected and measured along the pin axis and two perpendicular axes on the pebble equator. The average pebble diameter was found to be  $1.276 \pm 0.013$  cm (Note: Errors are based on the standard deviation of the measurement data set). Based on the average diameter measurement, the pebble volume is determined to be  $1.087 \pm 0.047$  cm<sup>3</sup>.

### 1.3.2.2 Pebble Mass and Density

Pebble mass measurements were performed with a calibrated balance with precision of 0.001g. For each measurement, the total mass of ten randomly selected pebbles was recorded. A total of 300 pebbles were sampled in 30 separate measurements. Based on this data, the instrumented pebble mass was found to be  $0.9173 \pm 0.0010$ g.

The resulting average density for the instrumented pebbles is  $0.844 \pm 0.026$  g/cm<sup>3</sup>. The measured density of the instrumented pebbles is approximately 6% lower than the nominal density of the polypropylene plastic, even with the additional mass of the tungsten wire insert. The discrepancy is the result of void defects present in the pebbles that form during manufacturing as the plastic is injected into the mold.

### 1.3.2.3 Coefficient of Restitution

The coefficient of restitution ( $C_R$ ) is an important parameter for DEM simulations to correctly model the damping of energy in the granular systems as pebbles move in contact with other pebbles and wall surfaces. The coefficient of restitution must be measured for each type of material interaction in the X-PREX facility. Tests were performed on four relevant plastic surfaces: polypropylene, cast acrylic, acetal resin, and polycarbonate. Additional measurements may be made if other materials (i.e. low friction plastics like Teflon) are used in future test sections in the X-PREX facility.

For each material, 20 drop tests were performed from an initial height  $h_1 = 57.5 \pm 0.1$ cm. A test tube clamp was used to release the pebble to minimize the initial velocity as the pebble falls. The coefficient of restitution was determined for each material using a clamped sheet with a thickness 1.3cm to minimize the energy absorbed due to vibrations of the sheet. Based on these drop tests, the coefficient of restitution may be simply evaluated from the kinematic relation:

$$C_R = \sqrt{\frac{h_2}{h_1}}$$

where  $h_2$  is the final height of the pebble after a single bounce. The drops were recorded using video at a frame rate of 60 frames per second that allows for the precise determination of the final height.

Table 1-2 gives the results of the drop tests with uncertainties are on the order of 2%. The coefficient of restitution for all plastic resins is observed to be on the order of 0.7 to 0.8, which implies that about half to two thirds of the kinetic energy in each pebble collision is lost. This supports the observation that granular materials are efficient in damping kinetic energy out of the system.

**Table 1-2. Bounce height and evaluated coefficients of restitution for instrumented pebbles on several plastic materials used in the X-PREX facility. The initial height for the drop tests was 57.5cm.**

Sheet Material	Bounce Height ( $h_2$ )	Coefficient of Restitution ( $C_R$ )
Polycarbonate (Pebble)	$35.1 \pm 0.8$	$0.781 \pm 0.014$
Cast Acrylic	$37.5 \pm 0.6$	$0.807 \pm 0.009$
Acetal Resin	$30.9 \pm 0.6$	$0.733 \pm 0.012$
Polycarbonate	$35.9 \pm 0.6$	$0.790 \pm 0.011$

#### 1.3.2.4 Coefficient of Friction

The coefficient of friction is also an important physical parameter in granular systems. The Coulomb (static) friction coefficient ( $\mu_c$ ) is used in DEM simulations as a physical upper bound on the friction forces applied to pebbles during interactions with other pebbles and wall surfaces. The static friction coefficient is also of crucial importance for granular materials to determine the angle of repose, which can lead to very different system behaviors in converging and diverging hopper geometries.

The Coulomb friction coefficient was evaluated for the instrumented pebbles and several plastic surfaces using a simple ramp test where the observed angle of the ramp at the initiation of motion gives the critical balance between the normal and tangent friction forces. A pebble cart (Figure 1-31) was fabricated to clamp four pebbles to ensure pure sliding motion and that no rotational motion could occur during the ramp tests.

Table 1-3 gives the result for the static friction coefficients from the ramp tests with polypropylene (pebble material), cast acrylic, acetal resin, and polycarbonate. Values are in the range of 0.3 to 0.4, which is common for dry materials. The static coefficient of friction for pebbles on the polypropylene sheet is 0.29, which implies an angle of repose of  $16^\circ$ .

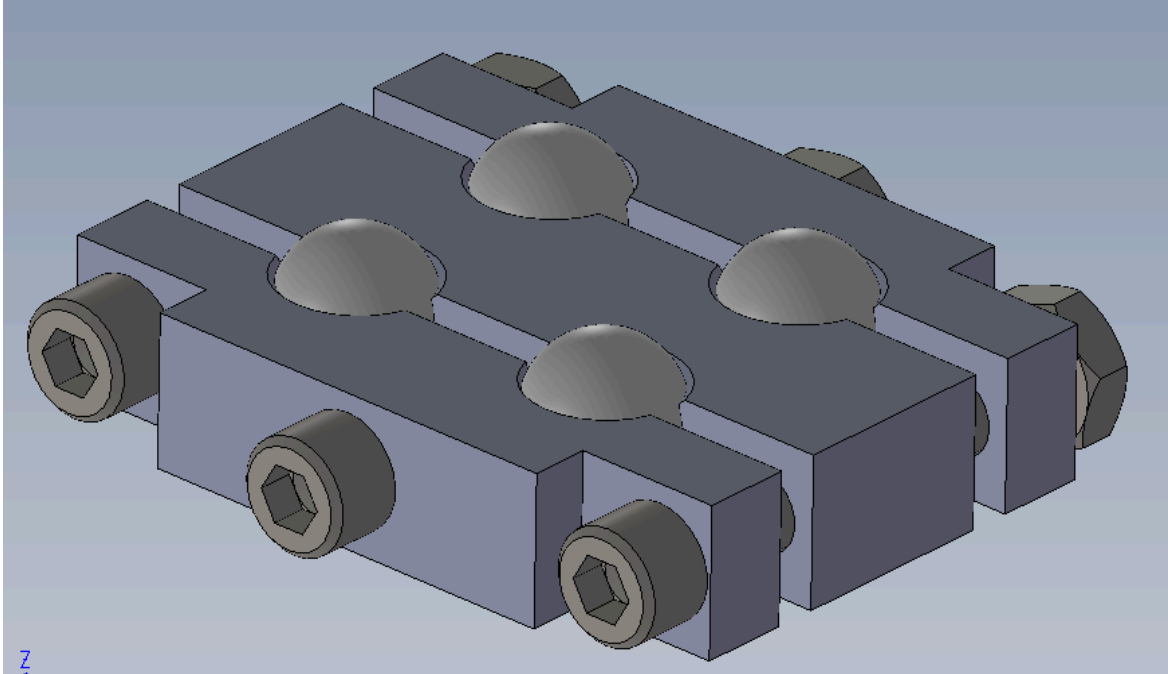


**Figure 1-31. Pebble cart used in static friction ramp tests to ensure pure sliding motion.**

**Table 1-3. Static friction coefficients derived from a ramp test for instrumented pebbles on several plastic materials used in the X-PREX facility.**

Sheet Material	Static Friction Coefficient ( $\mu_C$ )
Polypropylene (Pebble Material)	0.29
Cast Acrylic	0.39
Acetal Resin	0.29
Polycarbonate	0.41

## 1.4 Image Processing Methods

The development of novel image processing and computed tomography algorithms for the x-ray pebble recirculation experiment (X-PREX) facility is one of the most significant and challenging areas of work completed by U.C. Berkeley. The most difficult aspect of the X-PREX image processing methods involves extracting the position data for every pebble in a packed bed using a relatively small number of angular views. Figure 1-32 shows a sample of just five rotational views that can be used to reconstruct the pebble bed packing, which is far fewer than is commonly used in conventional CT scans that may use dozens or more x-ray images. This chapter describes the image processing methods developed for the X-PREX facility and the initial results from a verification test case.

Figure 1-33 shows the general structure of the image processing code modules for the X-PREX facility. From the initial set of x-ray images, three sequential modules are used to complete the reconstruction of the packed bed and track pebble motion for the step-wise motion of the system. In essence, each module adds one additional dimension to the pebble bed data. Module 1 scans all the x-ray images and produces a list of possible pin endpoints that represent a two-dimensional projection for each pin image from the x-ray tube focal point to the detector plan. Module 2 uses this two-dimensional data for a set of rotational views to reconstruct the three-dimensional packing configuration of the bed. Figure 1-34 shows a sample result from Module 2 for a simple test case of 20 pebbles arranged in an 'X' pattern and includes the equators for all pins based on the orientation of the tungsten wire insert. Finally, Module 3 is used to generate a mapping that tracks pebbles between motion steps. The resulting data on granular flow from the X-PREX facility is perhaps the highest fidelity data available to date and the only experimental data collected to date that includes the translation rotational motion for all particles in a packed bed.



**Figure 1-32. Sample x-ray images from the X-PREX facility from  $-45.0^\circ$  to  $+45.0^\circ$  in  $22.5^\circ$  increments.**

## X-PREX Image Processing Code Structure

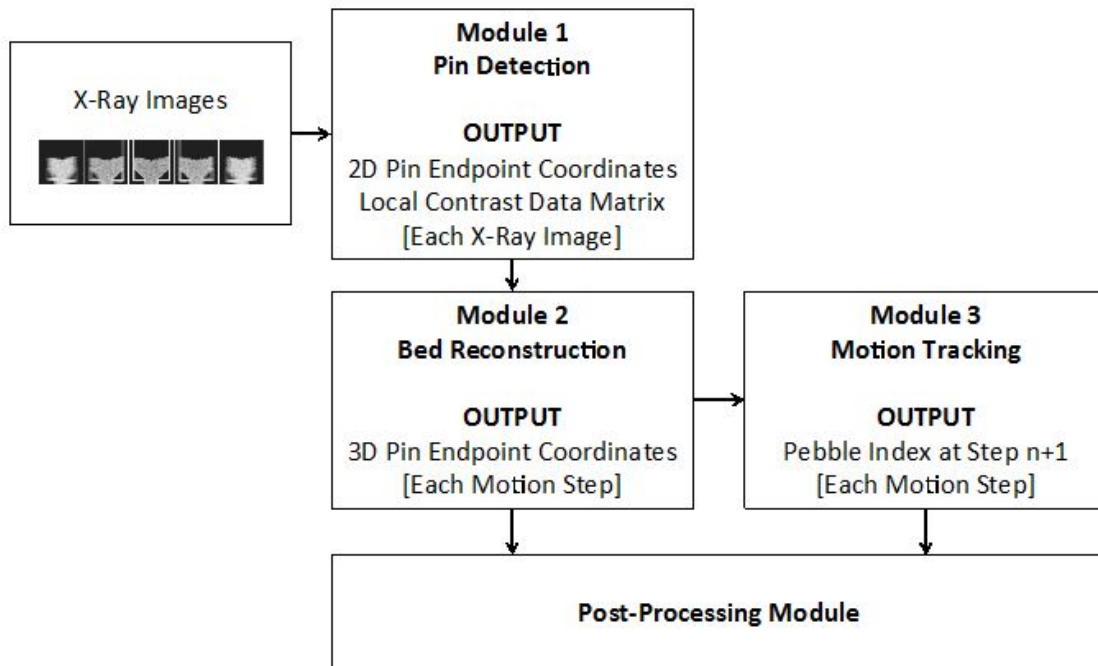


Figure 1-33. Block diagram of X-PREX image processing code structure and data flow.

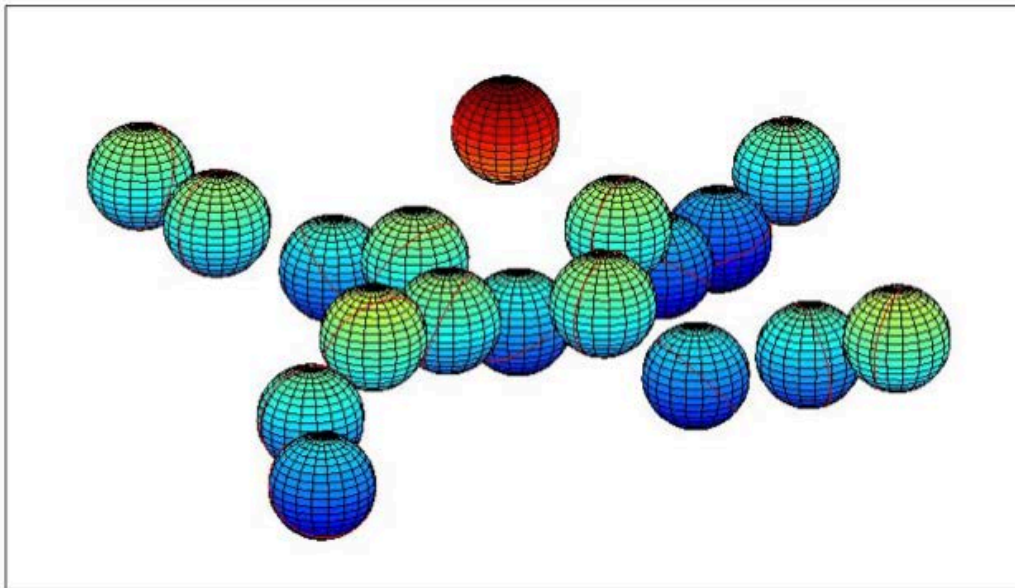
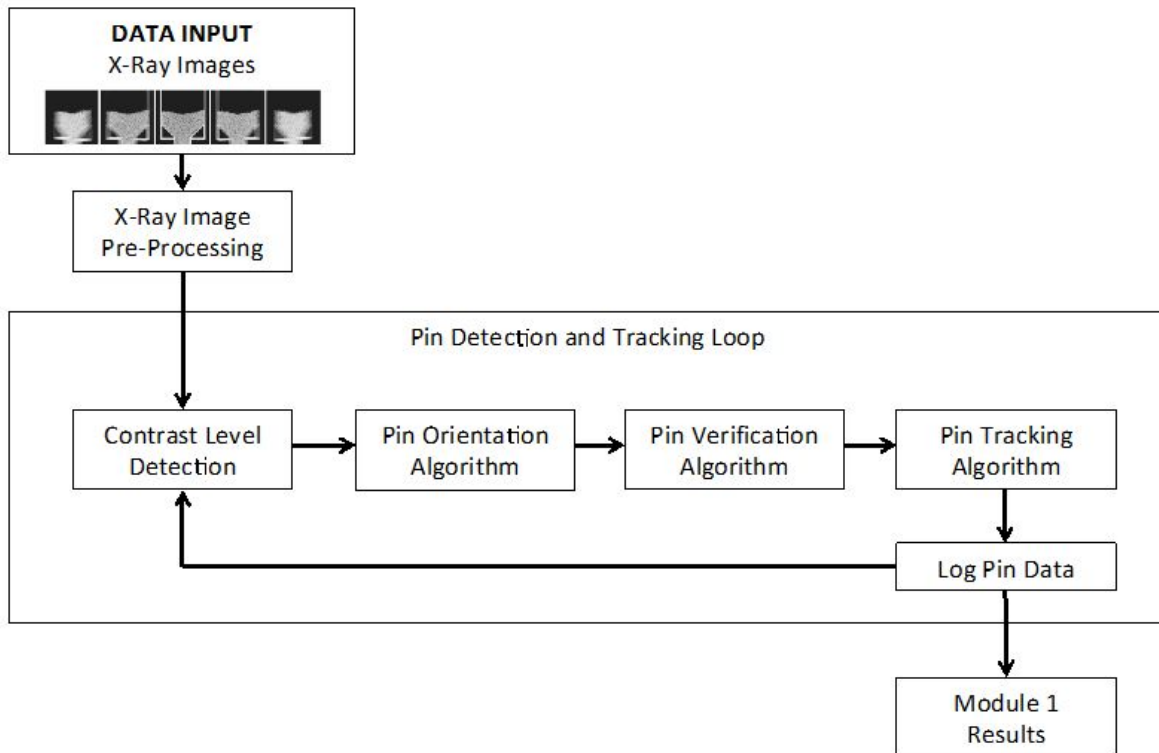


Figure 1-34. Sample results of the X-PREX image processing code for an arranged “X” pattern of pebbles with one pebble located above the “X” in the center. The thin red lines represent the equators of the pebbles based on the pin axis.

### 1.4.1 Module 1: Pin Image Detection

Module 1 of the X-PREX image processing software is a variation of a ridge detection algorithm that scans each x-ray image to generate a set of correlated two-dimensional pin endpoint positions. Figure 1-35 shows a schematic block diagram that includes the main algorithms and data pathways used to find the pin images. The methods used in each algorithm are described in the following sections.



**Figure 1-35. Block flow diagram for Module 1 image processing algorithms and data pathways.**

#### 1.4.1.1 X-Ray Image Pre-Processing

Before Module 1 scans an image to locate and track the pin images, a set of pre-processing routines is used to extract important data from the original luminosity data contained in the x-ray image file. The output of the pre-processing methods include local contrast data for each pixel in the image based on the cumulative difference in the luminosity level for that pixel and a set of surrounding pixels. The neighboring pixels used in the contrast calculation are located within minimum and maximum radii defined by the user. The pin images are approximately three pixels wide and a range of 2 to 4 pixels is effective in detecting the high attenuation of the x-rays through the tungsten wires. Figure 1-36 shows a crop of an x-ray image and the resulting contrast data that resolves the pebbles. The contrast data is very effective in thin regions, but the contrast decreases significantly in regions with many pin image intersections.

The Module 1 pre-processing method also generates an array of the local luminosity gradient data for each pixel location based on a central difference calculation.

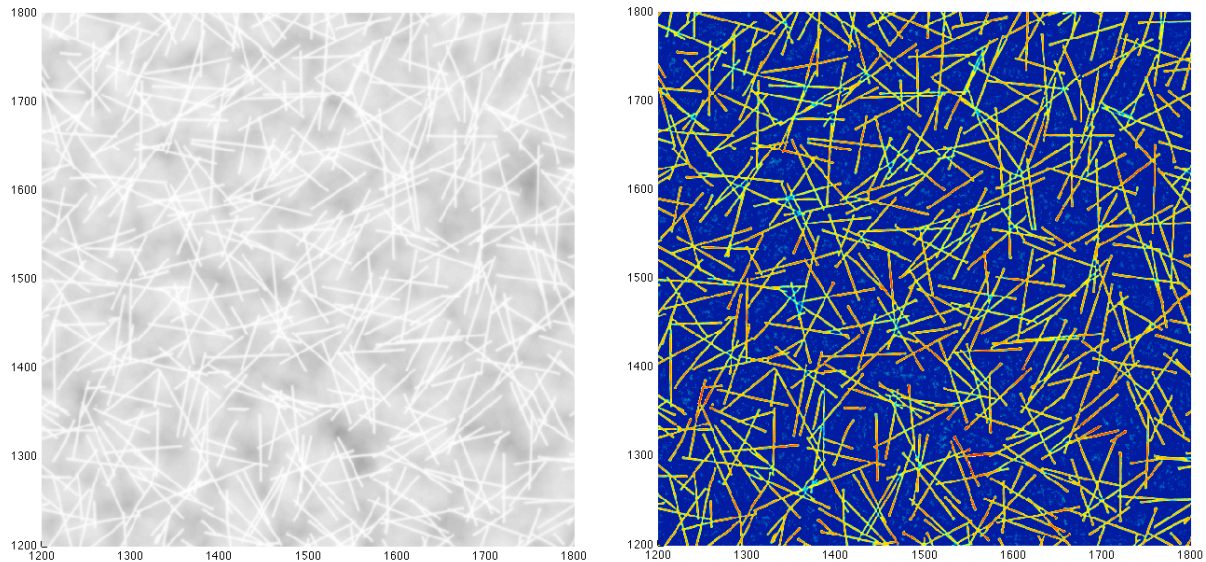


**Figure 1-36. Sample crop of original x-ray image (left) and contrast levels (right). Each image has dimensions of 600 x 600 pixels. The pin images are clearly established by the contrast data, though the contrast levels drop around pin intersections.**

#### *1.4.1.2 Contrast Level Detection Algorithm*

After the pre-processing methods are complete, the x-ray image is scanned from left to right sequentially for each row. The user defines a contrast limit threshold that is used to search for pin images and skip regions that are unlikely to contain any pins or have many pin intersections. When a pixel with a local contrast above the threshold is found, the local region above the pixel is scanned to find a neighbor pixel with the highest contrast level. If this pixel is a positive pin detection, this local maximum is likely to be within one pixel of the pin image and is subsequently used to determine the pin orientation.

#### *1.4.1.3 Pin Orientation Algorithm*

The pixel identified in the contrast level detection algorithm is used as the initial guess as the position of a pin image and the pin orientation algorithm is used to determine the direction of the pin axis that should be tracked to find the pin endpoints. To accomplish this orientation, the luminosity gradient values around the pixel at a fixed radius are interpolated with the ScanRing function. Figure 1-37 shows sample results from the ScanRing function for a pin endpoint and a middle section. The direction from the test pixel to the minimum gradient magnitude is a reasonable initial guess for the direction of the pin. The pin orientation is subsequently refined by using the average of the local gradient data normal to the pin image. Sub-pixel accuracy for the pin is also achieved by using a parabolic curve fit for the luminosity data normal to the pin direction near the test pixel. Figure 1-38 shows a quiver plot of the gradient data for a short pin and the resulting direction and start coordinates based on the refinement methods.

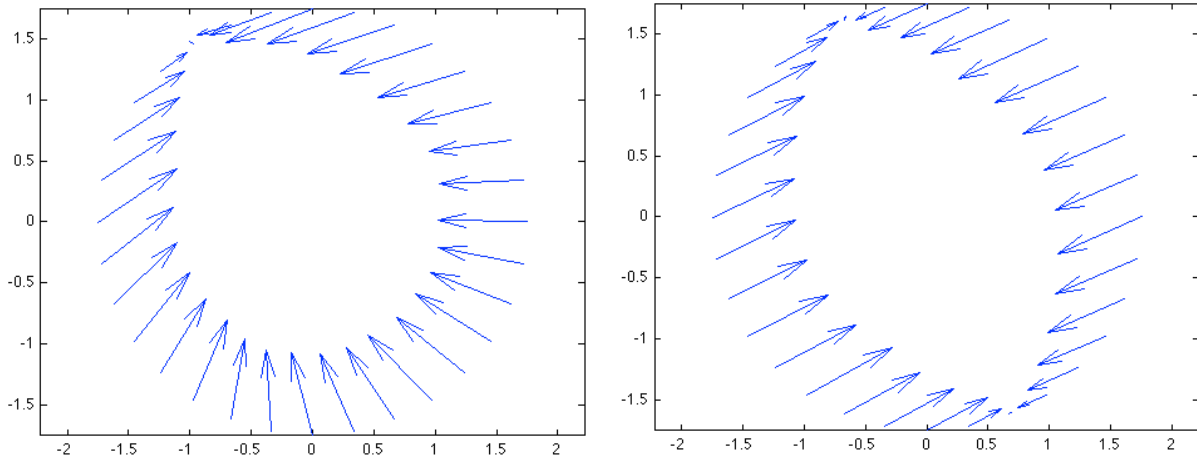


**Figure 1-37. Sample results of the ScanRing function for a pin endpoint (left) and middle section (right). The length of the arrows is proportional to the magnitude of the gradient. The direction of the minimum gradient magnitude is used as the initial guess for the pin direction.**

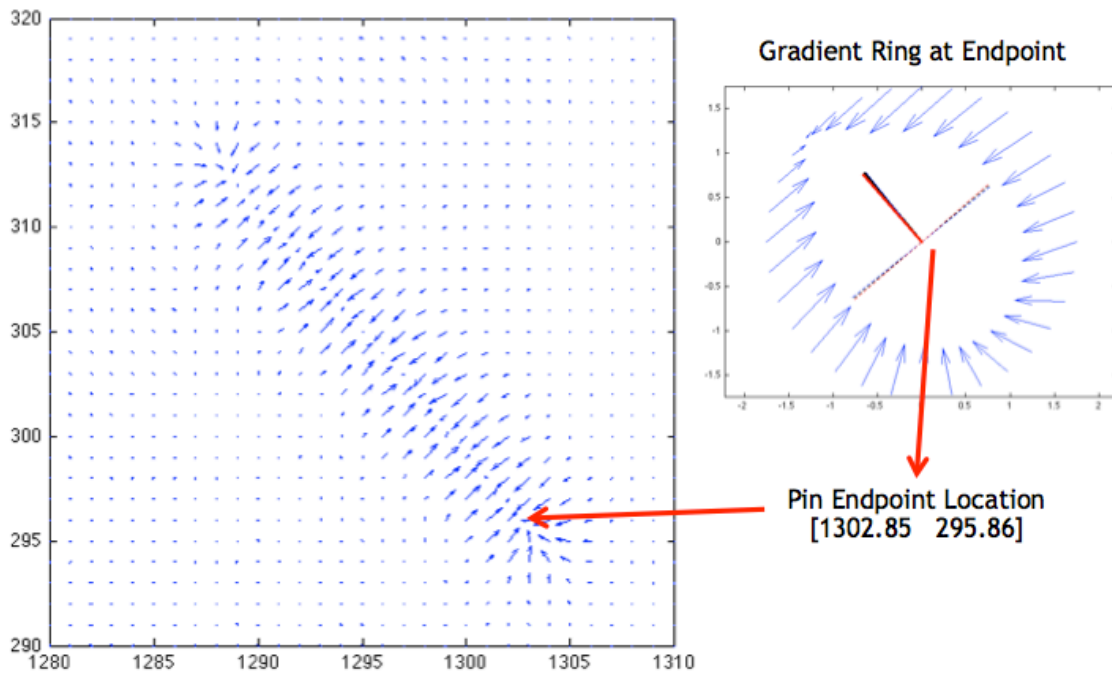


**Figure 1-38. Quiver plot of the local luminosity gradient vectors around a pin image and the local gradient ring located at one endpoint. The lengths of the arrows are proportional to the magnitude of the local gradient. Axis units are in pixels. Note that this pin image is relatively short compared to typical pin images due to the angle of view. The location of the pin endpoint is accurately determined with sub-pixel resolution.**

#### *1.4.1.4 Pin Verification Algorithm*

The pin verification algorithm confirms the detection of a pin image. This method steps along the pin axis using the initial position and direction from the pin orientation algorithm in increments of one pixel. At each new location, the direction of the pin image is determined based on the luminosity gradient normal to the pin direction and the position on the ridge is updated using a parabolic curve fit on the luminosity data, similar to that used in the pin orientation algorithm. The offset of the new ridge luminosity peak and alignment of the normal gradient data can be used to determine if the new position is aligned with the direction from the previous point. The tolerances in the pin verification method are set to be quite stringent so that high confidence is established that a single pin has been detected. This method is applied to a small number of steps, typically about 5, before the pin detection is confirmed.

#### *1.4.1.5 Pin Tracking Algorithm*

The pin-tracking algorithm uses the same methods as the pin verification algorithm, but with looser thresholds for tracking the pin image. This allows for more flexible tracking of pin images that may be slightly bent and to maintain tracking through intersections where the normal gradient data does not inform the pin orientation. From the initial length of pin detected in the verification method, the pin-tracking algorithm scans in both directions to find the pin endpoints. The pin endpoints are found when the luminosity data for the pin image falls below a set threshold level relative to the average value. Figure 1-39 shows the successful tracking of several pin images using this method, including a very short pin, several bent pins, and several pins with numerous intersections.

Due to the extremely large number of possible pin images and intersections, it is impossible to eliminate all errors from the pin-tracking algorithm. Figure 1-40 shows two particularly challenging pin configurations that are not practical to eliminate and must be corrected in Module 2 processing. In fact, there are often direct tradeoffs where the ability to track one type of pin image will make certain types of errors more frequent. For example, Figure 1-40(A) shows two pins in close alignment and the tracking that begins on one pin continues to the next before the tracking stops as the offset increases along the length. This error is inherent to Module 1 given the requirement to be able to track bent pin images described earlier. The elimination of this error by lowering the allowable offset would increase the number of errors in the tracking of non-straight pins.

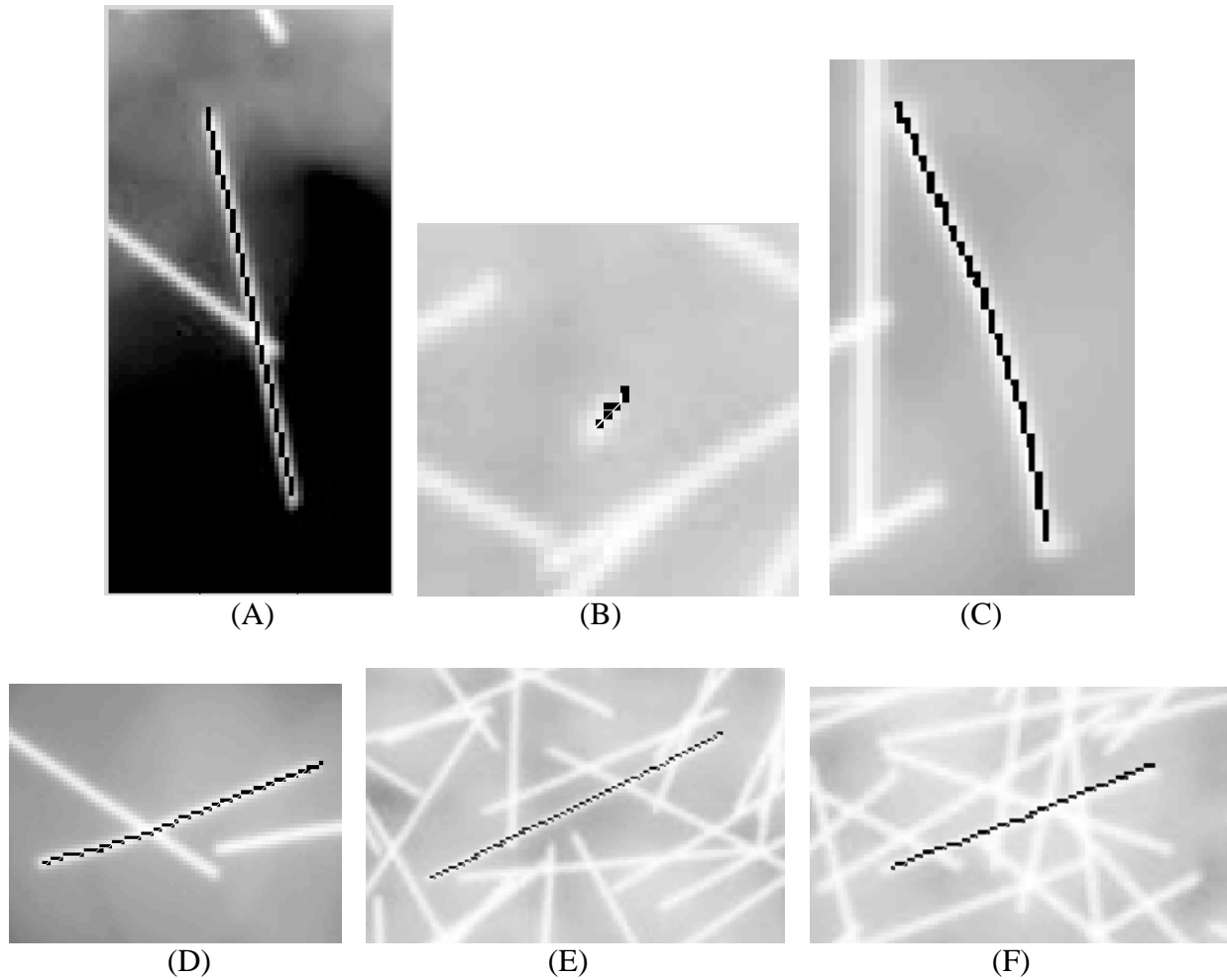


**Figure 1-39. Pin images that are successfully detected by Image Processing Module 1, including (A) a single pin with intersections, (B) a very short pin, (C)-(D) bent pins, and (E)-(F) long pins with many intersections.**

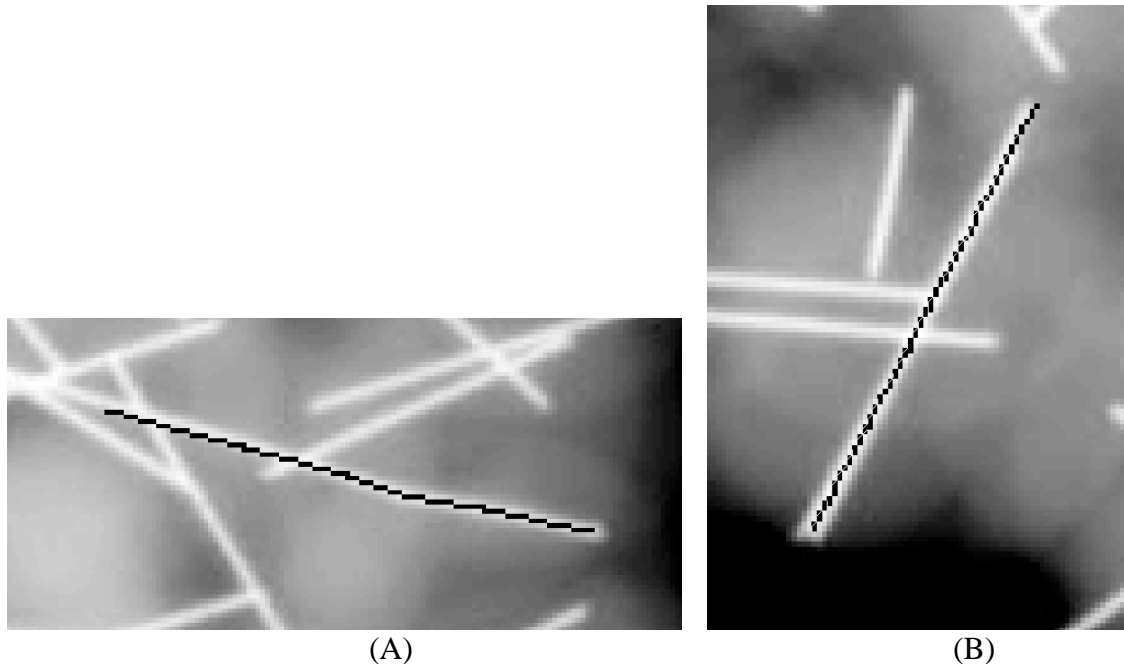


**Figure 1-40. Challenging pin configurations for Image Processing Module 1 including (A) intersecting pins with close alignment and (B) two nearly perfectly overlapping pins. These represent false negatives and false positives that must be corrected in Module 2.**

#### *1.4.1.6 Sample Results*

As described in the previous section, Module 1 includes a number of inherent tradeoffs in how the threshold values for pebble detection and tracking are set. In testing different threshold levels, it was generally found to be most valuable to set very tight threshold levels for pin verification, which ensures higher confidence that only true pins are detected, and relatively loose thresholds in the pin tracking, which helps to ensure that pins are tracked all the way to their endpoints. Figure 1-41 shows sample results from the two algorithms for the same region shown previously in Figure 1-36. The short green line segments are those detected in the pin verification algorithm and the red and blue segments that extend from both ends are the results of the pin-tracking algorithm in both directions. Figure 1-42 shows the original x-ray image with marked pin endpoints based on the results of Module 1 for the same region.

The results for Module 1 presented here are typical of those produced for a variety of packed bed geometries in that a large number of false positive pins (~10%) are recorded. These are most often associated with a pin segment that is found, but the tracking does not go all the way to one of the endpoints. This error is sometimes corrected when the undetected region of the pin is found and subsequently tracked back to the correct endpoint. This creates a kind of double pin image that must be eliminated through correlating the pin image with the rotation data in Module 2.

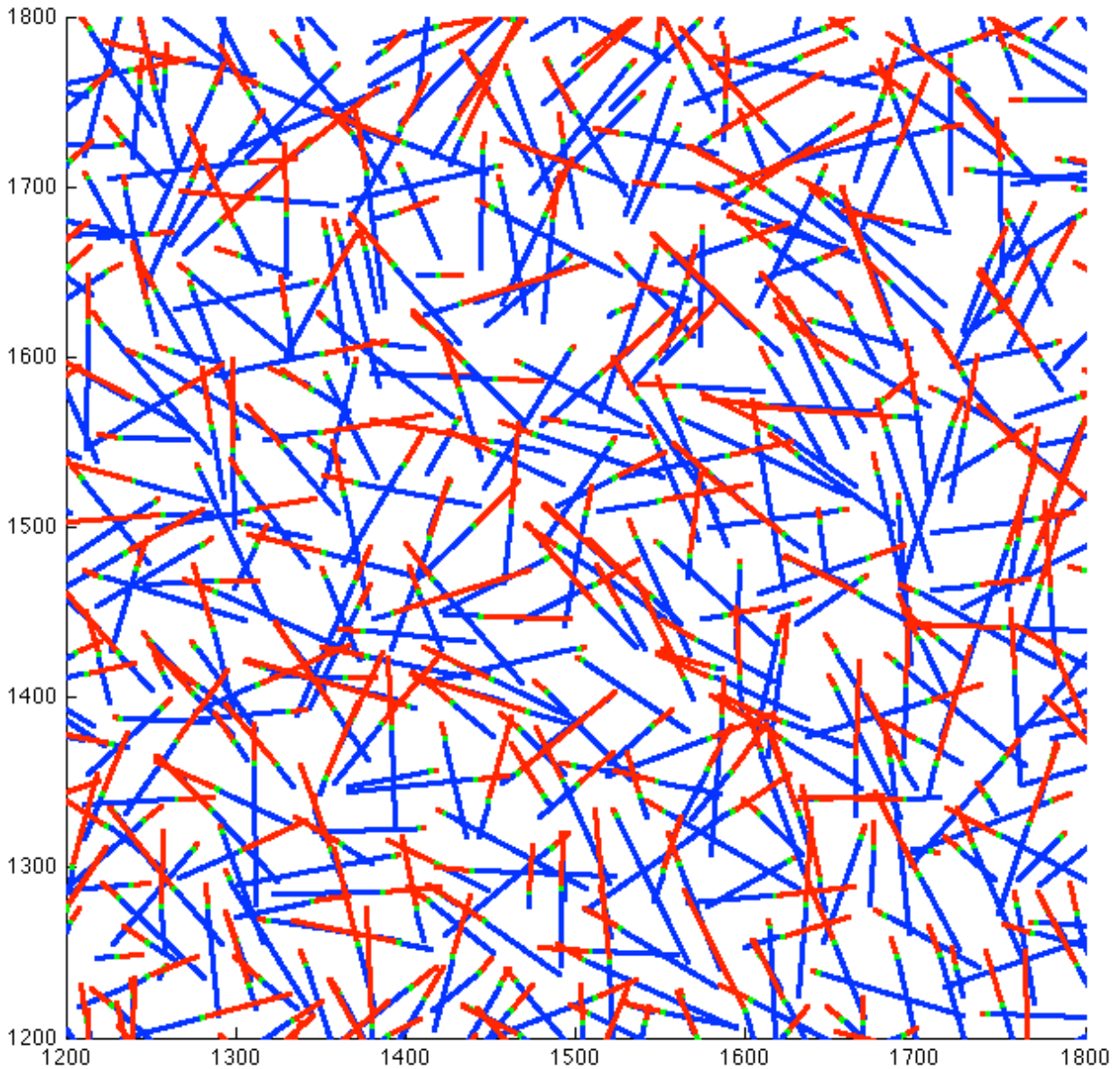


**Figure 1-41. Sample results for the pin tracking algorithm. The short green sections are the initial region of pin detection that meet the tight requirements of the pin verification algorithm. The red and blue sections extending from both sides are the resulting pin image from tracking in both directions.**

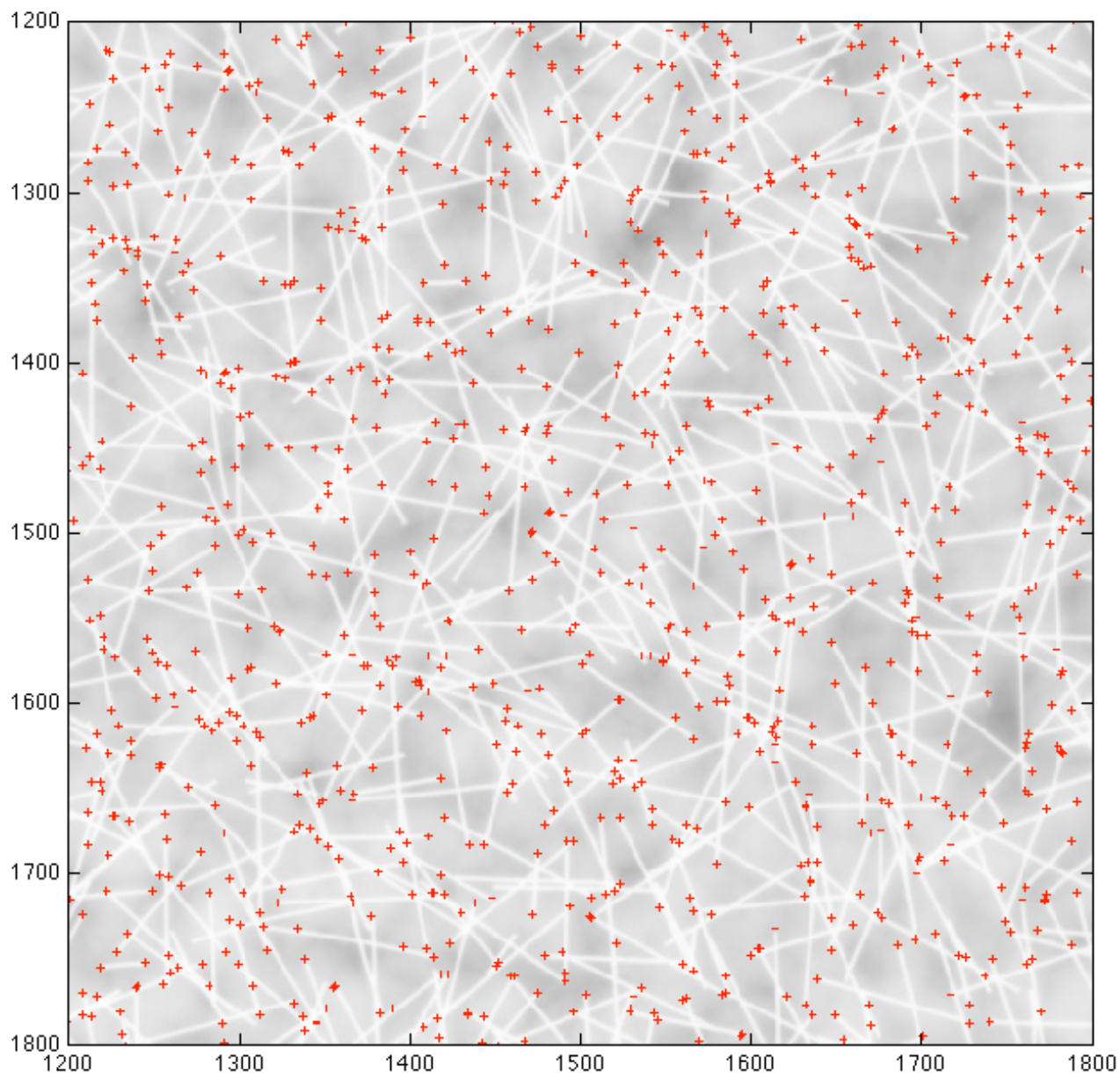


**Figure 1-42. Sample results from Module 1. The red '+' marks indicate the location of the detected pin endpoints. Approximately 10% more pin images are detected than are present in the image, which represent a significant number of false positives.**

### 1.4.2 Module 2: Packed Bed Reconstruction

Module 2 of the XPRES computer tomography suite uses the 2D results from Module 1 to reconstruct the 3D packed pebble bed. Module 2 uses a 3D reconstruction algorithm to find the 3D locations of pebbles using the endpoints of the tungsten wires, or “pins”, in x-ray images at several angles. The following sections describe this process.

The block diagram in Figure 1-43 shows the hierarchy of functions in Module 2 that are used to reconstruct a 3D pebble bed. Figure 1-44 shows the results from each phase. The following sections describe how each individual function performs its task.

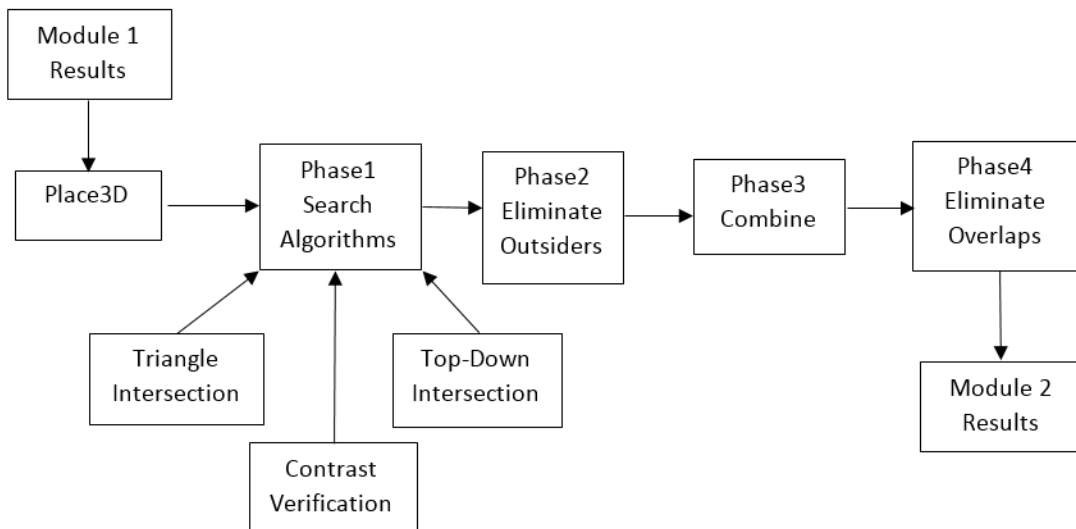


**Figure 1-43. Block diagram showing the Module 2 functions and data pathways.**

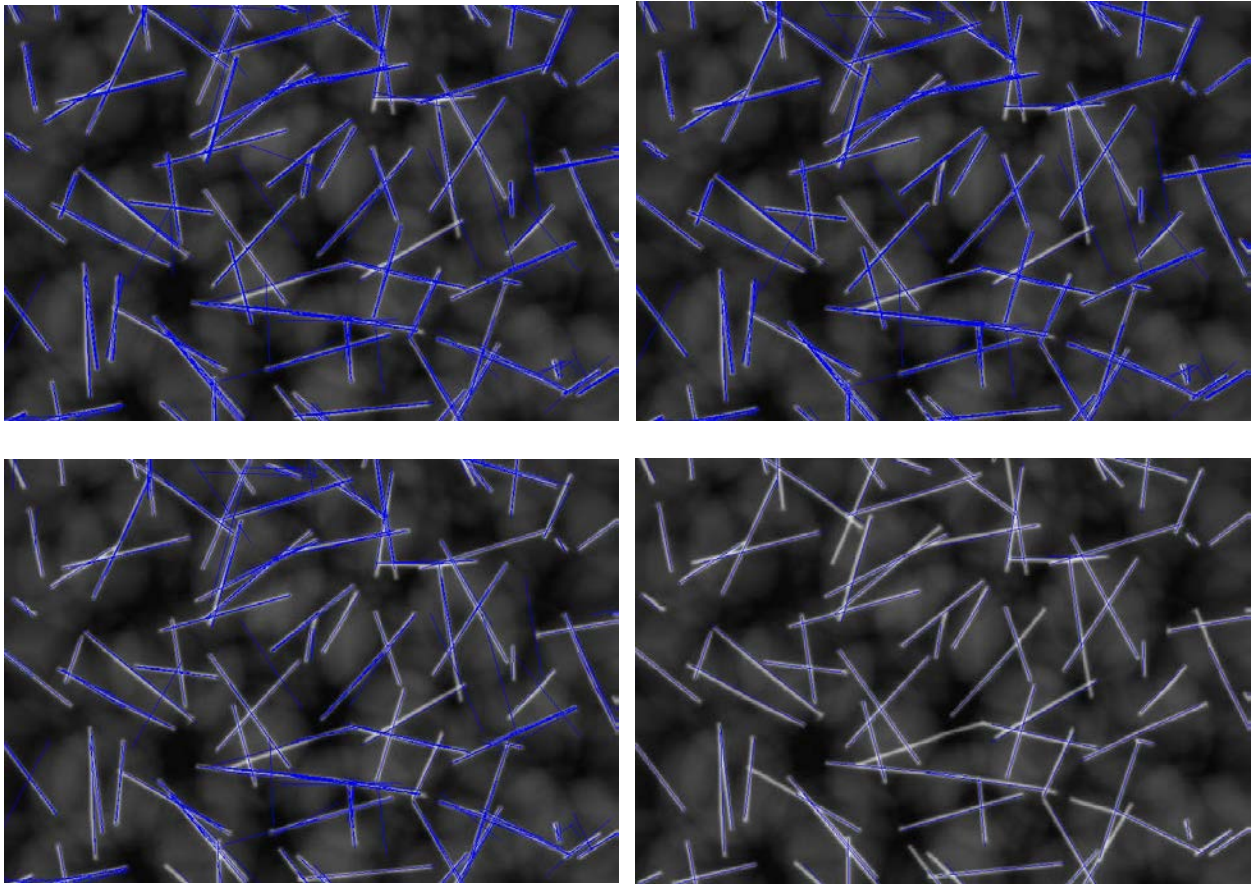


**Figure 1-44. Results from the four Module 2 phases. 3D solutions are projected as blue lines onto the original x-ray images. Top left: phase 1 output. Top right: phase 2 output. Bottom left: phase 3 output. Bottom right: phase 4 output (final results).**

#### *1.4.2.1 Place3D Function*

The Place3D function takes the 2-dimensional endpoint data from module 1 and places it in a 3-dimensional space. This function also adds the location of the x-ray point source for every image angle. The Module 1 results placed in 3-dimensional space by the Place3D function can be seen in Figure 1-45.

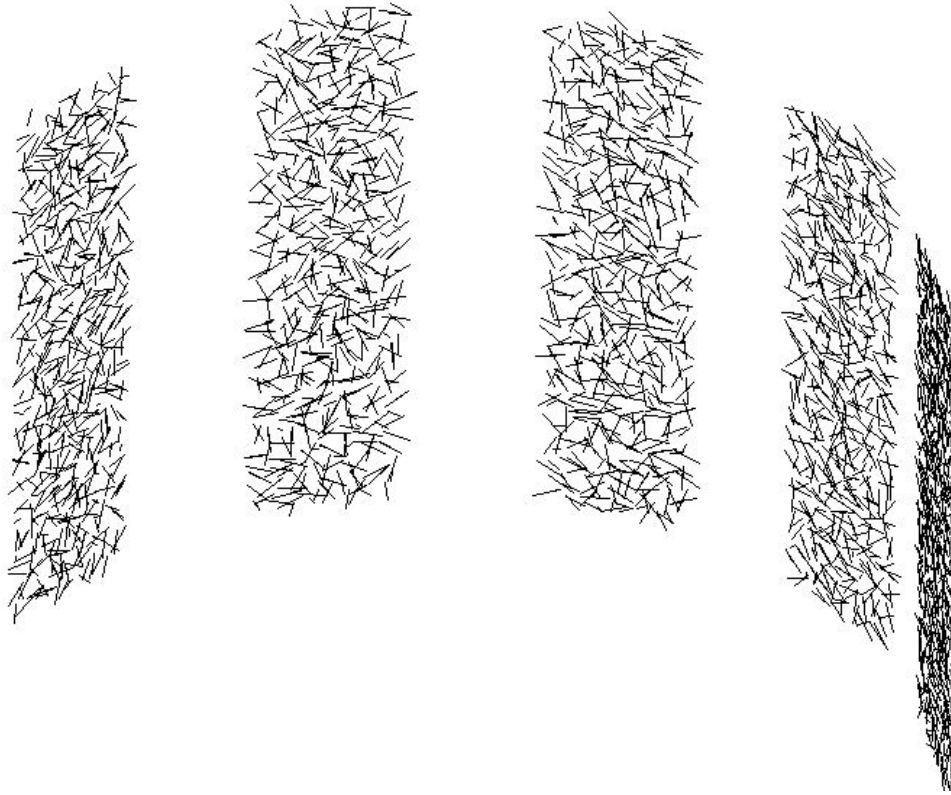


**Figure 1-45. Place3D results for five different images (0, 22.5, 45, 67.5 and 90 degrees).**

The black lines in Figure 1-45 represent the pebbles' tungsten wires that are seen in the x-ray images, and that are detected by Module 1. Five sets of black lines can clearly be seen in Figure 1-45 in five distinct 2-dimensional planes. Each 2-dimensional plane represents the detector plane at the given rotational angle.

#### *1.4.2.2 Phase 1 Search Algorithm*

Phase 1 is an iterative search algorithm that finds all possible 3-dimensional solutions for the 3D pebble bed reconstruction. A 3D solution is the possible translational and rotational constraints of an actual pebble in the physical 3D pebble bed. The search algorithm finds all possible 3D solutions that could result from a pair of x-ray images. The search algorithm is run for all possible pairs of images. Phase 1 is based on three main functions, described in sections 0 through 0.

#### **Triangle Intersection Function**

The intersection algorithms use vector calculus to assess whether a pair of endpoints from different angles in Figure 1-45 result from the same physical pebble in the actual pebble bed. The triangle intersection function does this by projecting triangles from the endpoints in each image to their respective x-ray source point, and examining the triangle intersection. A plot of this can be seen in Figure 1-46.

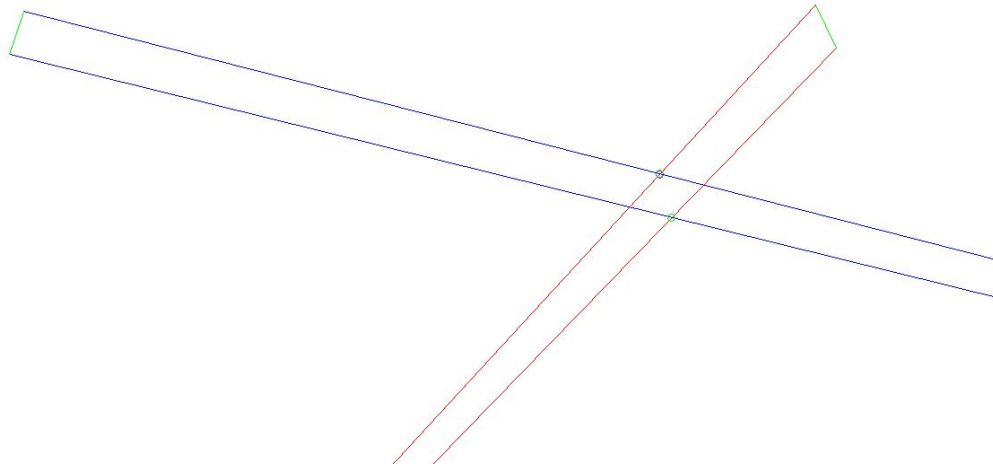


**Figure 1-46. Plot of the triangle intersection function.**

In Figure 1-46, the pebbles' tungsten wire can be seen as green lines in two x-ray image planes. The blue and magenta lines represent the triangles, with the third point (the x-ray source point) out of view. The intersection of the triangles can be seen marked with green circles.

If the green lines in Figure 1-46 (the two 2D endpoints from two images) belong to the same physical pebble, the two triangles should intersect perfectly in a line with a length equal to the diameter of a pebble. In practice, experimental error requires a small threshold to determine if the two triangles are close enough to count as an intersection. This intersection yields the translational and rotational data of an actual pebble in the pebble bed.

### **Top-Down Intersection Function**

The triangle intersection function works well for the majority of pebbles. Unfortunately, the error in the triangle intersection function increases dramatically as the tungsten wire in a pebble approaches a horizontal orientation. To remedy these select cases, a top-down intersection function is used.

The top-down intersection function projects the triangles seen in Figure 1-46 onto the horizontal plane. The function first finds the intersections in the horizontal plane, then locates the corresponding intersections in 3-dimensions. The 3-dimensional intersections are determined to be a pebble based on their spatial similarity and their length compared to a pebble diameter.

### **Contrast Verification**

The possible solutions found by the intersection functions are verified to be actual pebbles using the contrast verification function. Every possible 3D solution found in phase 1 is projected back onto the 2D x-ray images. The average contrast along the projected line is found using contrast data from Module 1. If the contrast is above a certain threshold in enough of the images, the solution is accepted.

#### 1.4.2.3 Phase 2 Eliminate Outsiders Algorithm

In this phase, possible solutions that are clearly outside of the testing volume are eliminated. The algorithm functions on the principle that any solution sufficiently far from the Module 1 results is probably a false positive and should be eliminated.

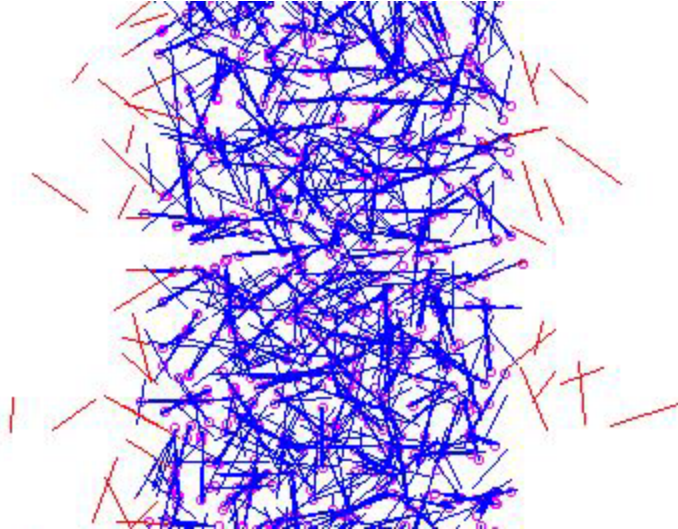


**Figure 1-47. Plot of Phase 2 outsiders elimination algorithm.**

In Figure 1-47, Module 1 results are plotted as circles, and possible Module 2 results are plotted as lines. The blue lines lie in the same range as the Module 1 results. The red lines lie outside of the Module 1 range, and are therefore eliminated.

#### 1.4.2.4 Phase 3 Combination Algorithm

Because any given solution is found from a pair of images, the solution set found from all five images contains many repeats. The Phase 3 Combination Algorithm iterates through all of the possible solutions, and combines those that are the same. Solutions that are sufficiently close together and oriented in the same direction are averaged and output as a probable pin. This algorithm is very computationally expensive and is sometimes circumvented for the purpose of speed.

#### 1.4.2.5 Phase 4 Eliminate Overlaps Algorithm

The final phase eliminates additional false positives by using the physical constraint of overlap. In the actual system, the pebbles do not overlap at all due to their hard surfaces. In the 3D solution, there will almost certainly be a small overlap between pebbles due to the uncertainty and error inherent in the system. If two pebbles overlap more than a set percentage, they are reassessed. The overlapping pebble that results in the higher contrast in the x-ray images is the more likely of the two, so the other pebble is eliminated.

### 1.4.3 Module 3: Pebble Motion Tracking

Module 3 of the X-PREX image processing software takes the packed bed data from Module 2 and tracks pebble motion between each time step. The methods used here have been adapted from algorithms used previously at U.C. Berkeley to track pebble motion at a transparent visible surface and are similar in concept to particle image velocimetry methods, but also allows pebbles to be tracked over relatively longer distances. Figure 1-48 shows a simplified block flow diagram for Module 3 that includes the key algorithms and data pathways. The follow sections describe the methods used in each of these algorithms.

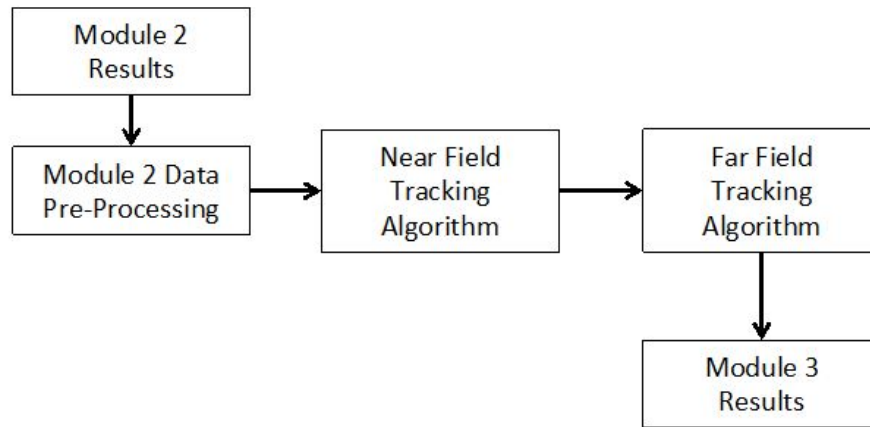


**Figure 1-48. Block flow diagram for Module 3 image processing algorithms and data pathways.**

#### 1.4.3.1 Near Field Tracking Algorithm

The purpose of the near field tracking algorithm is to track the motion of pebbles that move a small distance between each motion step. This may apply to all pebbles in the packed bed for experiments with very small motion steps, but is most likely to apply to granular plug flow (i.e. near uniform downward motion) in constant area regions of a test section. For these cases, the user defines the upper and lower elevation of the near field flow region based on the known system geometry.

With the defined region of interest, the near field tracking algorithm will map pebbles in time step  $n$  to the nearest pebble located in the direction of motion in time step  $n+1$ . However, not all pebbles in time step  $n$  are required to be mapped to pebble positions in time step  $n+1$ . The user may define a maximum horizontal displacement for tracked pebbles, which is appropriate in plug flow where pebbles will move predominantly in the vertical direction. Values on the order of 0.5 pebble diameters are appropriate to use for this purpose.

### 1.4.3.2 Far Field Tracking Algorithm

The far field tracking algorithm is used to track pebble motion in regions with larger displacements or with larger and unpredictable horizontal velocity components. This method is based on the observation in granular flows that local pebble packing configurations are relatively stable and therefore local motion is often highly correlated for small regions. Based on the tracking data from the near field algorithm, predicted positions are generated for the pebbles sequentially extending above and below the plug flow region. The nearest neighbor in time step  $n+1$  to the predicted position is assigned to the pebble and used to generate the predicted position for the next neighboring pebbles evaluated. Similar to the near field algorithm, not all pebbles must be mapped and a tracking will be cancelled if a subsequent pebble in time step  $n$  is better tracked to the same pebble in time step  $n+1$ . Figure 1-49 shows a sample result of this algorithm for downward pebble motion at the bottom of a converging region.

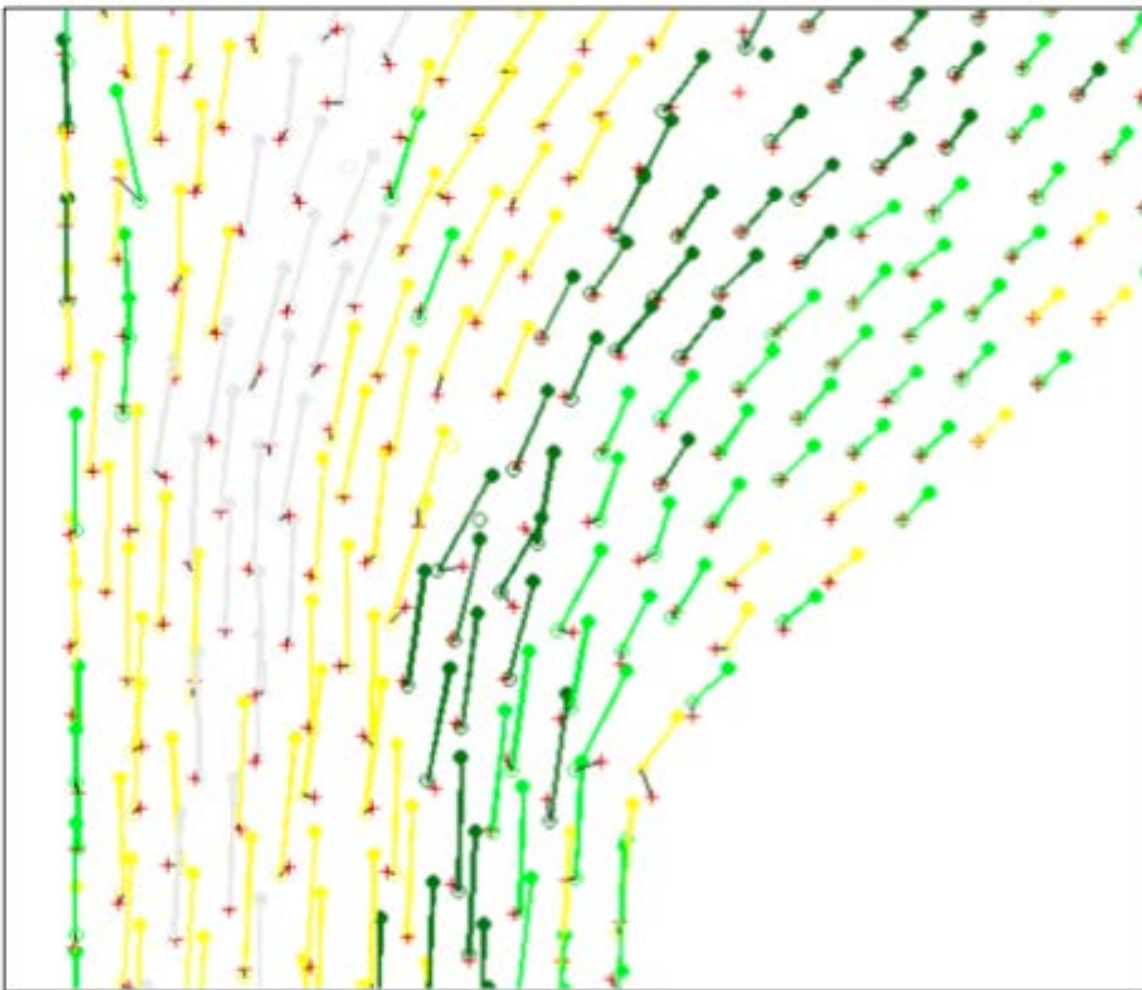


**Figure 1-49. Sample result from image processing Module 3 that tracks pebble motion between time steps. In this example, the pebbles are moving down and the thick lines show the pebble displacement between the two time steps. The red “+” indicates the predicted position.**

#### 1.4.4 Code Verification

The complete functionality of the X-PREX image processing modules was tested using a relatively simple test case from the modular test bay: the motion of pebbles in a small tube as a result of pebble circulation from the continuous discharge device. Figure 1-50 shows the test setup used for this verification test with a total of 470 instrumented pebbles in the upper cylindrical region of inner diameter 5.5 pebble diameters  $d$ . This test case is also useful as the boundary condition for future tests with the cylindrical silo test section. A total of 17 motion steps were recorded with an average of 17.6 pebbles discharged per step. Figure 1-51 shows the front and side view x-ray images for the initial packing configuration.



**Figure 1-50. Continuous discharge device set up for testing and verification of the X-PREX image processing modules. The upper section within the x-ray imaging area contains 470 pebbles.**

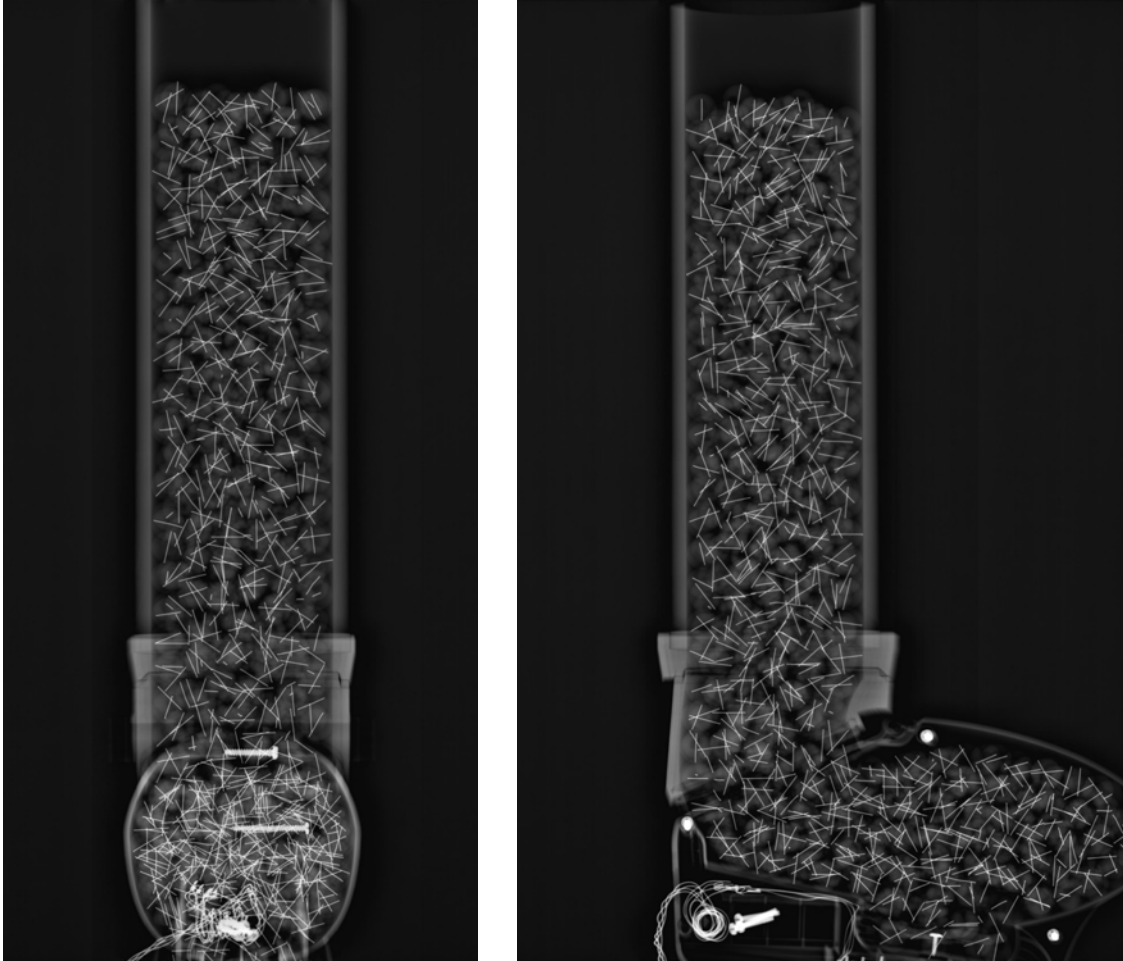


**Figure 1-51. Front (left) and side (right) x-ray images of the discharge hopper.**

The results from Module 1 included the detection of 697 pin images. This represents approximately a 50% false positive rate, which is higher than that observed during the previous code development effort. Figure 1-52 shows the resulting pin endpoints over the original x-ray image in the upper tube region. Closer inspection of the pin endpoints showed that the relatively thin bed depth resulted in slightly wider regions of high contrast and therefore the same pins were picked up several times. This is consistent with the relatively small number of false positives that are observed visually.

Module 2 subsequently found a total of 430 pebbles in the packed bed reconstruction algorithm. Figure 1-53 shows the reconstructed packed bed, which matches the geometry of the cylindrical tube. These results indicate a pebble detection rate above 90%. The resulting packing fraction from the reconstructed bed is 53%, which is noticeably lower than the measured packing fraction of 58% in the cylindrical column. Figure 1-54 shows a top view of the pebble positions in the initial test configuration. From this result, the ordered packing is clearly visible throughout the entire test section, where the central axis is less than three pebble diameters from the wall. This is the first experimental data known to the authors that shows this kind of detailed packing information for a granular material.

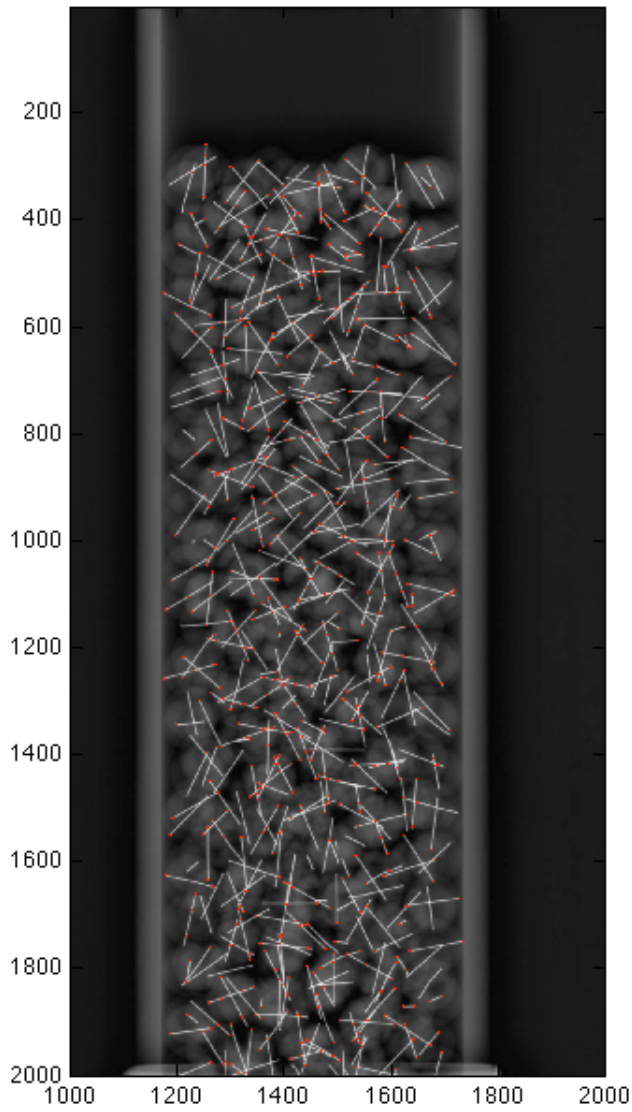


**Figure 1-52. Module 1 results for discharge hopper test. The detected pin endpoints are marker in red. Module 1 detected 697 pin images in this time step with approximately 50% false positives.**

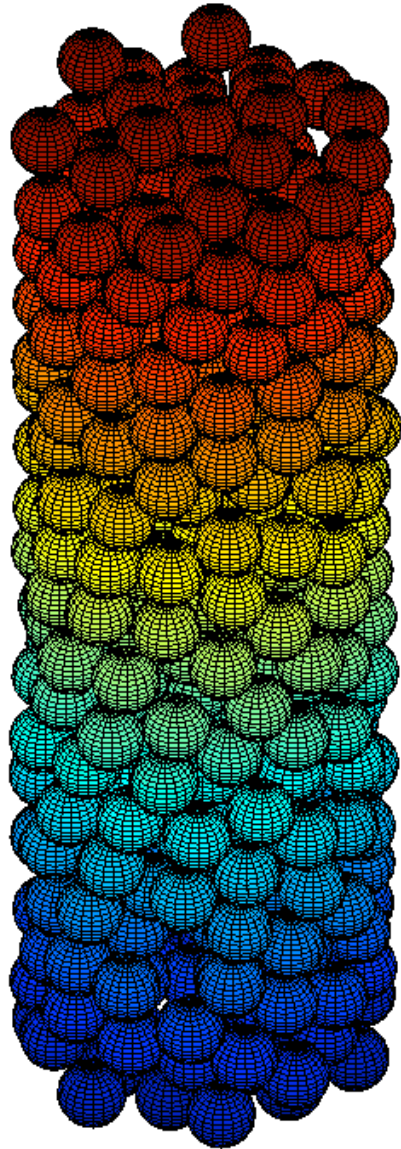


**Figure 1-53. Packed bed from Module 2 results for the initial configuration of the hopper discharge test. 430 of 470 pebbles were located, indicating a detection rate above 90%.**

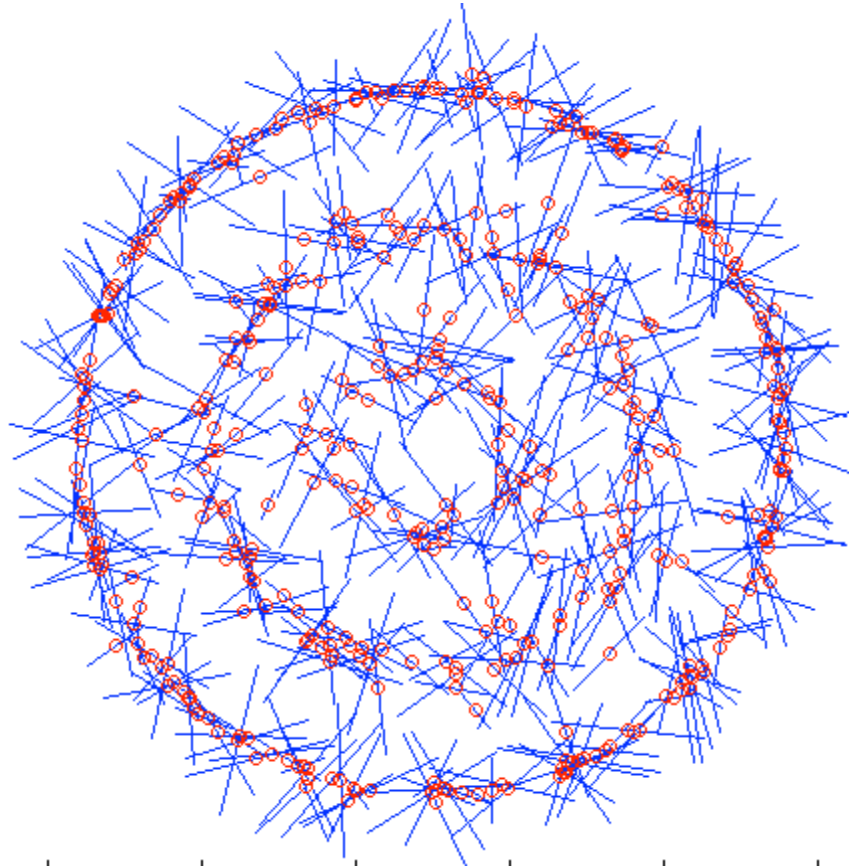


**Figure 1-54. Top view of pebble center positions (red circles) and orientations (blue lines) from the Module 2 results for the initial configuration of the hopper discharge test. Ordered packing is clearly visible throughout the narrow cylindrical channel with an inner diameter of 5.5 pebble diameters.**

Module 3 was successful in tracking the near-vertical displacement of pebbles from the hopper discharge test for a variety of motion steps up to about 1.2 pebble diameters. Figure 1-55 shows the side view of the cylinder with the vertical displacements marked for the first motion step. In each motion step, approximately 90% of the pebbles were tracked. This is consistent with the assumption that Module 2 will find a similar number of pebbles in each motion step and that the false negatives will be randomly distributed. It is therefore reasonable to assume that Module 3 tracked nearly all of the possible pebble displacements for which there was sufficient data.

Figure 1-56 shows the average vertical and horizontal displacement for pebbles in each motion step compared to the number of discharged pebbles. As expected for a plug flow region, the vertical displacement is approximately linear with the number of discharged pebbles and the horizontal displacements are small ( $\sim 0.1$  pebble diameters). Finally, based on the measured packing fraction of 58% in the cylindrical column, the predicted and measured vertical displacements for each motion step is compared in Figure 1-57. This result shows that the best-fit line is within 3% of the predicted values.

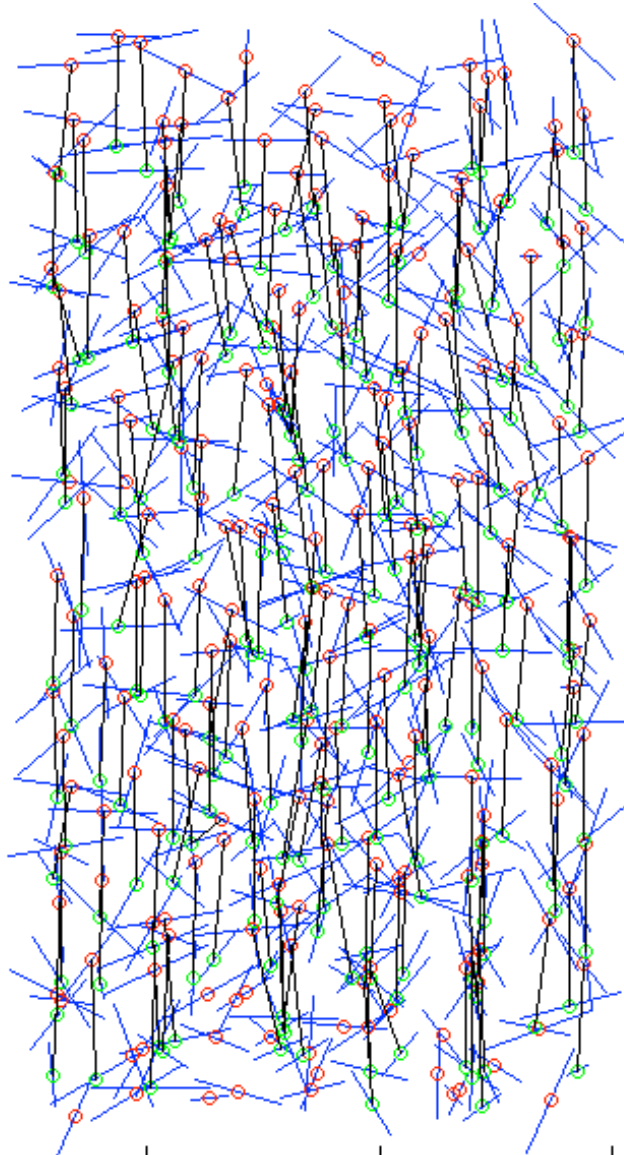


**Figure 1-55. Side view of Module 3 results for the first motion step of the hopper discharge test. 410 of 430 pebbles were tracked, indicating a tracking rate above 95%. The vertical displacement is  $0.533 \pm 0.084$  pebble diameters and the horizontal displacement is  $0.078 \pm 0.066$  pebble diameters.**

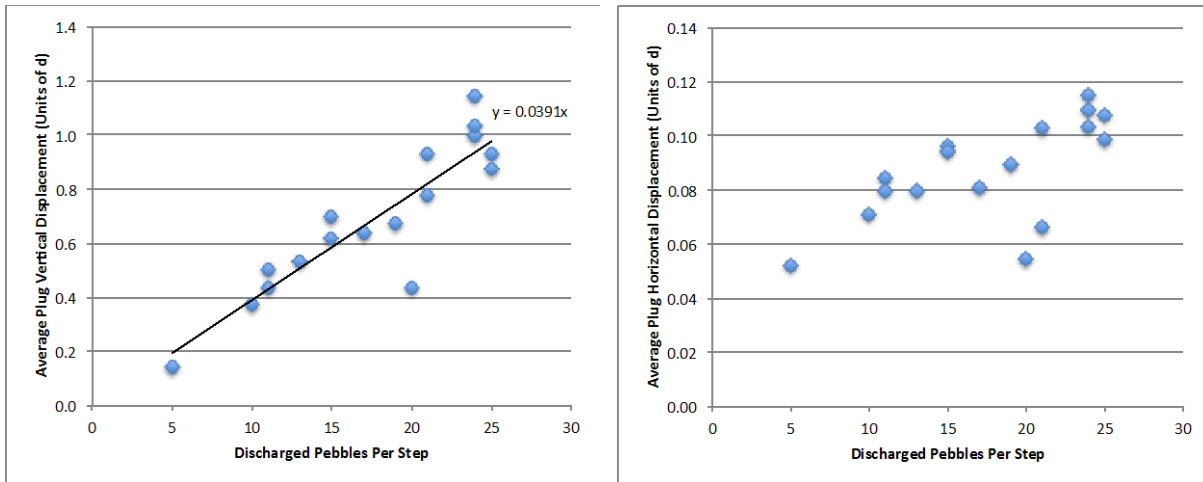


**Figure 1-56. Average vertical (left) and horizontal (right) displacement for each motion step against the number of discharged pebbles. Displacements are given in pebble diameters.**

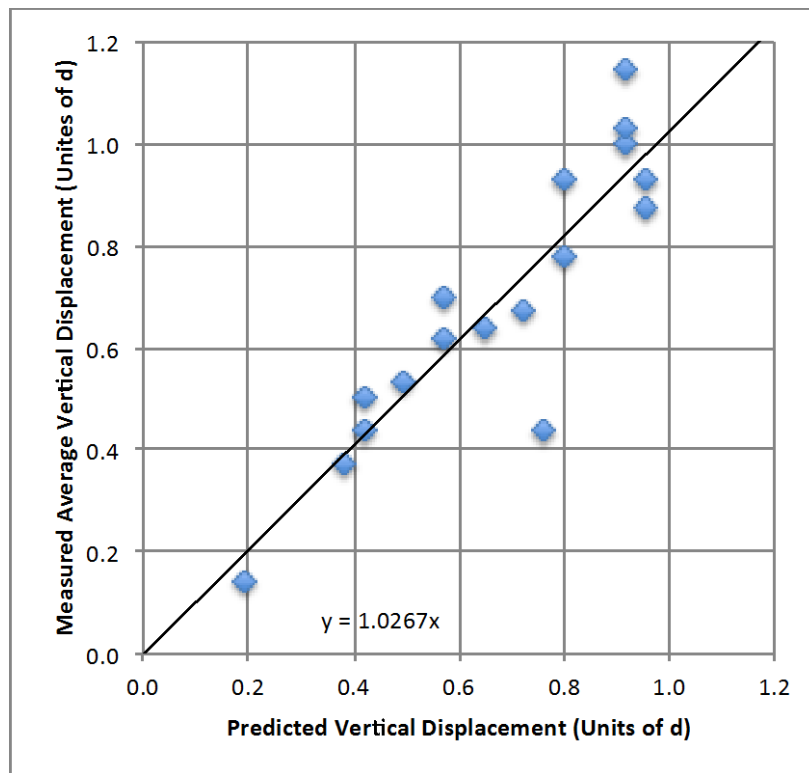


**Figure 1-57. The measured average vertical displacement compared to the predicted vertical displacement based on the column packing fraction (0.58) and the number of discharged pebbles. The best-fit line is within 3% of the predicted values.**

## 1.5 Quality Assurance

U.C. Berkeley has adopted a graded approach to quality assurance for the X-Ray Pebble Recirculation Experiment (X-PREX) based on the requirements to ensure the safe operation of a radiation producing machine and proper documentation of facility design, operation procedures, and experimental results. This chapter presents a high level overview of some key components of the X-PREX Quality Assurance Plan and how they are applied in the facility.

### 1.5.1 Facility Safety and Records Requirements

The X-PREX facility includes an x-ray generator that is classified as a radiation producing machine (RPM) and oversight for its safe operation is provided by the U.C. Berkeley Office of Environment, Health and Safety (EH&S). EH&S issues a Radiation Use Authorization that allows the facility to operate and requires the facility users to keep proper records in accordance with the university and state requirements. This documentation overlaps significantly with the requirements to maintain quality records on the facility design and operation.

Table 1-4 gives a select list of facility procedures, records, and templates that are used for the facility to maintain compliance with EH&S requirements and ensure quality records for data collection. Critical documents for facility safety include the operator training procedure, standard operating procedure, and dose rate verification procedures. Additional records such as key control and operator tags that must be used any time the x-ray generator is energized help to ensure that only qualified and approved facility users have access to the RPM. The Project Manager, the Project Safety Officer, or the Principal Investigator must review and approve all facility procedures. However, with the adopted graded quality assurance approach, reports are not required to receive approval before being stored in the X-PREX facility digital records.

In addition to maintaining proper procedures and records of authorized users, EH&S requires RPM users to keep detailed records that include every shot fired from the x-ray tube. All facility users are required to maintain these records when they use the facility. This can be done with the generic Study Log Template (XPRES-TEMPLATE-001) or the Data Collection Study Log Template (XPRES-TEMPLATE-008). As these records are already required to maintain the facility RUA, additional information relevant for data records is also included in these templates that are included in the record keeping for all data collection studies completed in the X-PREX facility.

Figure 1-58 shows a sample X-Ray Data Collection Study Log used for a drainage study of the Cylindrical Silo Test Section with a 45° cone angle. In this case, all shots were fired at 75 kVp and 20 mAs and eight rotational positions were recorded for each motion step from 0.0° to 157.5° in 22.5° intervals. The position data recorded is the number of discharged pebbles read on the counting scale and TARES are logged every 1,000 pebbles. This information is critical to determine the boundary condition for any simulation for this configuration. For each data run, the Data Collection Study Log is scanned and included as an appendix in the Data Collection Report for that run.

**Table 1-4. Selection of X-PREX procedures, records, and templates.**

<i>Document ID</i>	<i>Name</i>
XPRES-PROC-001	Operator Training Procedures
XPRES-PROC-002	Facility Operating Procedures
XPRES-PROC-003	Dose Rate Verification Procedure
XPRES-PROC-004	Detector and X-Ray Tube Level Adjustment Procedure
XPRES-REC-001	Facility Operating Procedures Training Log
XPRES-REC-002	Dose Rate Verification Procedure Training Log
XPRES-REC-003	Dose Rate Verification Log
XPRES-REC-004	Facility Key Log
XPRES-REC-005	Operator Tag Log
XPRES-REC-006	Laboratory Notebook Log
XPRES-REC-007	Shielding Enclosure Signage
XPRES-REC-008	Description and Safety Case of Facility Indicator Light
XPRES-REC-009	Radiation Use Authorization
XPRES-REC-010	Test Section Design Guidelines
XPRES-REC-010	Generic Data Collection Guidelines
XPRES-TEMPLATE-001	Study Log Template
XPRES-TEMPLATE-002	Key Labels
XPRES-TEMPLATE-003	Operator Tag Labels
XPRES-TEMPLATE-004	Event Log Template
XPRES-TEMPLATE-005	Procedure Template
XPRES-TEMPLATE-006	Report Template
XPRES-TEMPLATE-007	Data Collection Study Log Template
XPRES-TEMPLATE-008	Data Collection Report Template



UNIVERSITY OF CALIFORNIA, BERKELEY  
 NUCLEAR ENGINEERING DEPARTMENT, THERMAL HYDRAULICS GROUP  
 X-RAY PEBBLE RECIRCULATION EXPERIMENT (X-PREX)

X-Ray Data Collection Study Log

PATIENT ID	003-C-45-001
STUDY ID	20141230-01/02/03/04
STUDY DESCRIPTION	Data Collection
OPERATOR	MRL
PRINCIPLE INVESTIGATOR	PPF

kVp	mAs	Orientation								
75	20	0.0	22.5	45.0	67.5	90.0	112.5	135.0	157.5	

STUDY ID		20141230-01									Notes
Step	Position	Image Number									
1	C	1	2	3	4	5	6	7	8	Card Stack 7→8 → Reject?	
2	200	9	10	11	12	13	14	15	16		
3	403	17	18	19	20	21	22	23	24		
4	600	25	26	27	28	29	30	31	32		
5	801	33	34	35	36	37	38	39	40		
6	1007	41	42	43	44	45	46	47	48	TARE	
7	200	49	50	51	52	53	54	55	56		
8	400	57	58	59	60	61	62	63	64		
9	603	65	66	67	68	69	70	71	72		
10	802	73	74	75	76	77	78	79	80		
11	1001	81	82	83	84	85	86	87	88	TARE → 38 Non-Instrumental	
12	201	89	90	91	92	93	94	95	96		

STUDY ID		20141230-02									Notes
Step	Position	Image Number									
13	400	1	2	3	4	5	6	7	8		
14	600	9	12	13	14	15	16	17	18	+10 Exposure +11 Exposure	
15	801	19	20	21	22	23	24	25	26	+23 Software Lead	
16	1000	27	28	29	30	31	32	33	34	TARE → 12 Non-Instrumental	
17	201	35	36	37	38	39	40	41	42	0° Photo Post Imaging	
18	402	43	44	45	46	47	48	49	50		
19	600	51	52	53	54	55	56	57	58		
20	800	59	60	61	62	63	64	65	66		
21	1000	67	68	70	71	72	73	74	75	+69 Position TARE → 9 Min	
22	201	76	77	78	79	80	81	82	83		
23	406	84	85	86	87	88	89	90	91		
24	603	92	93	94	95	96	97	98	99		

DATE 12/30/14

PAGE 1 OF 2

Figure 1-58. Sample completed x-ray data collection study log.

### 1.5.2 Data Processing Management

Studies completed in the X-PREX facility produce a large amount of data in various forms ranging from digital x-ray images to data files containing pebble motion data. This data requires procedures to ensure that all records are organized in a standard and convenient form and results are preserved for future use.

The first set of data from the X-PREX facility is the original digital x-ray images recorded at the remote operator workstation. The image files are backed up on external drives and on local U.C. Berkeley computers for security. After converting from the DICOM image format, the images for each study are batch processed with the following naming convention:

YYYYMMDD\_ID\_TYPE\_###\_ANGLE

With the following definitions:

YYYYMMDD – Date of the x-ray imaging session

ID – ID of the x-ray imaging session for the imaging date

TYPE – ‘X’ for x-ray images or ‘V’ for visual images

### - Motion step index number

ANGLE – Four-digit rotational angle to 0.1 degree precision (no decimal point)

This naming convention allows for all the important data to be extracted from the file name during for the tomography image processing and reduces the amount of manual input required. The images are organized and batch processed in a photo management program (either Apple Aperture or Adobe Lightroom) so that each study has folders for the x-ray and visual images and subfolders for each rotational position. Figure 1-59 is a screenshot of how the photos are organized for easy use with these data management procedures.

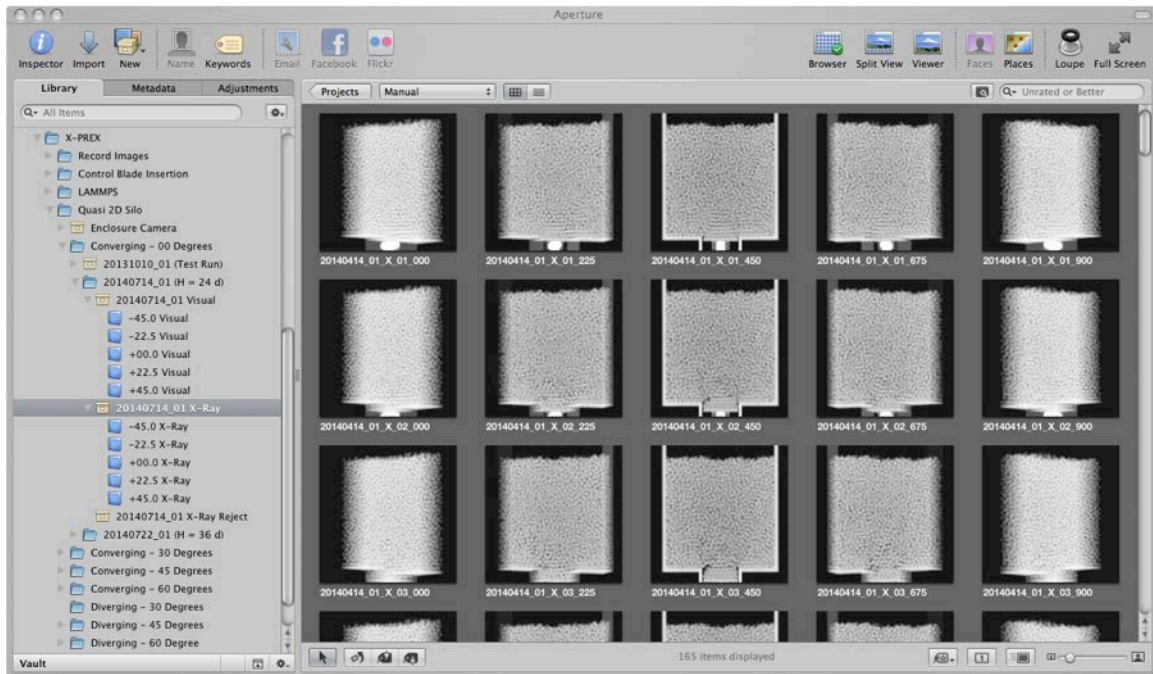


**Figure 1-59. Screenshot example of the image management system for the X-PREX facility. Each study includes folders for the x-ray and visual images and subfolders for each rotational position. In the sample shown, each column includes one rotational position for the 00-degree Converging Quasi-2D Silo test section from -45.0 to +45.0 degrees.**

Quality record keeping for the image processing software and final data is also an important component of the X-PREX quality assurance program. The tomography image processing software for the X-PREX facility is still in the prototype phase and therefore many versions of the code exist. In order to reduce confusion on the code development, new versions of the code are created for each development day or multiple versions may be created in a single day if significant changes are being made. Comments are included at the top of the code in the ‘Code Log’ detailing the important changes made for each version. Data processed with the image processing software is always stored with the version of the image processing code used.

Once the image processing code is completed, new procedures will be put in place to archive the final data from X-PREX data collection runs with appropriate documentation on the file contents. These records will also include all the original x-ray and visual images and a data collection report for each study that includes the data collection study log and describes the test geometry, pebble loading and motion. Final data from the X-PREX facility will be archived on the remote operator computer with a backup on the secure server in the Thermal Hydraulics Laboratory. These procedures will ensure that data from the facility is safely stored and adequately documented for any future use.

## 2 Experimental Program

### 2.1 Quasi Two-Dimensional (2D) Silo Experiment

The Quasi Two-Dimensional (2D) Silo (Figure 2-1) is a geometry configuration that has been previously studied through experiment, simulation, and analytic methods in order to gain insights into the fundamental behavior of slow dense granular flow.<sup>2,3</sup> This geometry was selected for initial studies in the X-PREX facility due to its relevance for reactor core pebble flow, relative simplicity, and the flexibility to study different geometric configurations with a modular test section design. The experimental results for the Quasi-2D Silo test section will also provide the best available comparison to DEM simulation results for model validation.



**Figure 2-1. Quasi-2D Silo test section in the X-PREX facility. For the test show here, 3,000 pebbles were initially loaded into the test section then downward motion of the pebbles occurs as a piston plate in the orifice chute moves in incremental steps of  $d$ .**

---

<sup>2</sup> Jaehyuk Choi, Arshad Kudrolli, and Martin Z Bazant, “Velocity Profile of Granular Flows Inside Silos and Hoppers,” *J. Phys.: Condens. Matter*, (January 2005).

<sup>3</sup> Chris Rycroft et al., “Dynamics of Random Packings in Granular Flow,” *Physical Review E* 73, no. 5 (May 2006).

## 2.1.1 Experimental Methods and Setup

### 2.1.1.1 Physical Description

The Quasi-2D Silo test section is a modular design that can be used to study pebble drainage in converging and diverging hoppers with several different hopper angles. Figure 2-2 shows the design of the Quasi-2D Silo. The silo has width 30.48 cm ( $24d$ ) and depth 10.16 cm ( $8d$ ). The total height of the wide region (top in Figure 2-2) is 25.40 cm ( $40d$ ). The orifice is centered and has width and depth 10.16 cm ( $8d$ ) and the total height of the narrow region (bottom in Figure 2-2) is 22.86 cm ( $36d$ ).

In addition to the zero-degree hopper configuration, wedges of 30, 45, or 60-degrees (Figure 2-3) can be installed in the wide region near the orifice to adjust the hopper angle. Figure 2-4 shows the Quasi-2D Silo test section during three preliminary data collection runs configured with converging geometry and hopper angles of 0, 30, and 60 degrees. In these runs, a mixture of instrumented pebbles unmodified high density polyethylene (HDPE) pebbles were used to help visualize the flow patterns.

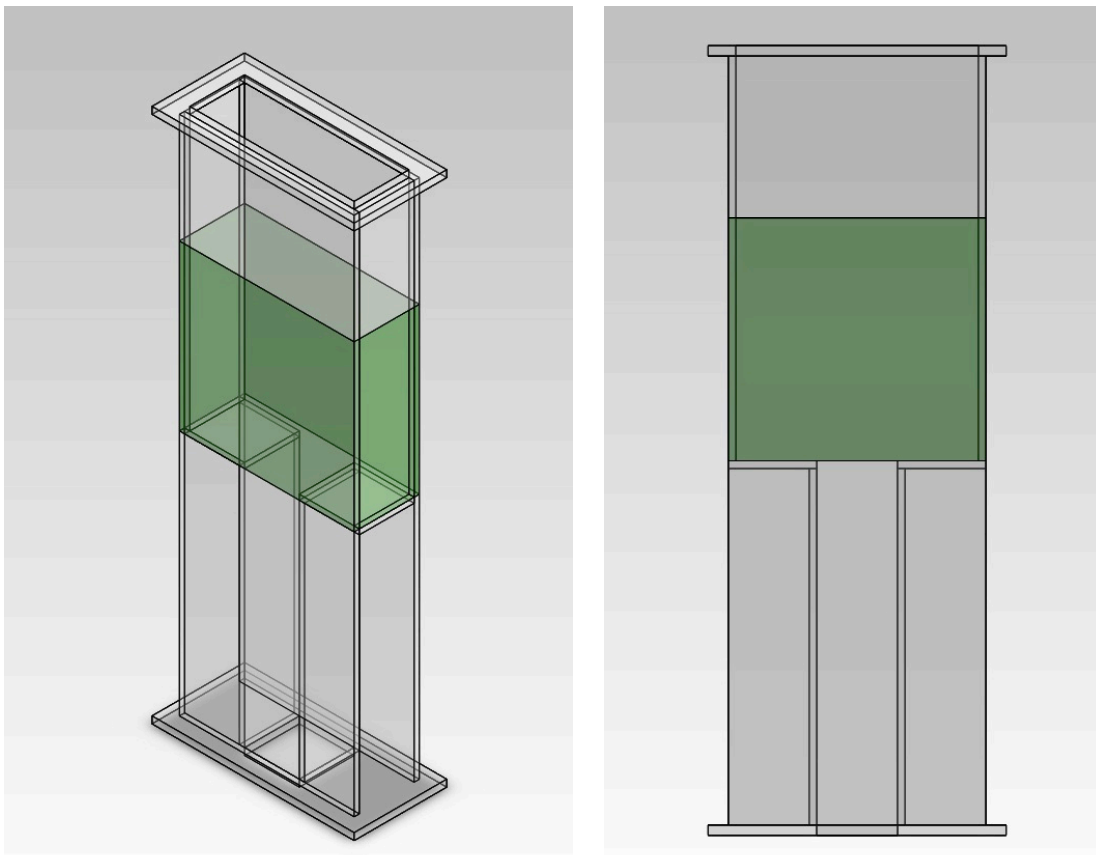


**Figure 2-2. Isometric (left) and front (right) view of Quasi-2D Silo test section design. The green region is the imaging zone where pebbles are tracked with the digital x-ray tomography.**



**Figure 2-3. Detail views of the 60-degree wedge installed on the test section (left) and the 45 and 30-degree wedges (right).**

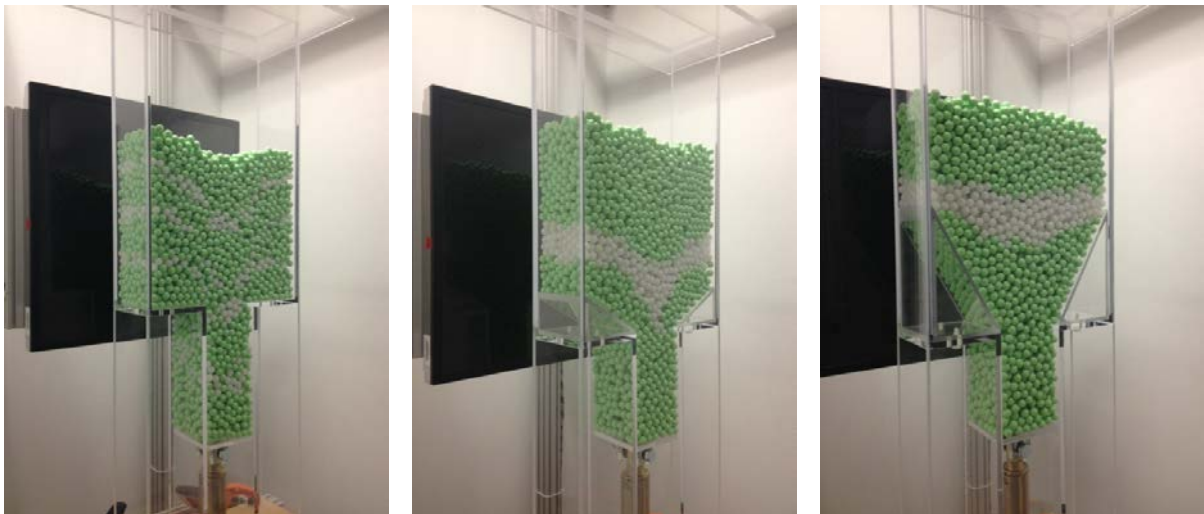


**Figure 2-4. Images of the Quasi-2D Silo Test Section in the modular test bay during data collection for the 0-degree (left), 30-degree (center), and 60-degree (right) converging configurations. The white pebbles in the images are instrumented with tungsten wires, while the green pebbles are unmodified HDPE pebbles.**

The Quasi-2D Silo test section was designed to study both converging and diverging granular flow behavior with minimal modifications or adjustments. Figure 2-5 shows the test section in the X-PREX facility during data collection runs with the 45-degree for converging and diverging pebble flow. To convert from converging to diverging geometry, the test section can be simply flipped upside down. Special precautions must be taken in the diverging configuration to make sure that the linear actuator that controls the pebble motion boundary condition is not extended while pebbles are loaded in the test section. This is due to the limited degrees of freedom in the system and the large forces transferred into the packed bed that could damage the test section.



**Figure 2-5. Converging (left) and diverging (right) configurations of the Quasi-2D Silo test section with a 45-degree hopper angle.**

The motion boundary condition for the Quasi-2D Silo is set by the step-wise motion of a piston plate located at the bottom of the packed bed. Figure 2-6 shows flat piston plates fabricated from cast acrylic for both the converging and diverging geometry. The motion of the piston plate provides an appropriate boundary condition that can be approximated in DEM simulations. For the diverging geometry, the linear motion of the piston plate is also a reasonable representation of the plug flow that would be expected at the top of a constant area region. Some distortions may exist along the sidewalls, where some additional pebble hold up may occur even in constant area regions.

During early studies with the diverging configuration, a significant amount of ordered packing was observed on the surface of the flat piston plate in the x-ray images. Based on this result, U.C. Berkeley used pebble packing data from DEM simulations and three-dimensional printing facilities to produce a random packing piston plate (Figure 2-7) to better simulate the disorganized packing expected at the top of a constant area region in a large packed bed. Figure 2-8 shows a comparison of the x-ray images for the flat and random piston plates. The random packing plate effectively eliminates the ordered packing effect and should be used in all subsequent diverging geometry tests.

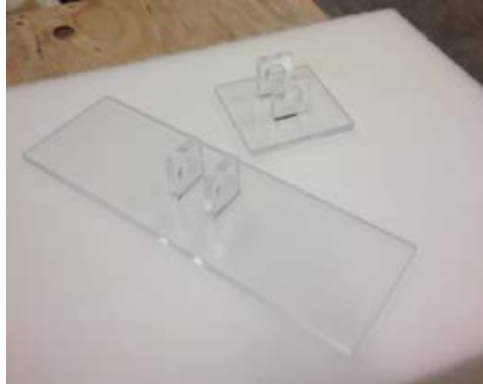


**Figure 2-6. Flat piston plates to enforce plug flow boundary conditions for the quasi-2D test section for diverging and converging geometries.**



**Figure 2-7. Random packing configuration from DEM simulation (left), CAD model (center), and FDM-manufactured random pebble packing piston plate (right).**

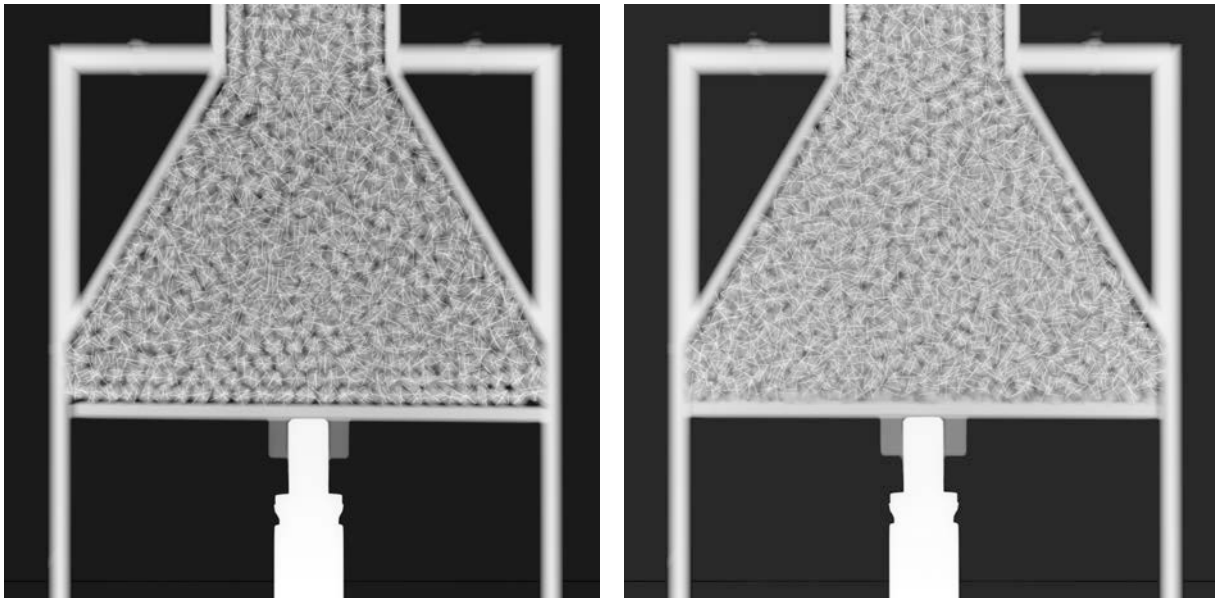


**Figure 2-8. Comparison of pebble packing configurations for the 60-degree Diverging Quasi-2D Silo with the flat (left) and random packing (right) piston plate.**

### 2.1.1.2 Test Procedure

For each data collection run with the Quasi-2D Silo, the total number of pebbles loaded into the test section is determined using digital counting scale. The motion boundary condition for motion in the Quasi-2D Silo is set by the piston plate (either flat or random pebble surface) mounted to the top of the linear actuator in the X-PREX modular test base. For the converging studies, the initial position of the piston plate is set at the orifice slit. For the diverging studies, the linear actuator is extended so that the flat surface is located 20.3 cm ( $16d$ ) below the orifice slit. After initial pebble loading of the silo to the determined height, downward step-wise motion is achieved by retracting the linear actuator. Step sizes of 1.27 cm ( $1d$ ) and 0.42 cm ( $d/3$ ) were used between each rotation image series for the converging and diverging configurations, respectively. The ratio of step sizes matches the area ratio in the main test section and the small area region, therefore the diverging tests should give an average vertical pebble displacement of 1.27 cm ( $1d$ ) in the small area region.

During each data collection run, 32 motion steps were completed to give total actuator displacements of 40.64 cm ( $32d$ ) and 13.44 cm ( $10.67d$ ) for the converging and diverging cases, respectively. At each position, x-ray and visual images were recorded at five rotational position:  $-45.0$ ,  $-22.5$ ,  $0.0$ ,  $+22.5$ , and  $+45.0$  degrees.

### 2.1.1.3 Test Plan

The initial test plan for the Quasi-2D Silo includes three preliminary runs with the converging silo geometry with a mixture of instrumented and unmodified pebbles (previously shown in Figure 2-4) that allow for the overall flow pattern to be observed.

For the converging silo configuration, the test plan includes two data collection runs for each hopper angle with packed bed heights of  $24d$  and  $36d$ . Figure 2-9 shows the initial and final bed configuration for the two heights with the zero-degree hopper. No additional pebbles were added to the top of the packed bed for these tests. The study of the packed bed to a height of  $24d$  is important for the DEM validation effort because all of the pebbles in the system are visible in the x-ray images and can be used as the initial packing configuration in the simulation model. The height of the test section limits studies of packed beds up to a height of  $36d$ , which is a better representation of the type of packing relevant for granular flow in reactor cores.

The test plan for the diverging geometry includes studies with no pebble reloading and a single pebble reload for the 30, 45, and 60-degree hopper angles. These tests were completed with the flat piston plate. Figure 2-10 shows the initial and final bed configuration for the 45 and 60-degree tests with no pebbles loaded after the initial packing. Additional studies were completed with the 45 and 60-degree hopper angles with the random packing plate and regular pebble additions during the run.

Figure 2-11 shows an example of the visual and x-ray images collected at each rotational view for the 45-degree converging test at the initial and final packing configuration. The initial height of the packed bed in this case is  $24d$ .

Initial Height = 24 d

Initial Height = 36 d

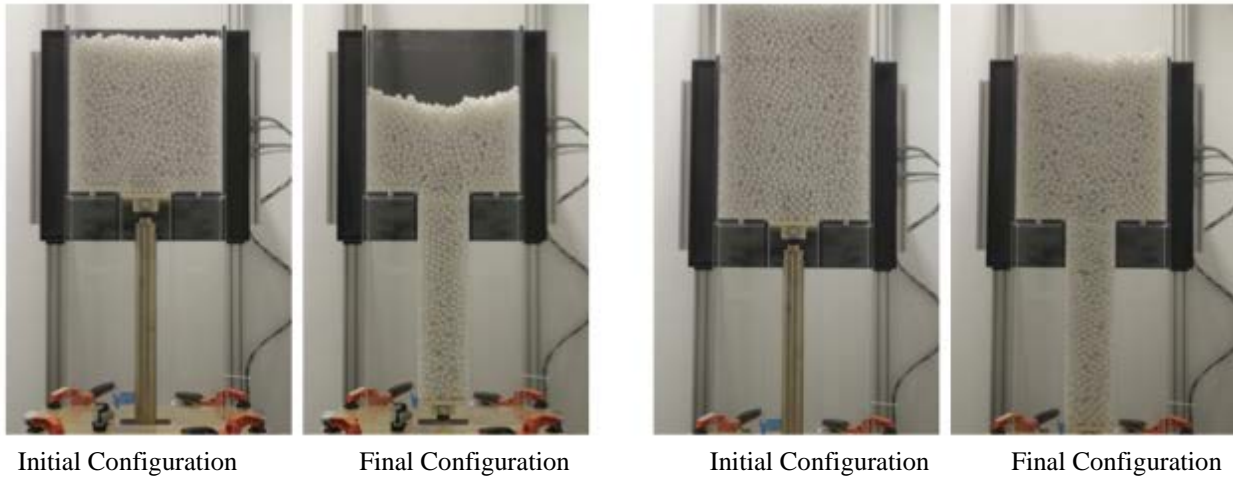


**Figure 2-9. Initial and final bed configurations for the converging Quasi-2D Silo in the zero degree hopper configuration. The left images are for an initial bed height of 24 d (30.5 cm) and the right images are for an initial bed height of 36 d (45.7 cm).**

45-Degree Diverging Silo

60-Degree Diverging Silo

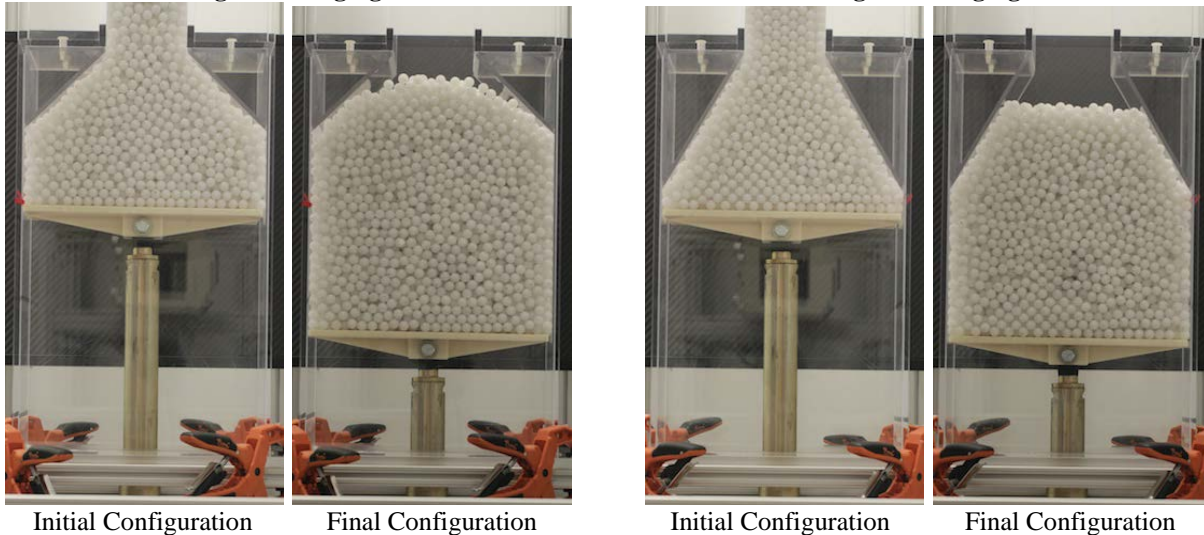
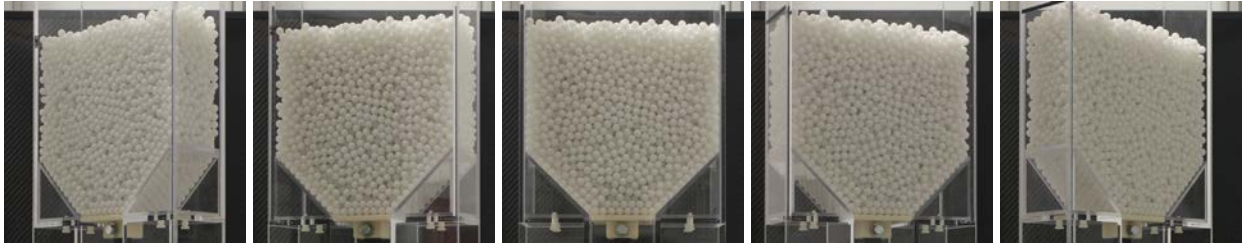


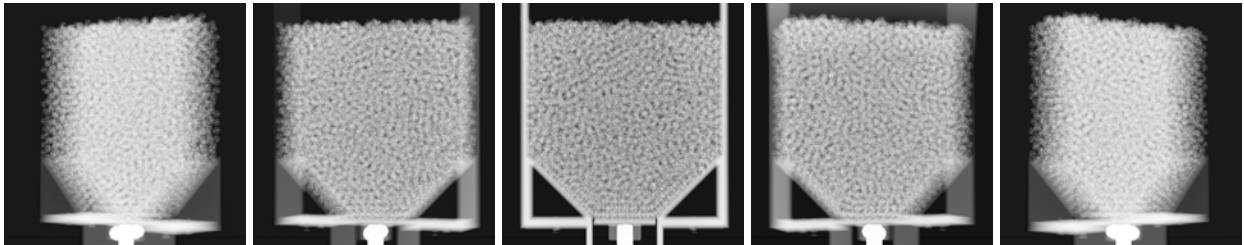
**Figure 2-10. Initial and final bed configurations for the diverging Quasi-2D Silo in the 45-degree (left) and 60-degree (right) hopper configuration. These data runs were completed without pebble addition.**

*Piston Displacement = 0 d*

Visual Image Sequence



X-Ray Image Sequence



*Piston Displacement = 32 d*

Visual Image Sequence



X-Ray Image Sequence

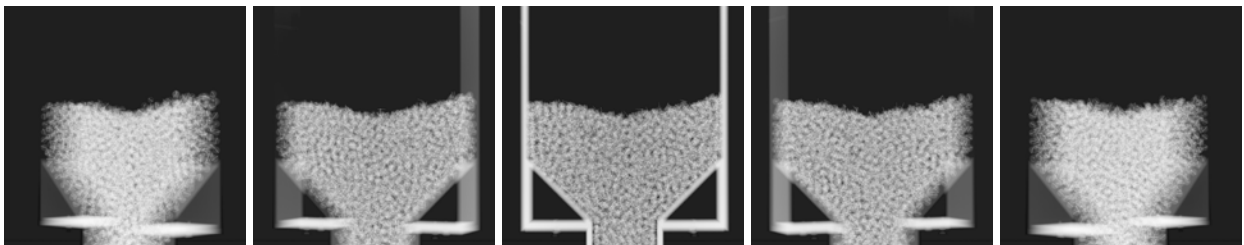


**Figure 2-11. Rotational image sequences for the Quasi-2D silo for initial and final packing configurations of the 45-degree hopper loaded to an initial height of  $24d$ . For each position step, the upper row includes the visual images of the surface and the lower row are the x-ray images. From left to right, each sequence gives the views for  $-45.0$ ,  $-22.5$ ,  $0.0$ ,  $+22.5$ , and  $+45.0$  rotational positions.**

### 2.1.2 Results

The data collection studies for the Quasi-2D Silo were completed during summer and fall in 2014 before the installation of the lower stabilizer bearing in the X-PREX Modular Test Bay. After the verification of the image processing software, it was determined that the geometry in these studies was not precise enough to successfully complete the computed tomography analysis of the packed bed motion. Small misalignments of the rotation axis due to wobble in the precision turntable are the main reason this data cannot be processed. Therefore the results from the completed data studies are primarily qualitative and can be used to inform future test programs in the X-PREX facility.

Results are presented here for the converging silo configuration from the flow visualization test runs and the data collection runs with an initial packed bed height of  $24d$  that can be used to evaluate the packing structure of the free surface. The data from the diverging silo configurations is omitted due to the fact that the bed remains packed and little information can be gained from the still images in the data collection runs. It should be noted that stop-motion video of the images in these runs show interesting behavior that will be studied in more detail in the future.

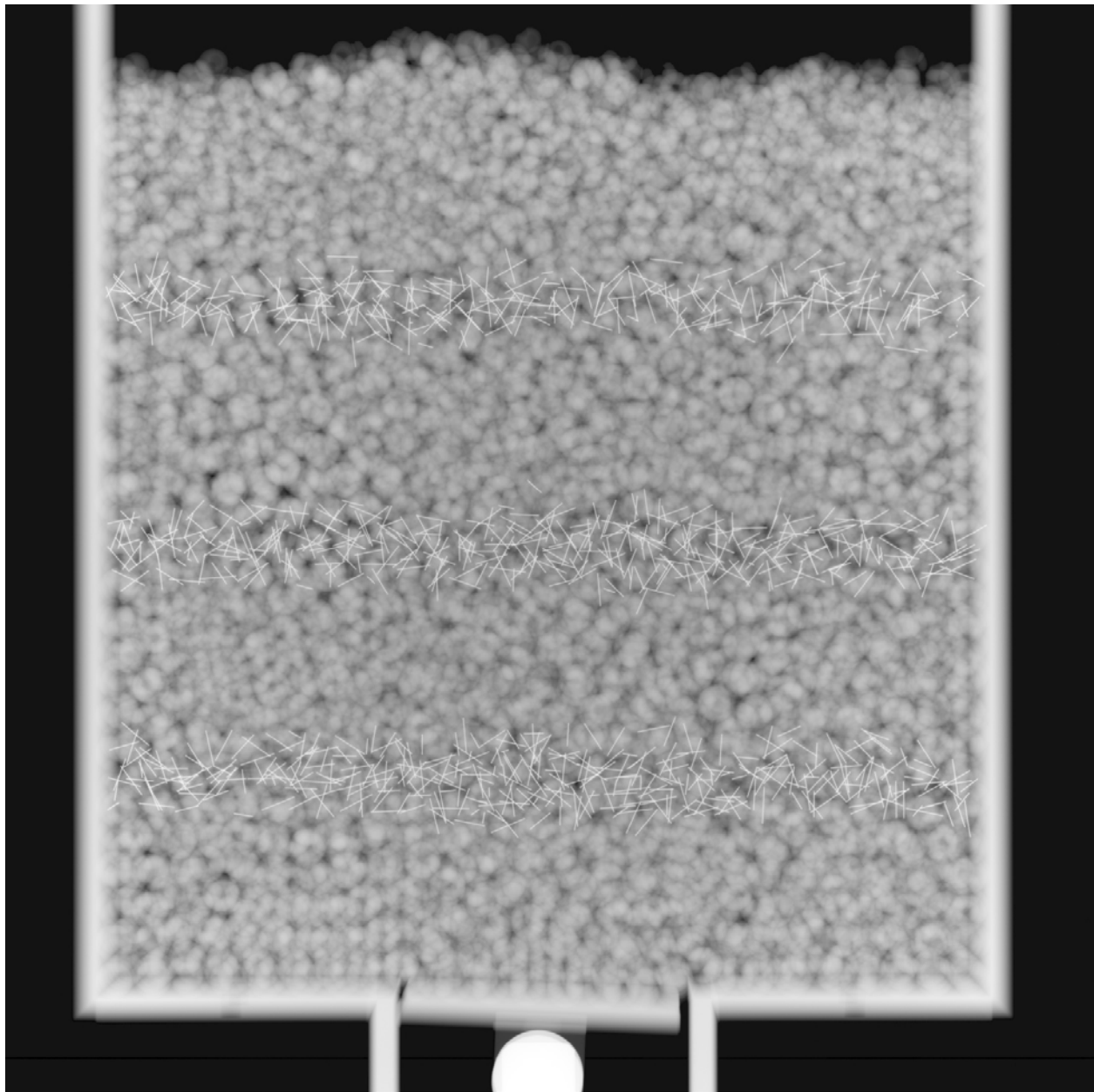
The flow visualization test runs completed with layers of instrumented and unmodified pebbles are useful to get an intuitive understanding of the granular flow behavior in systems like the Quasi-2D Silo. Figure 2-12A-F shows the front view of the test section in the zero-degree converging silo with three layers of instrumented pebbles separated by piston displacement of  $6d$ . From these images, the channeling of the flow above the orifice region where pebbles move much more quickly than those near the sidewalls is clearly visible. Stagnant regions can also be observed on both sides of the orifice extending up from the corners of the defueling chute at approximately 60-degrees. These results are consistent with phenomena previously observed in experiments and DEM simulations. They also point to the promise of the results from the X-PREX facility to provide additional insights through the tracking of rotation data this kind of system geometry.

Figure 2-13A-C and Figure 2-14A-C show the flow visualization test runs for the converging 30 and 60-degree silo configurations, respectively, with a single layer of instrumented pebbles initially located several pebble diameters above the start of the hopper region at the initial, middle, and final piston displacements. Both image series show that there is no stagnation region in these geometries, though significantly greater pebble hold up is observed in the 30-degree hopper. These results support the conclusion that larger hopper angles will produce significantly smaller variations in residence times for pebbles circulating through the core in pebble bed reactors.

Finally, in order to provide some initial validation of DEM simulations using results from the X-PREX facility, Figure 2-15, Figure 2-16, and Figure 2-17 show the change in the surface packing configuration for runs with the 0, 30, and 60-degree hoppers, respectively. These figures show the structure of the free surface at the initial packing, which is nearly flat in all cases, and with piston displacements of  $16d$  and  $32d$ . The results from the 0 and 30-degree hoppers show similar structures due to the channeling of flow in the center region and a heap structure based on the angle of repose. The results from the 60-degree hopper show a significantly more level free

surface, which is consistent with the more uniform velocity profile for pebbles near the sidewalls.

Piston Displacement =  $0 d$



**Figure 2-12-A. Pebble flow visualization run for zero-degree converging silo.**

Piston Displacement =  $6d$

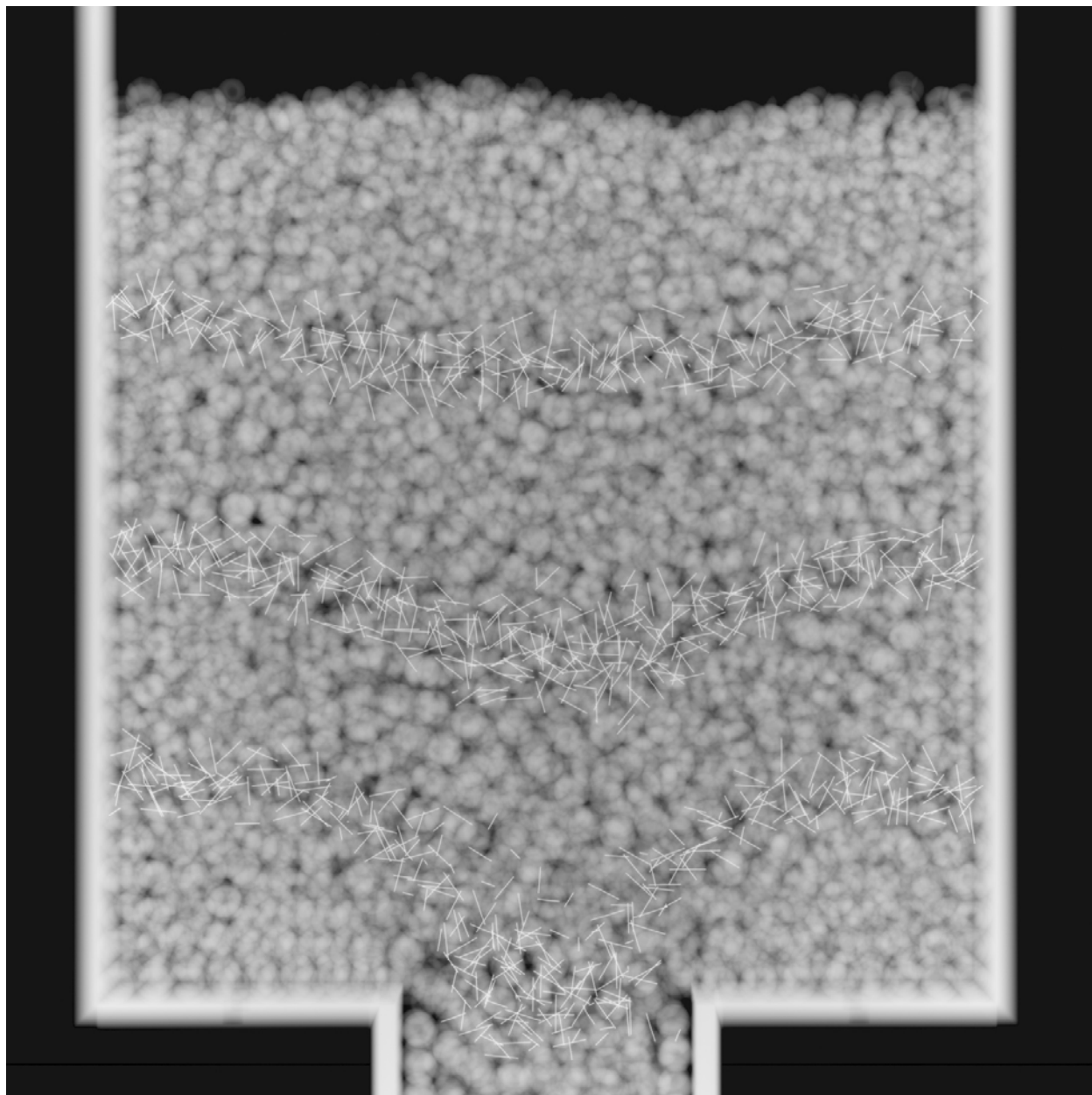


**Figure 2-12-B. Pebble flow visualization run for zero-degree converging silo.**

Piston Displacement =  $12 d$

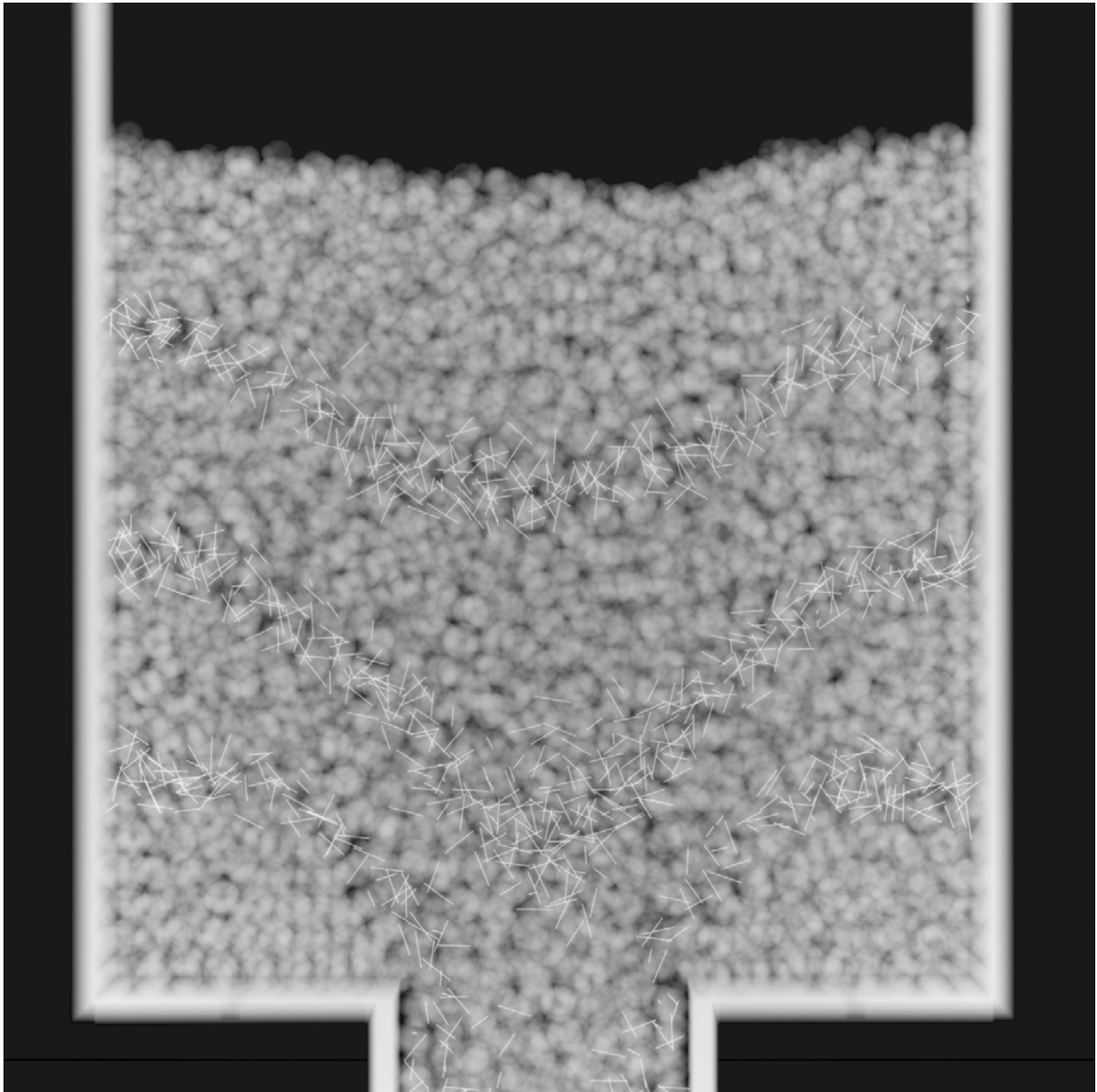


**Figure 2-12-C. Pebble flow visualization run for zero-degree converging silo.**

Piston Displacement =  $18 d$

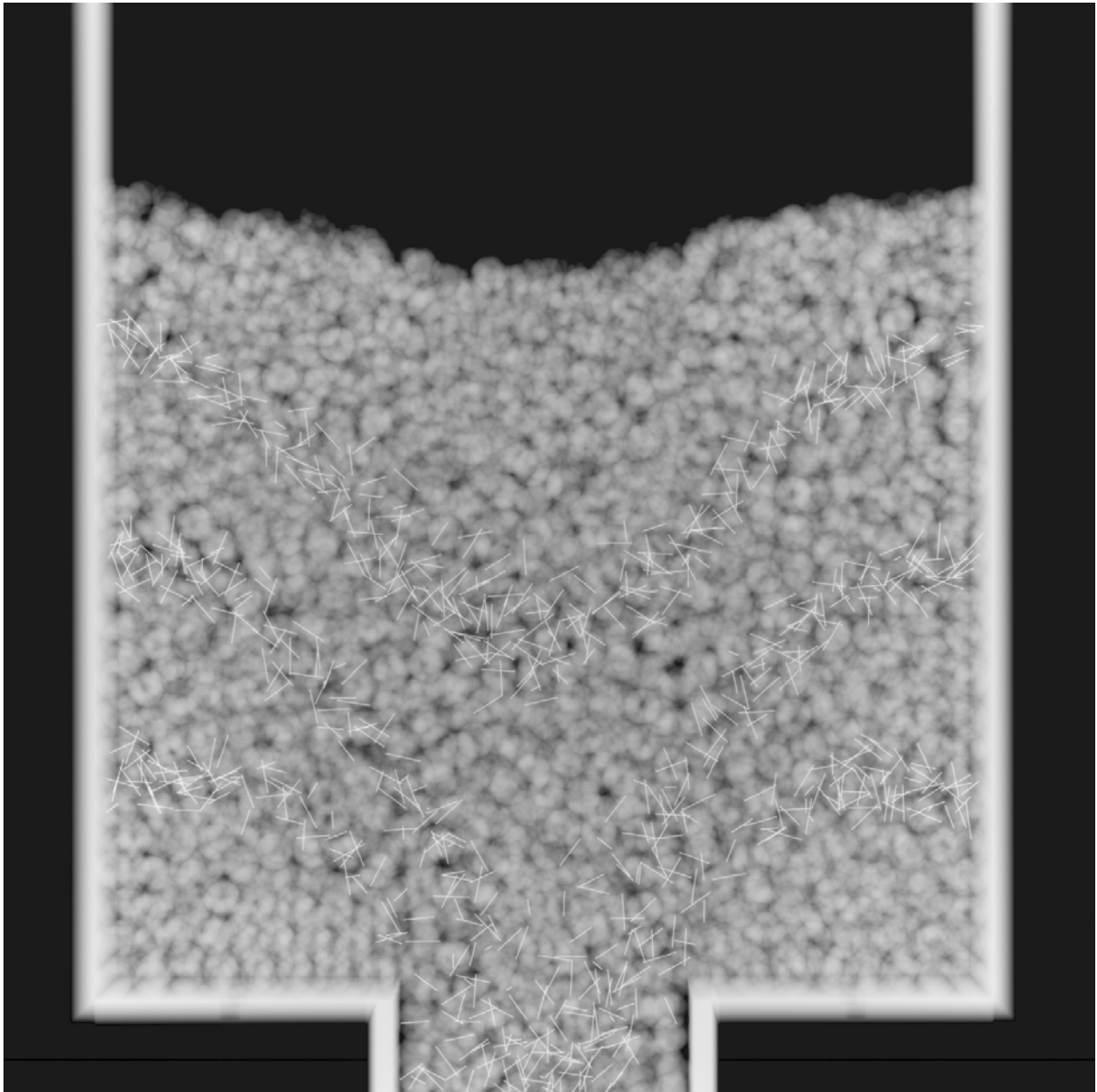


**Figure 2-12-D. Pebble flow visualization run for zero-degree converging silo.**

Piston Displacement =  $24 d$

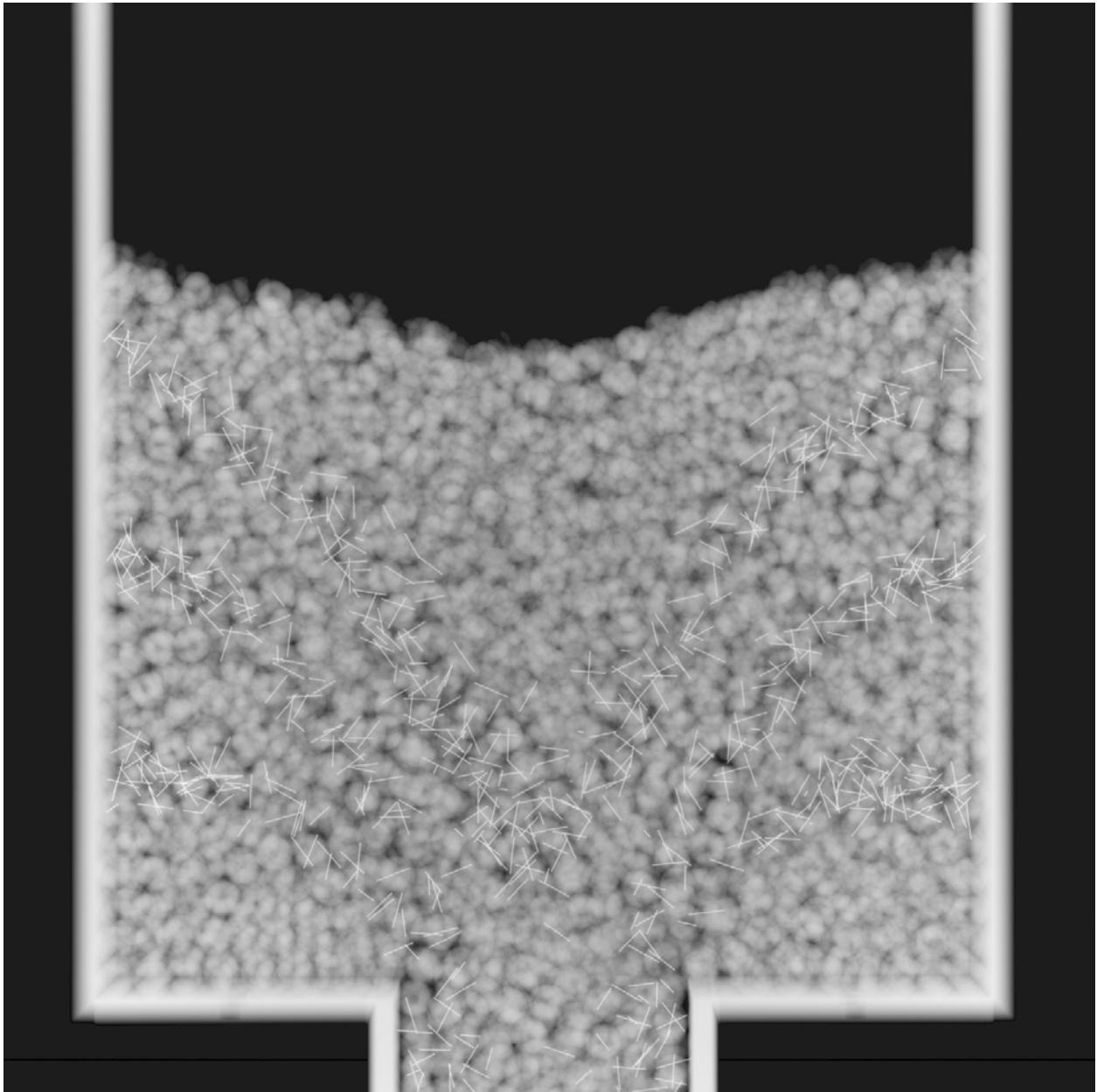


**Figure 2-12-E. Pebble flow visualization run for zero-degree converging silo.**

Piston Displacement =  $30 d$

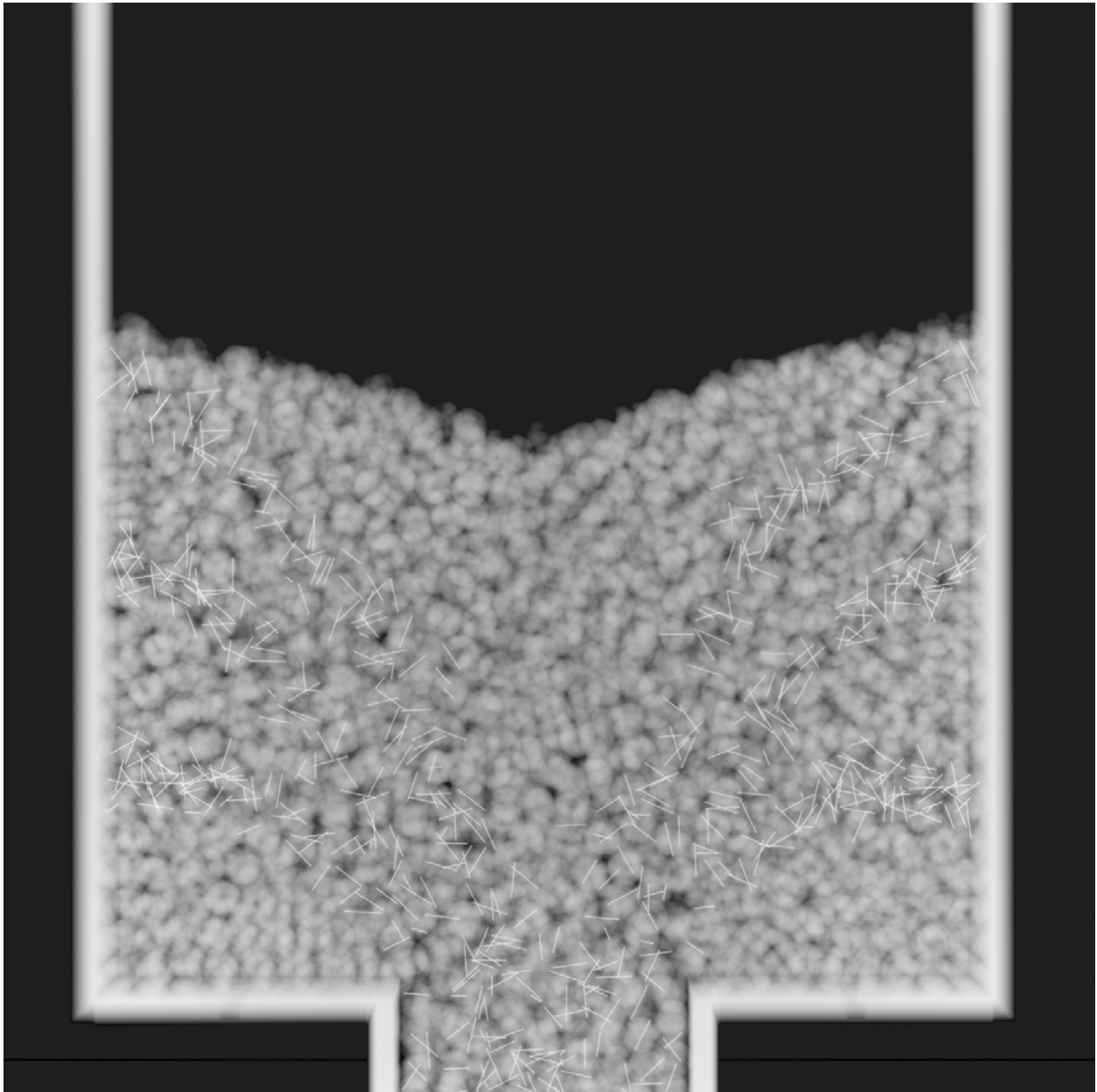


**Figure 2-12-F. Pebble flow visualization run for zero-degree converging silo.**

Piston Displacement = 0 *d*

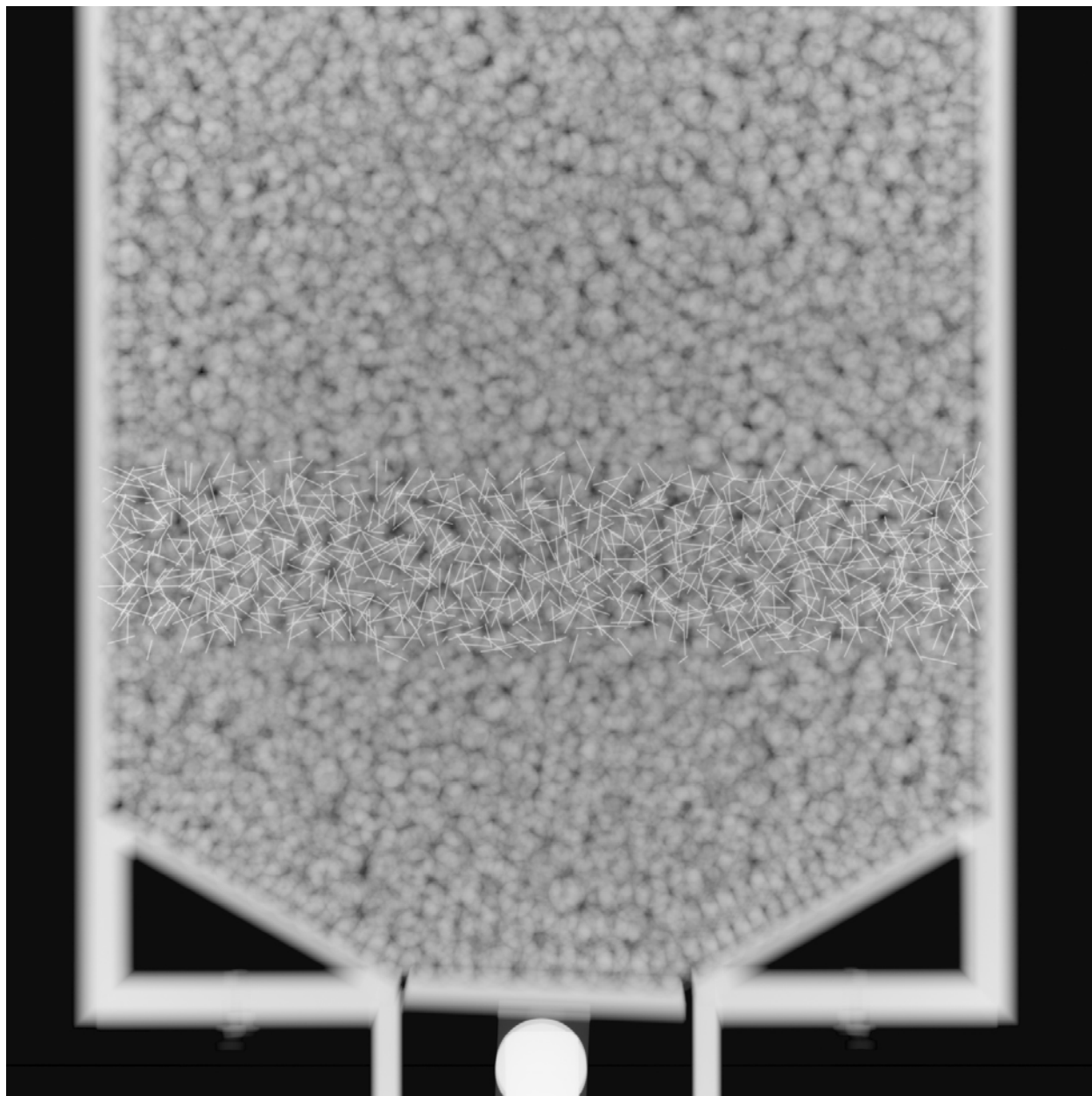


**Figure 2-13-A. Pebble flow visualization run for 30-degree converging silo.**

Piston Displacement =  $16 d$

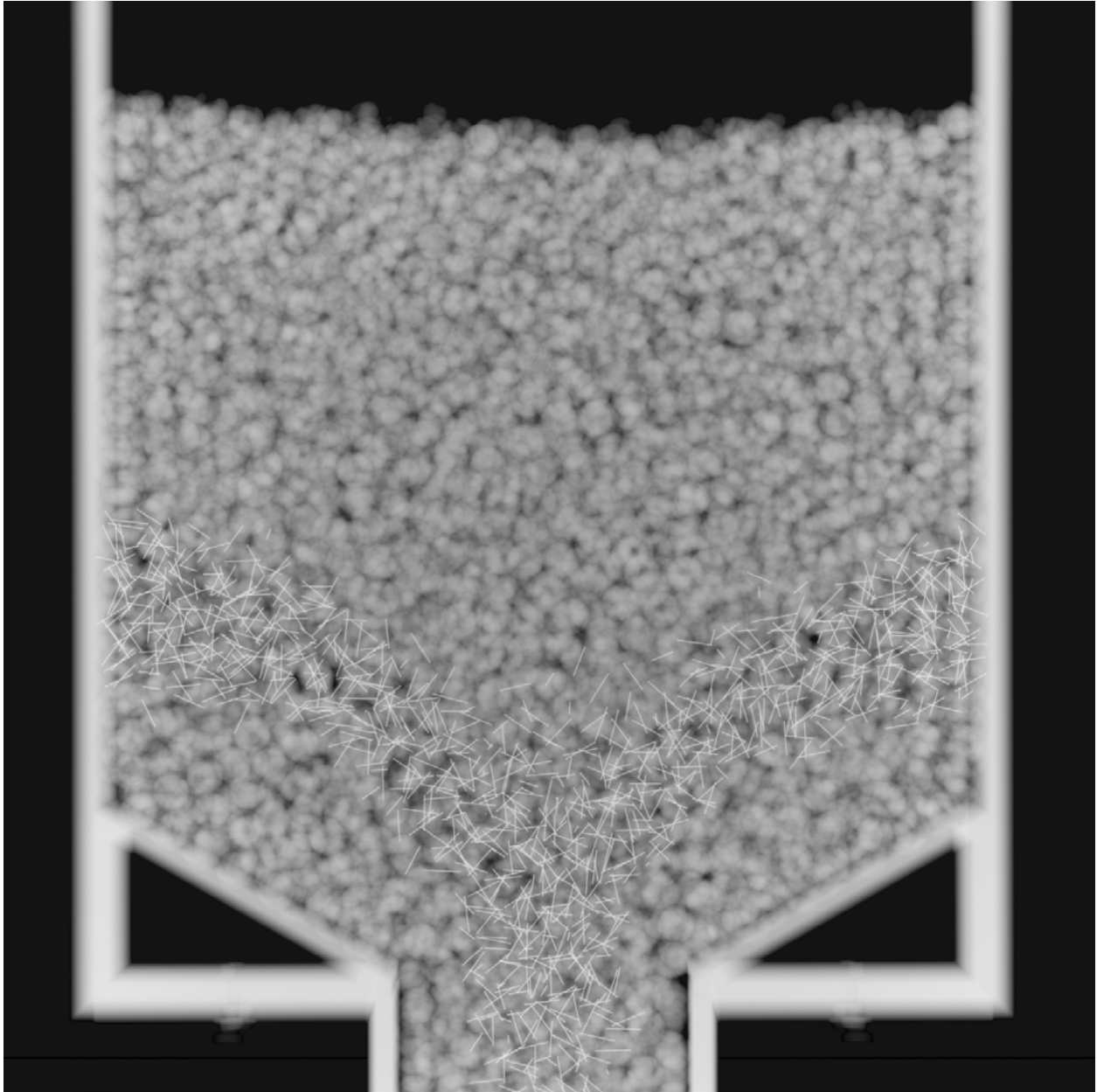


**Figure 2-13-B. Pebble flow visualization run for 30-degree converging silo.**

Piston Displacement =  $32 d$

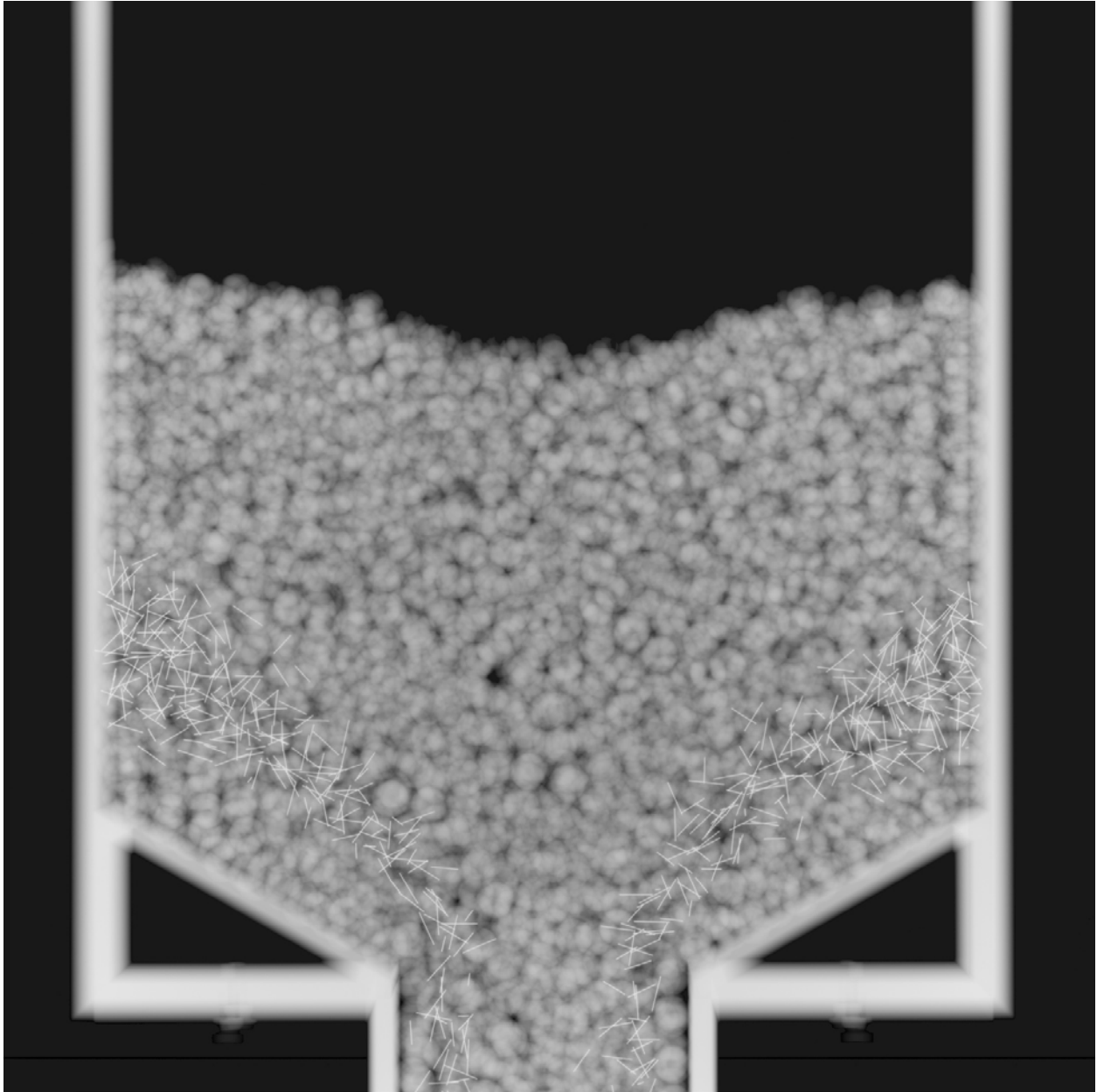


**Figure 2-13-C. Pebble flow visualization run for 30-degree converging silo.**

Piston Displacement = 0 *d*

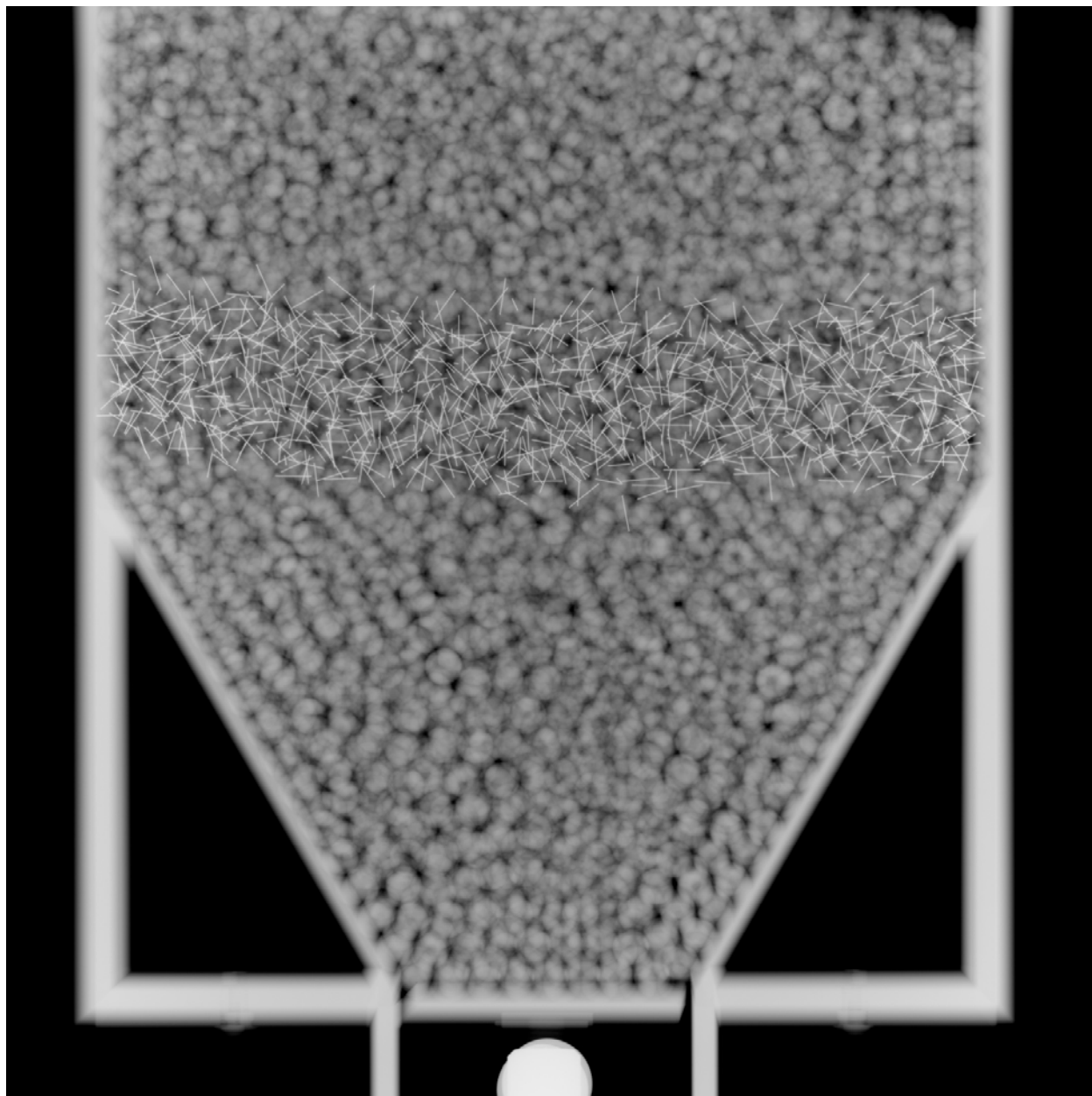


**Figure 2-14-A. Pebble flow visualization run for 60-degree converging silo.**

Piston Displacement =  $16 d$

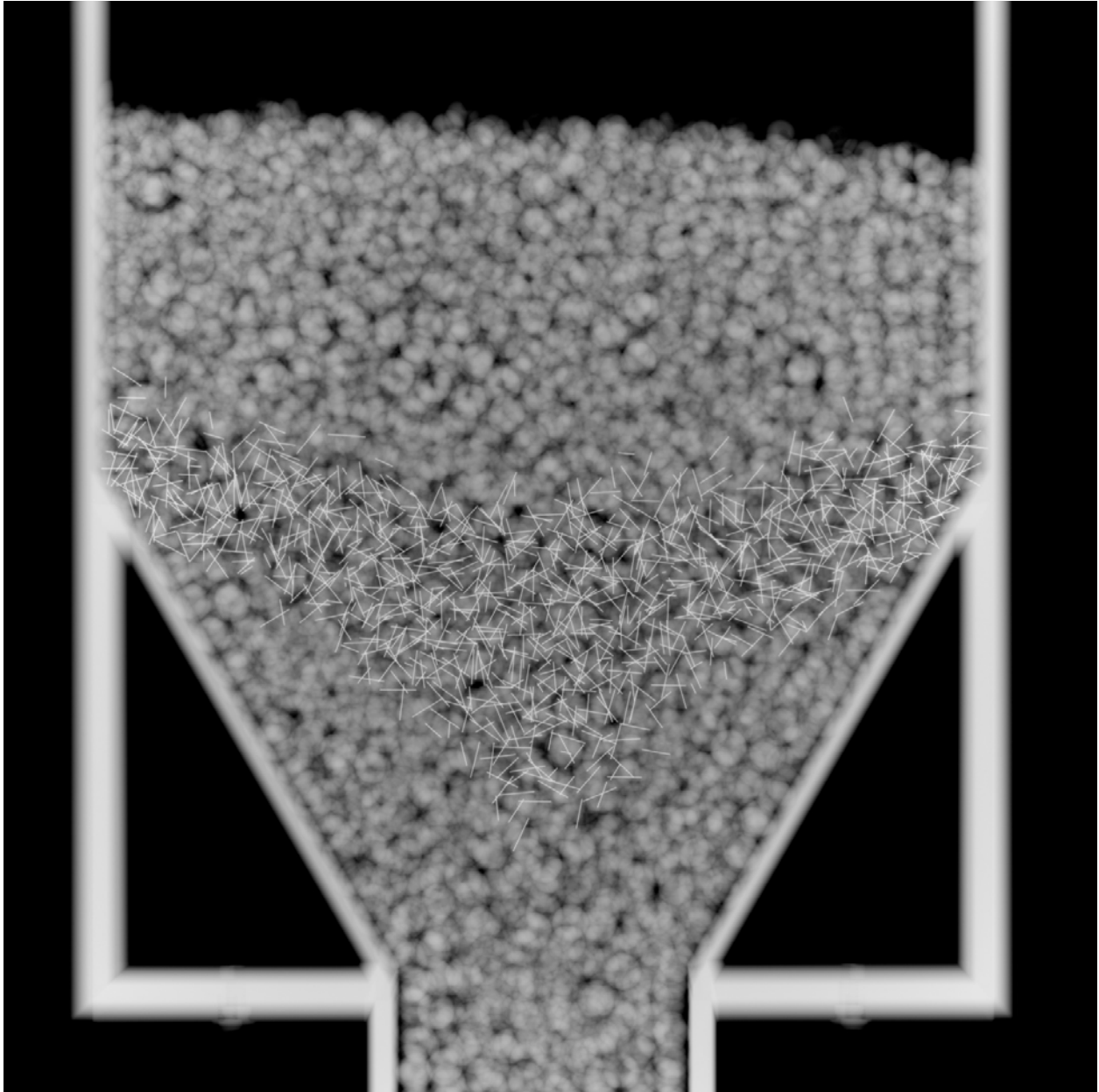


**Figure 2-14-B. Pebble flow visualization run for 60-degree converging silo.**

Piston Displacement =  $32 d$

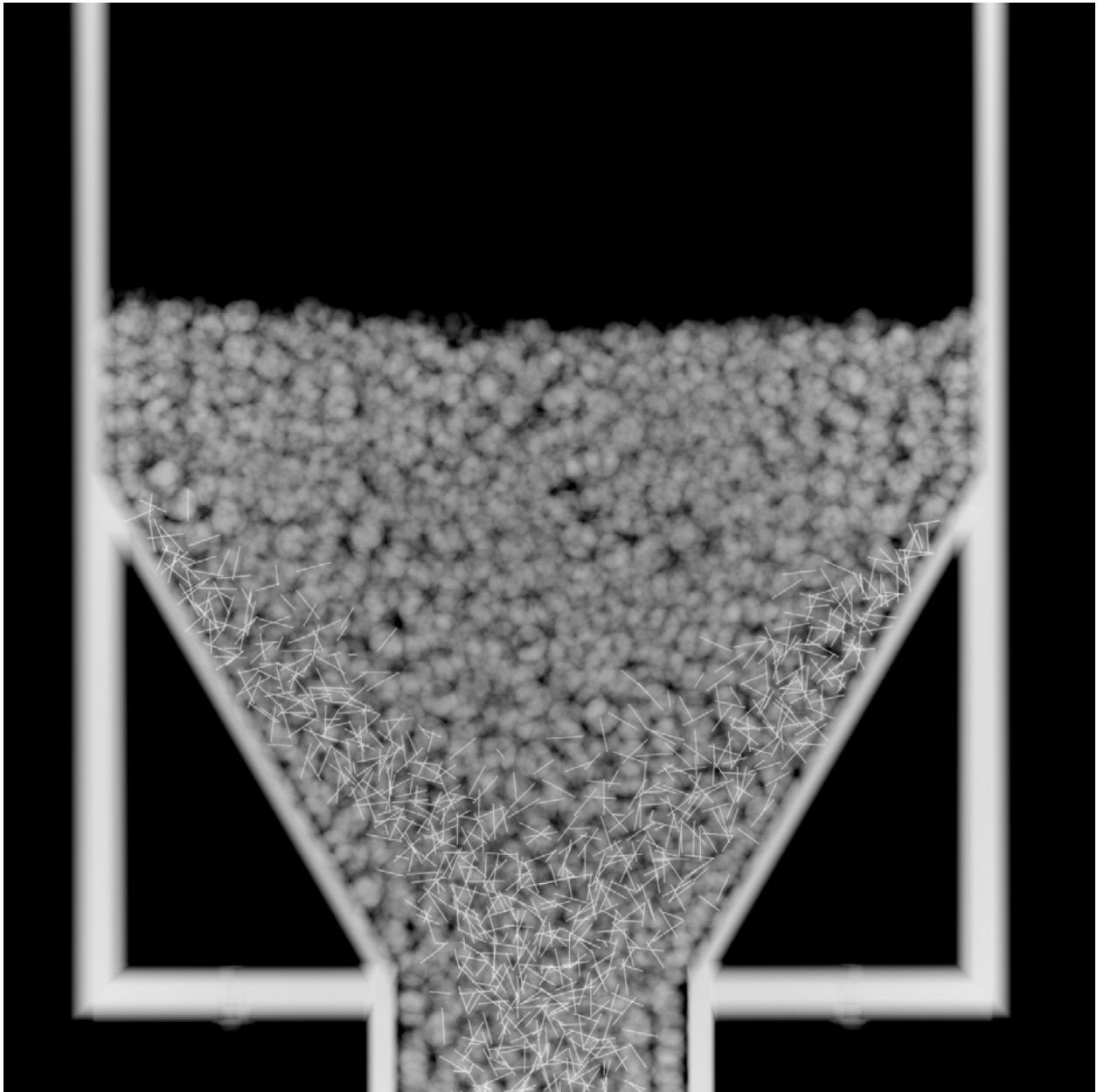
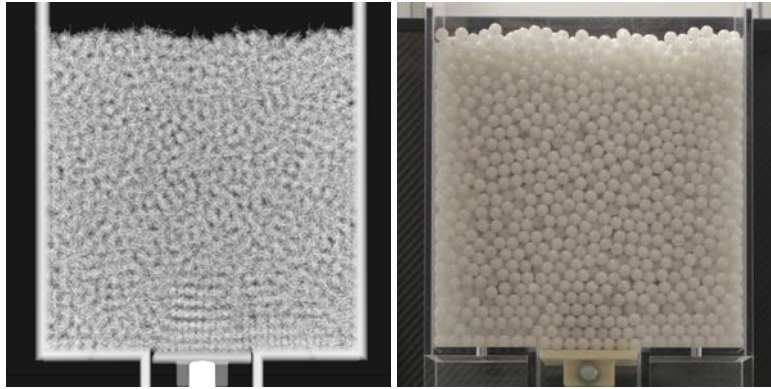
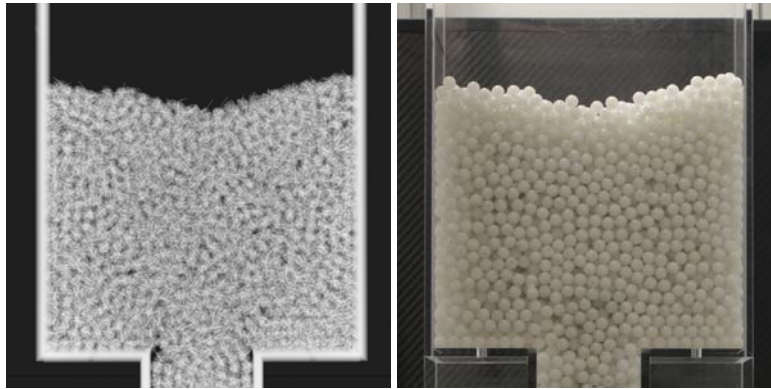


**Figure 2-14-B. Pebble flow visualization run for 60-degree converging silo.**

Piston Displacement = 0 d



Piston Displacement = 16 d



Piston Displacement = 32 d

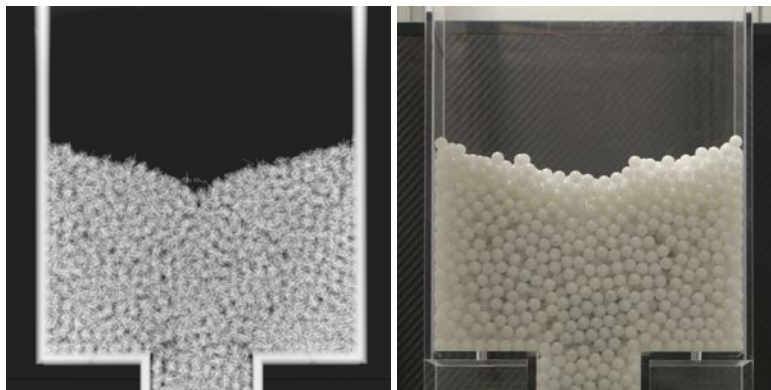
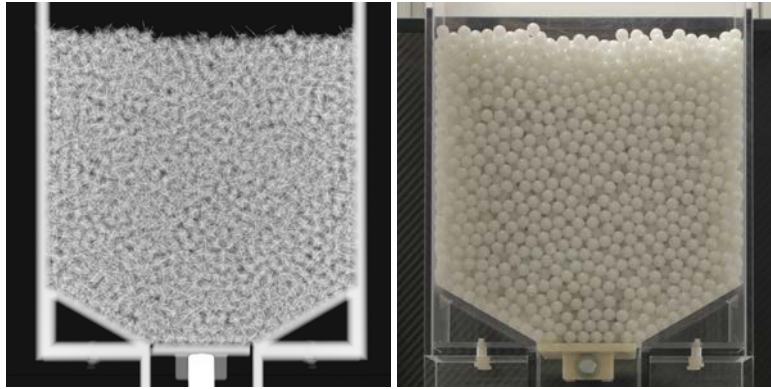
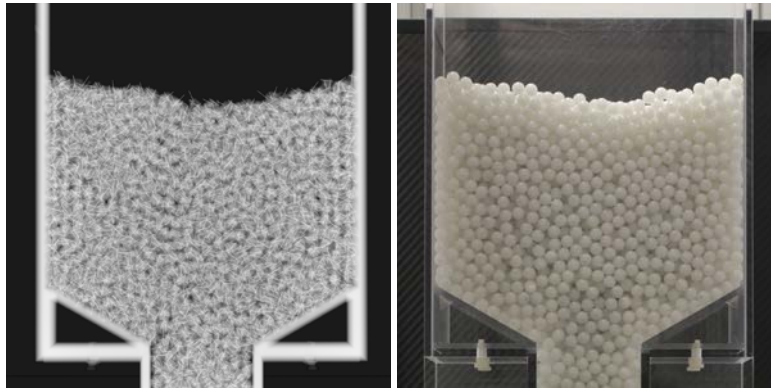


**Figure 2-15. Comparison of the front view for the x-ray image (left), and photograph image (right) for the step drainage of the Quasi-2D Silo test section without wedges for piston displacements of 0, 16, and 32 d.**

Piston Displacement = 0 d



Piston Displacement = 16 d



Piston Displacement = 32 d

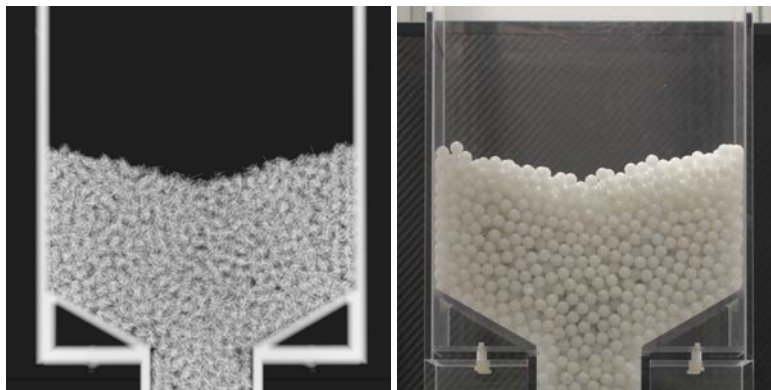
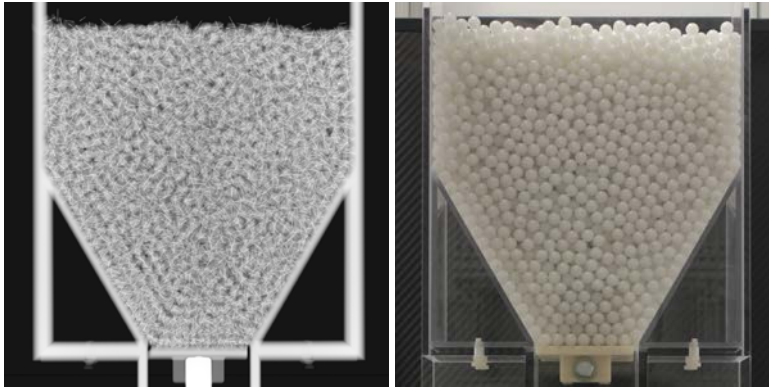
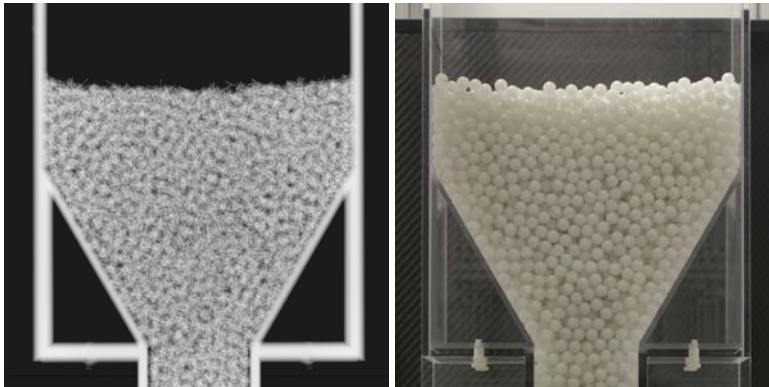


**Figure 2-16. Comparison of the front view for the x-ray image (left), and photograph image (right) for the step drainage of the Quasi-2D Silo test section with 30-degree angle for piston displacements of 0, 16, and 32 d.**

Piston Displacement = 0 d



Piston Displacement = 16 d



Piston Displacement = 32 d

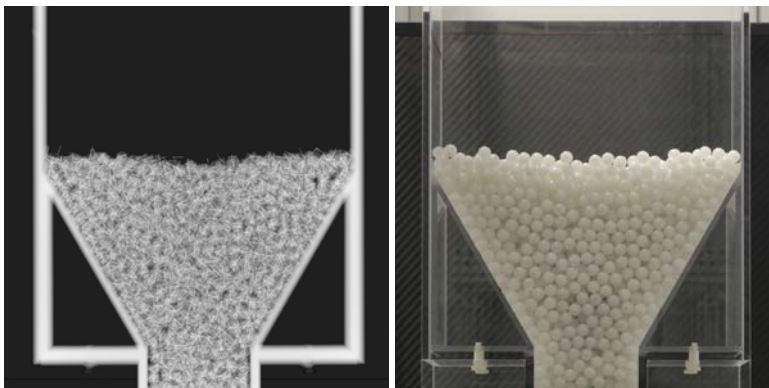


**Figure 2-17. Comparison of the front view for the x-ray image (left), and photograph image (right) for the step drainage of the Quasi-2D Silo test section with 60-degree angle for piston displacements of 0, 16, and 32 d.**

### 2.1.3 Conclusions

This chapter describes the design and preliminary results from the Quasi-2D Silo test section in the X-PREX Facility. The fabricated test section is modular and can be adapted to study a wide variety of hopper angles in both converging and diverging geometries. The motion for these tests is controlled by the retraction of a piston plate attached to the end of a linear actuator in the X-PREX Modular Test Bay. These boundary conditions are well suited to what can be implemented in discrete element method simulations of granular flow.

Innovative design and manufacturing methods were used to develop a random pebble packing piston plate that can be used in the diverging geometry configuration to eliminate the distortions of ordered pebble packing near the surface of a flat piston plate. This packing geometry better represents the true packing in a tall constant area region below the diverging hopper.

Due to the lack of precise geometry in the completed data collection runs, the X-PREX image processing software could not be applied to the collected x-ray images for the Quasi-2D Silo test runs. Instead, qualitative results for the flow visualization with layers of instrumented pebbles and for the evolution of the free surface packing structure are presented. These results are consistent with previously observed behavior for quasi-2D silo drainage. The free surface packing geometry may be used for initial comparison to DEM simulations. These results and animations from the sequence of x-ray images, which cannot be shown in a written report, point to the great potential in the results that will be generated in the future with the X-PREX facility.

## 2.2 Control Blade Insertion Experiment (CoBIE)

In 2013, U.C. Berkeley identified the insertion of a control blade into a packed pebble bed as one of the key technical questions for the Mk1 Pebble Bed Fluoride-Salt Cooled High Temperature Reactor (PB-FHR) design. The significant additional reactivity worth of these shutdown elements (compared to the control rods inserted into channels in the center graphite reflector) make them a highly desirable option for redundant and diverse shut down capabilities.

The force of a control blade inserted directly into a packed bed of spheres is a very important parameter to determine the viability of this kind of shutdown system. Such a design would provide a large amount of shut down worth and generate confidence in the shutdown margins. This strategy was adopted for the THTR gas-cooled pebble bed reactor in Germany, but the forces on pebble bed led to a large number of broken pebbles and complicated the initial operation of that facility. In the salt-cooled pebble bed reactor designs, the insertion of a control blade from the top of the bed may prove to be more feasible due to the reduced body forces in the positively buoyant system and the lubricity provided by the coolant. In core designs with an unconstrained free surface at the bottom of the bed, there are additional degrees of freedom for pebble motion that should also reduce the stress and potential for damage to fuel pebbles.

The x-ray pebble recirculation experiment (X-PREX) facility is uniquely suited to study this safety-related design feature by tracking the positions of pebbles as the control blade displaces them. These results can be used to validate Discrete Element Method (DEM) simulations, which compute the forces on individual pebbles.

In 2014, U.C. Berkeley developed and operated the Control Blade Insertion Experiment (CoBIE). The experiment was designed to examine the feasibility of blade insertion directly into a packed pebble bed. The experiment measures the insertion forces required to drive a control blade directly into a packed pebble bed, as well as the pebble displacements due to such an insertion. By doing this, the experiment will help to inform control blade design unique to direct pebble bed insertion. This chapter presents the results and conclusions from studies conducted in 2014, and also recommends experiments for future work.

### 2.2.1 Experimental Methods and Setup

The X-PREX facility is uniquely suited for the operation of CoBIE. The Data Acquisition (DAQ) system and the linear actuator control system provide the capability to drive the control blade insertion with precision linear motion, while gathering accurate insertion force measurements. Additionally, the X-Ray tomography software provides the capability of pebble displacement tracking during a control blade insertion.

### 2.2.1.1 Physical Description

CoBIE is designed as an acrylic test silo that can be combined with modular wedge inserts, a variety of control blade designs, and a packed pebble bed of variable height. The pebbles used for this experiment are 1.257 cm in diameter (approximately 0.5 inches), and are instrumented with tungsten wires for the purpose of x-ray imaging. The silo can be mounted on the X-PREX turntable assembly in the imaging region (see Figure 2-18 below).

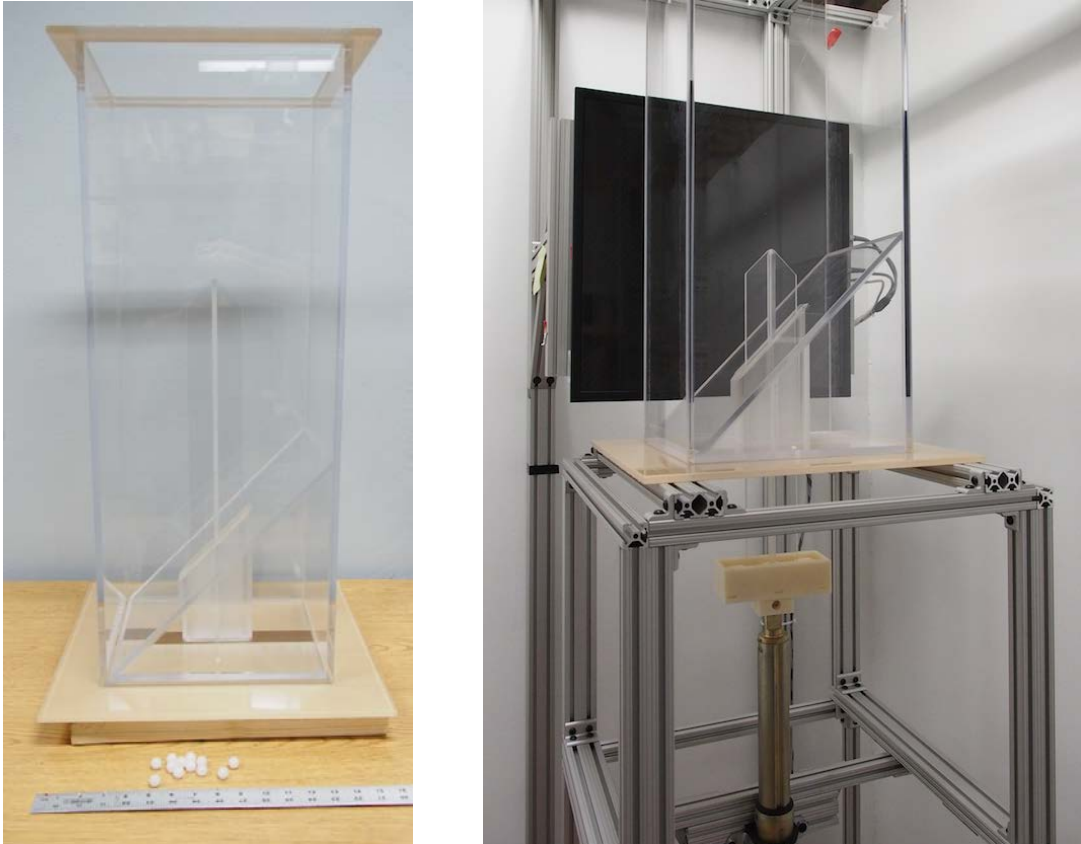


**Figure 2-18. CoBIE test silo physical arrangement without a packed pebble bed. Left: acrylic test silo with 45-degree wedge insert, control blade, and instrumented pebbles. Right: acrylic test silo mounted on the X-PREX assembly with linear actuator partially extended and x-ray detector in-view.**

The CoBIE test silo currently has the option of two different wedge inserts. Each wedge offers a different pebble bed interface plane angle. One wedge has a pebble interface plane that is parallel to the horizon (the “0-degree wedge”), which serves as a separate effects test for blade tip geometry. The other wedge has a pebble interface plane that is inclined at 45 degrees to the horizon (the “45-degree wedge”, shown in Figure 2-18), in order to better represent the inner reflector in an annular PB-FHR core. Both wedges have a Teflon sleeve that acts as a low-friction stabilizing channel for the control blade insertion path. Both wedges can be seen in Figure 2-19.

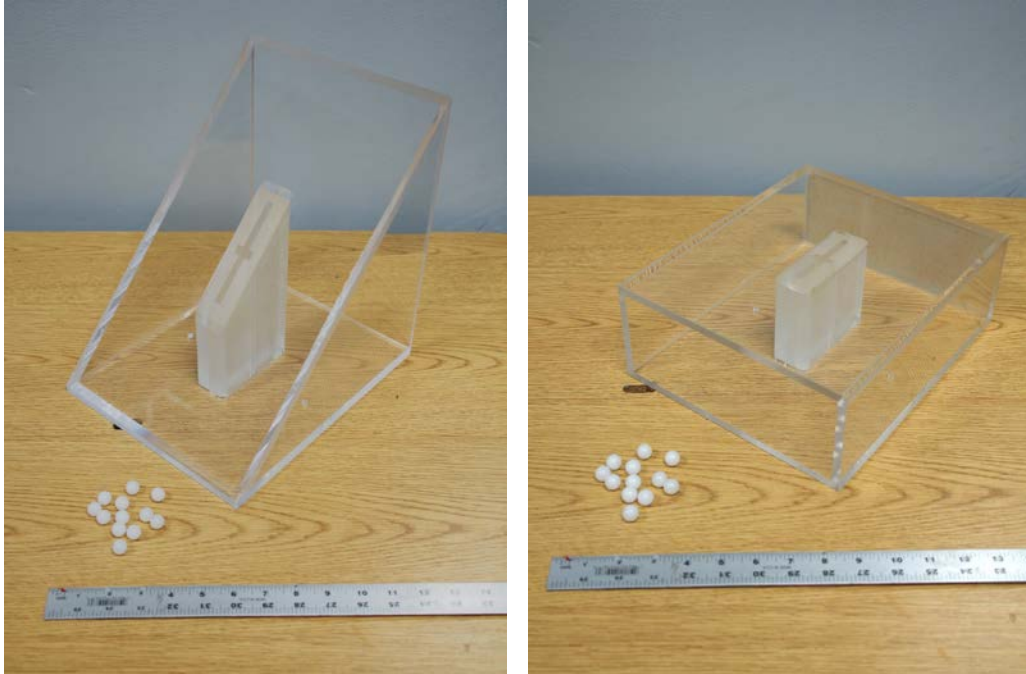


**Figure 2-19. Detailed view of the modular inserts that feature Teflon sleeves for low friction blade insertion. Left: the 45-degree wedge. Right: the 0-degree wedge.**

The primary blade design consists of a flat blade with stiffening ribs, creating a cruciform cross section. The cruciform blade is designed such that it can be fabricated out of 0.635 cm (0.25 in) polycarbonate sheets.

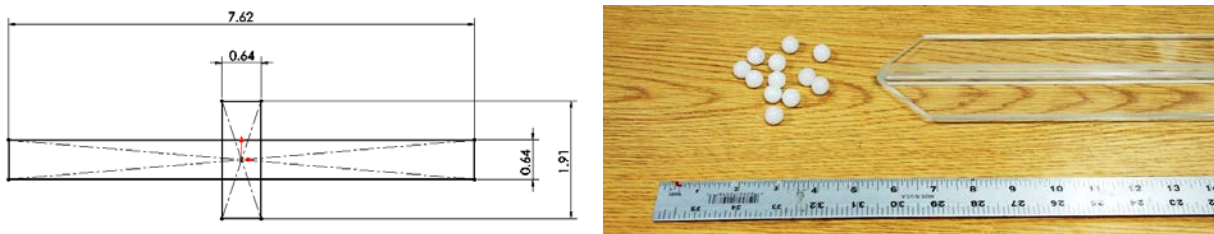


**Figure 2-20. Primary control blade design. Left: cruciform cross section (dimensions in centimeters). Right: Actual blade compared to the 1.257 cm diameter pebbles.**

To date, seven unique blade tip geometries have been studied. The two main tip geometry designs consist of a tip with two variable angles, and a tip with three variable angles. The naming convention is perhaps not so intuitive, so it is important to note that the blade tip with two variable angles has a third angle that is constrained at 90-degrees. It is also important to note that the designated angle of a blade tip is measured from the horizontal, such that a 30-degree blade is blunt compared to a 60-degree blade. The naming convention and tip geometries are shown here for the 30-degree two-angle and three-angle blades:

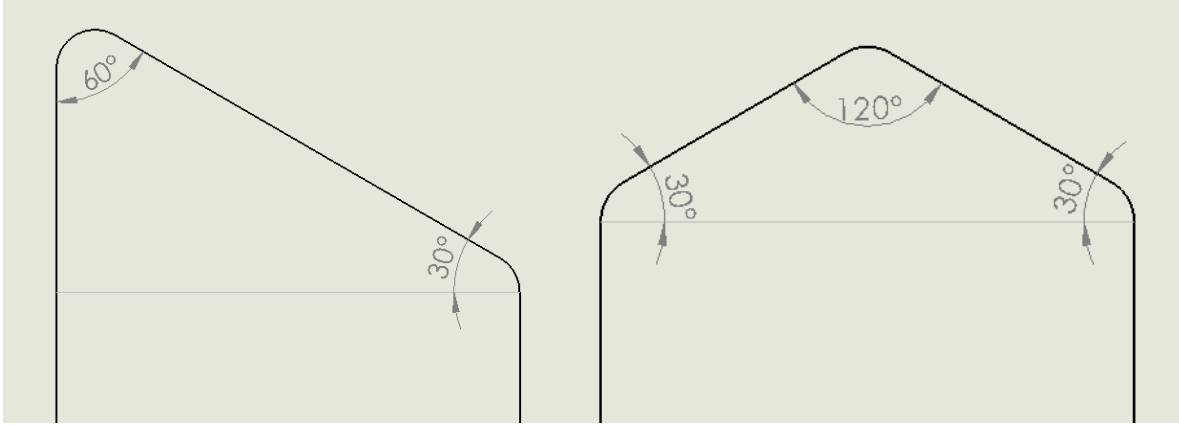


**Figure 2-21. Two blade geometries with annotations showing the unconstrained angles in the tip. Left: 30-degree two-angle blade. Right: 30-degree three-angle blade.**

### 2.2.1.2 Controls and Sensors

The linear actuator, which drives the control blade into the pebble bed is actuated using a relay switch controlled by a National Instruments (NI) DAQ-6009. The position of the actuator can be measured with sub-millimeter precision using a potentiometer built into the actuator. Blade insertion forces are measured using two Tekscan FlexiForce A401 piezoresistive force sensors. Rubber bumpers are adhered to either side of the forces sensors for uniform load distribution. Each force sensor is wired using a simple voltage divider circuit with a 1 M $\Omega$  resistor (see Figure 2-22). The voltage drop across the force sensors are measured using another NI DAQ-6009, which is kept separate from the DAQ-6009 that controls the linear actuator, in order to eliminate electrical noise.

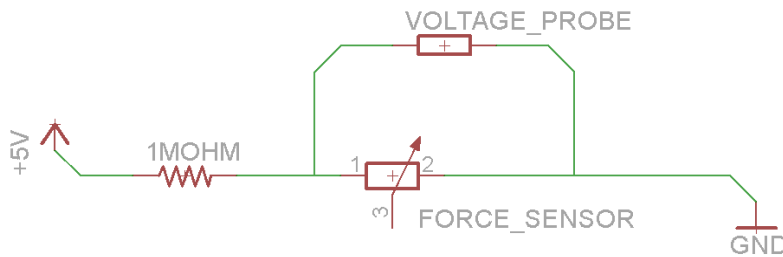


**Figure 2-22. Wiring schematic for the force sensors. Voltage probe is representative of the DAQ-6009.**

Samples are collected at a rate of 16,000 samples per second by a custom NI LabVIEW Virtual Instrument (VI). The VI records approximately 30 data points per second. Each data point consists of a moving average of 100 samples, in order to eliminate electrical noise for a more accurate measurement.

The two force sensors are calibrated before and after the experiment using a seven-point calibration test. Weights are hung on each force sensor using a cantilever beam assembly, in order to evenly distribute the weight on the sensor, while keeping the center of mass below the sensor, for maximum stability. As specified by the manufacturer, the resistance of the force sensors is not linearly proportional to the force applied. Accordingly, a logarithmic function is used to fit the calibration data points. As seen in Figure 2-23, the fit function is quite precise both before and after the experiment.

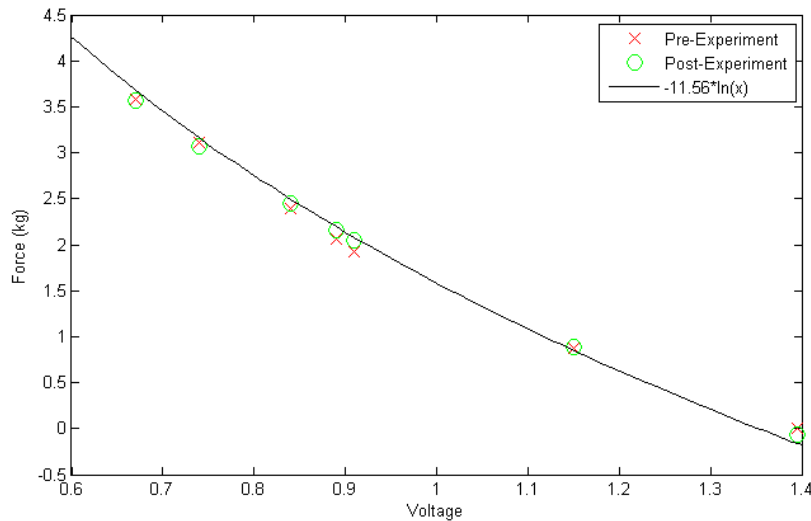


**Figure 2-23. Seven-point calibration of a Tekscan FlexiForce A401 Sensor with resulting fit function. The fit function does not have a Y-axis reference because that value is “zeroed” during the actual experiment.**

During the experiment, the two force sensors are used to measure the vertical insertion force of the blade into the pebble bed. The force sensors are arranged in parallel in an interface between the actuator and the control blade (Figure 2-24). Two sensors are used instead of one to ensure that each sensor is operating within its force limit.

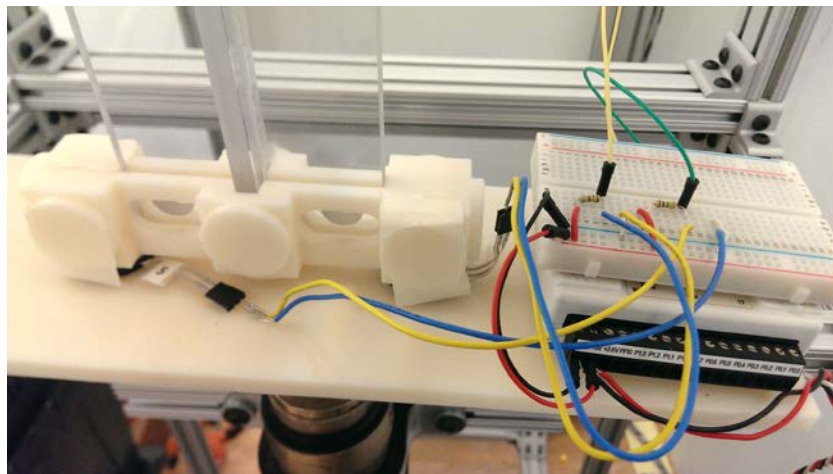


**Figure 2-24. Detailed view of force sensor setup during an experiment.**

The 3D-printed interfaces (beige-colored in Figure 2-24) create parallel contacts between the blade and the actuator for nominal force sensor contact. Blue and yellow wires lead to the two force sensors. The device on the right in Figure 2-24 is the NI DAQ-6009 device with a wiring breadboard mounted on top.

### 2.2.1.3 Test Procedure

There are two separate procedures for tests that collect only insertion forces, and for tests that collect insertion forces in addition to x-ray images.

For tests that collect only force data, the LabVIEW control VI is the only necessary piece of software. Before starting an experiment, the operator should verify that the actuator and force sensors are properly connected and powered. The operator should also establish an extension limit on the actuator (using the custom LabVIEW control VI), so that the actuator does not drive the blade too far and damage the test silo. The operator then fills the test silo with pebbles until the desired pebble bed height is reached. Pebble bed heights are measured from the point of blade entry into the pebble bed to the approximate height of the pebble bed. The two force sensors should be “zeroed” with the control blade stationary in the Teflon sleeve before the tip of the blade contacts the pebbles. The friction caused by the blade sliding through the Teflon sleeve should be very low and can be subtracted from the results later. The operator then uses the LabVIEW VI to simultaneously actuate the linear actuator, driving the blade into the pebble bed, while recording data from the two force sensors. If set correctly, the extension limit should automatically stop the blade insertion at the correct stopping point. The recorded data should be exported to Microsoft Excel using LabVIEW’s built in features. Before performing another experiment, it is important that the operator completely empty and refill the test silo with pebbles. Performing subsequent blade insertions without completely emptying and refilling the pebbles dramatically affects insertion forces, as can be seen in the results section.

For tests that additionally collect x-ray images, the procedure is modified slightly. The additional pieces of software required are the turntable control software, the digital camera control software, and the x-ray image acquisition software. While filling the silo with pebbles, the operator may want to implant a channel of instrumented pebbles around the blade insertion path surrounded by non-instrumented pebbles. This can be achieved by fabricating a makeshift sleeve to regulate where pebbles are placed. Once the silo is filled, the data collection can begin. While collecting x-ray images, the blade is inserted in a stepwise fashion in motion steps of  $\frac{1}{2}$  or  $\frac{1}{4}$  of a pebble diameter. At every blade insertion position, the test silo should be rotated to five different angles using the turntable software. X-ray and camera images should be collected each rotation angle. Once all necessary images are collected for a given motion step, the blade should be inserted an additional motion step. The magnitude of a motion step can be changed in the LabVIEW control VI. Images are then collected at the new motion step. This procedure is repeated until the blade is fully inserted and five x-ray and camera images at five different angles have been collected at each motion step.

#### 2.2.1.4 Test Matrix

The CoBIE setup allows for many degrees of freedom utilizing modular and replaceable pieces. A summary of the possible tests can be seen in Table 2-1 below. Completed tests are marked with a check-mark.

**Table 2-1. CoBIE test matrix.**

	0 Degree Wedge Insert	45 Degree Wedge Insert	Variable Pebble Bed Height	Variable Insertion Speeds	Secondary Insertions
0 Degree Flat Tip	✓	✓	✓		✓
30 Degree 3-Angle	✓	✓	✓		✓
45 Degree 3-Angle	✓	✓	✓		✓
60 Degree 3-Angle	✓	✓	✓		✓
30 Degree 2-Angle		✓	✓		✓
45 Degree 2-Angle		✓	✓	✓	✓
60 Degree 2-Angle		✓	✓		✓

The tests completed in 2014 (Table 2-1) measured insertion force results and not x-ray images, due to the continued development of the x-ray tomography software. The purpose of these initial insertion force tests are to identify ideal blade tip geometries for further study with x-ray tomography and DEM simulation, as is detailed in the future work section.

#### 2.2.2 Results

The tests completed in 2014 have returned detailed insertion force results for many CoBIE testing configurations. These results are summarized in section 2.2.2.1 below. X-ray image collection has only been completed for one configuration (section 2.2.2.2), and sufficient tomography software has not yet been developed to process these images. The insertion force results do however indicate several potential blade designs that are recommended for future x-ray tomography studies, as detailed in the following sections.

### 2.2.2.1 Insertion Force Study

Figures 8 through 14 detail the insertion force results for various CoBIE configurations. Insertion forces are normalized by one pebble mass (one pebble weighs approximately 0.917 grams), and lengths are normalized by one pebble diameter (1.257 cm).

Figure 2-25 shows how different blade tip angles affect the insertion force (note that the 0-degree tip is the most blunt and 60-degree tip is the sharpest). All tests in Figure 2-25 use the 0-degree wedge insert, so the initial contact area of a blade with the pebble bed is directly proportional to how blunt the blade is (inversely proportional to the blade angle).

It is hypothesized that the most blunt blade will have the sharpest increase of force during initial contact with the pebble bed. This expectation is due to the largest initial contact area, which consequently attempts to displace the maximum amount of pebbles. The empirical results of Figure 2-25 support this hypothesis, showing the sharpest force peak with the 0-degree blade.

It is also hypothesized that the sharper the blade, the lesser the maximum insertion force. This is because a sharper blade should tend to displace pebbles laterally instead of vertically, decreasing the displacement force on the tip of the blade. The empirical results support this hypothesis for the 0, 30 and 45 degree blades. The 60 degree blade shows an increase in maximum force compared to the 30 and 45 degree blades. This result is attributed to the stochastic nature of the packed pebbled bed.

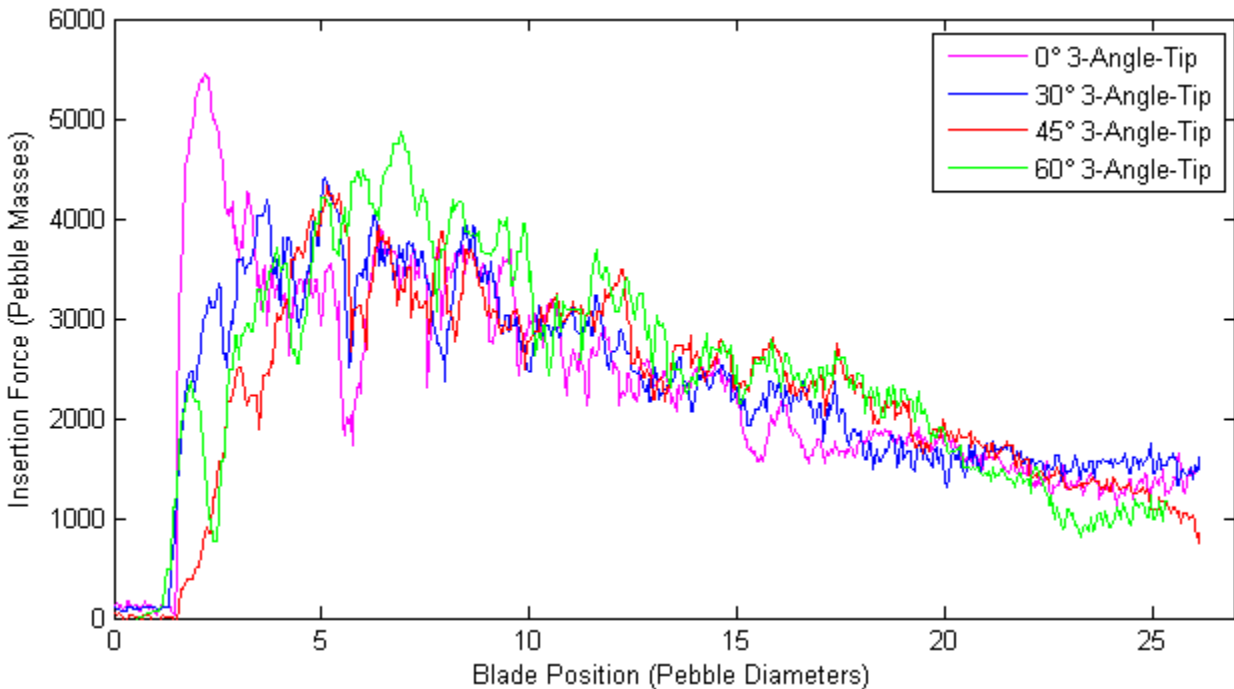


**Figure 2-25. Insertion force vs. blade position for four different 3-angle tips with the 0-degree wedge insert and a pebble bed height of 24 pebble diameters above the entry location.**

The results from Figure 2-25 suggest that a blade tip with a leading edge parallel to the pebble bed interface plane (the wedge insert plane in CoBIE) will have the greatest initial insertion force. To test this, the two-angle blade tips are inserted into the packed pebble bed with the 45-degree wedge insert. Figure 2-26 supports this claim, showing that the 45-degree blade inserted through the 45-degree wedge results in a dramatically larger initial force than the other two blades.

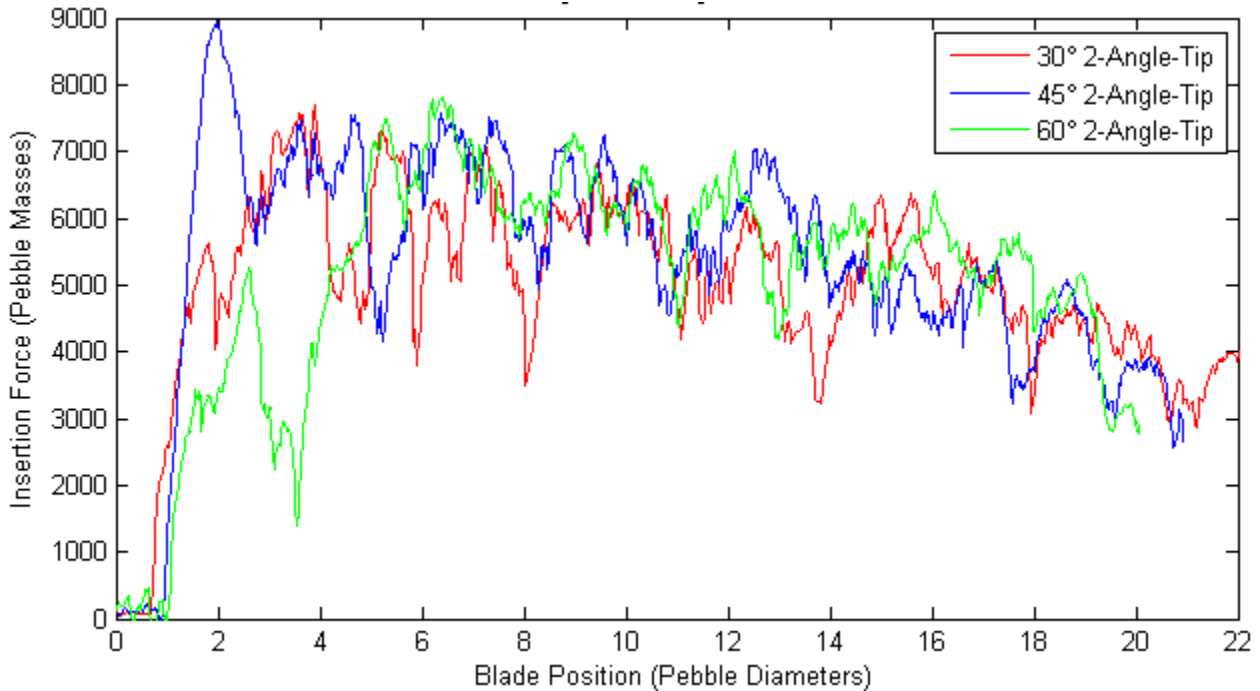


**Figure 2-26. Insertion force vs. blade position for three different 2-angle tips with the 45-degree wedge insert and a pebble bed height of 36 pebble diameters above the entry location.**

Because of the dramatic initial peak in force seen in Figure 2-26 for the 45-degree 2-angle blade, this blade is used to study insertion force as a function of pebble bed height. The insertion force profiles as a function of blade position for four different bed heights can be seen in Figure 2-27.

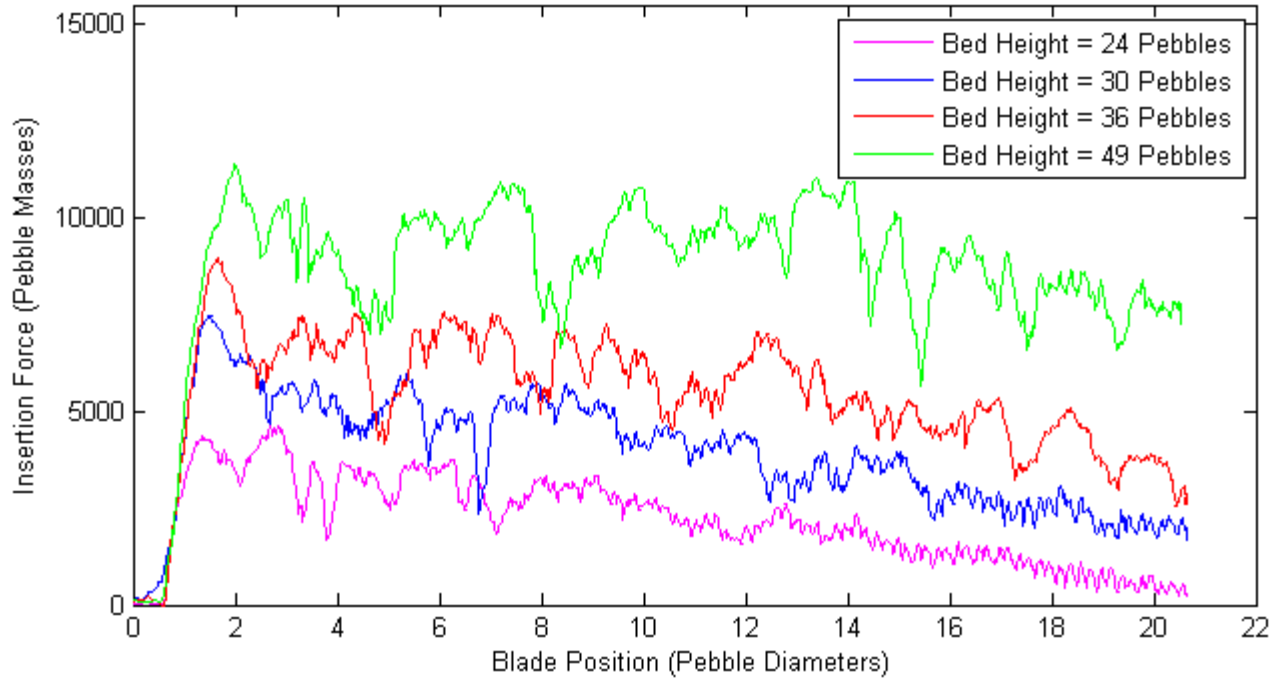


**Figure 2-27. Insertion force vs. blade position for the 45-degree two-angle blade into four different pebble bed heights with the 45-degree wedge insert.**

Clearly, a taller pebble bed results in an increase of insertion force, as would be expected. It is hypothesized that the maximum force required to drive a blade into a packed pebble bed reaches an asymptotic value as the bed height increases. Figure 2-28 supports this hypothesis, plotting the maximum insertion forces from Figure 2-27 against the four bed heights.

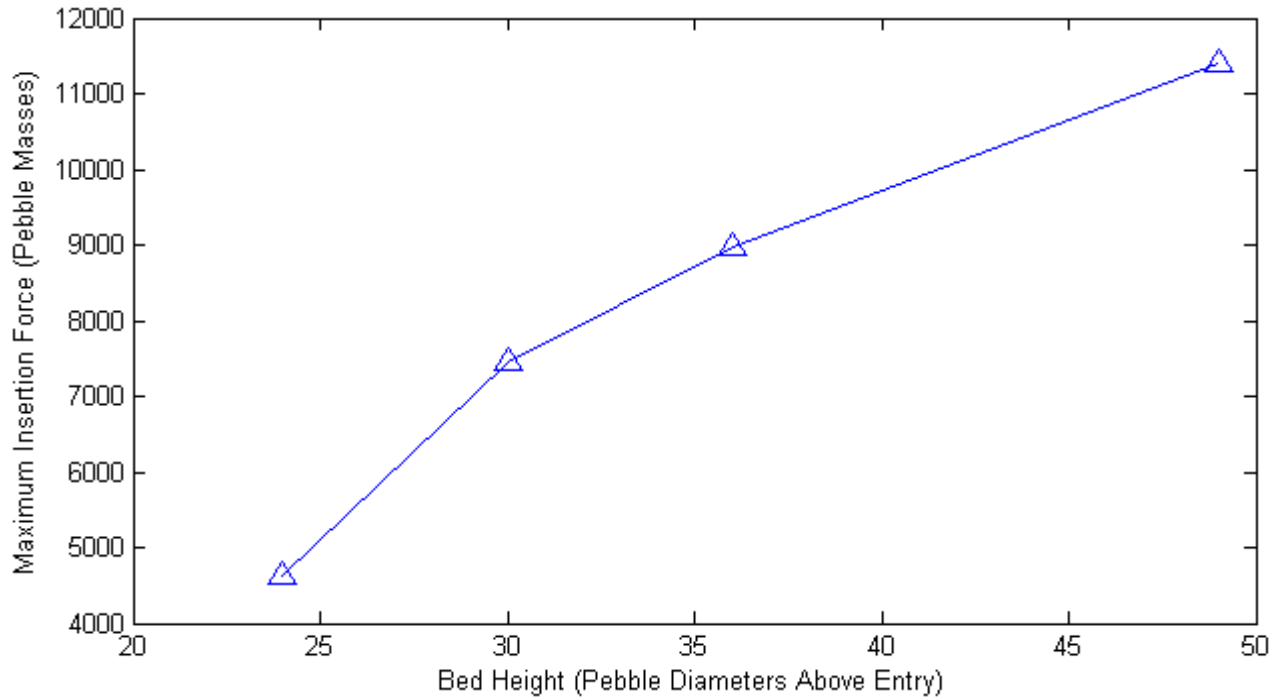


**Figure 2-28. Maximum insertion force vs. bed height for the 45-degree two-angle blade with the 45-degree wedge insert.**

A comparison of the 2-angle and 3-angle tip geometries is vital to the design of control blade shutdown elements for pebble beds. It is likely that the two tip designs will displace different amounts of pebbles in different directions. Consequently, the maximum force on pebbles will be different for the two tip designs. A force study of the two designs shows that the insertion forces required for the two designs is comparable, but that the force required to insert a 2-angle tip is larger than the force required to insert a 3-angle tip. This result can be seen in Figure 2-29.

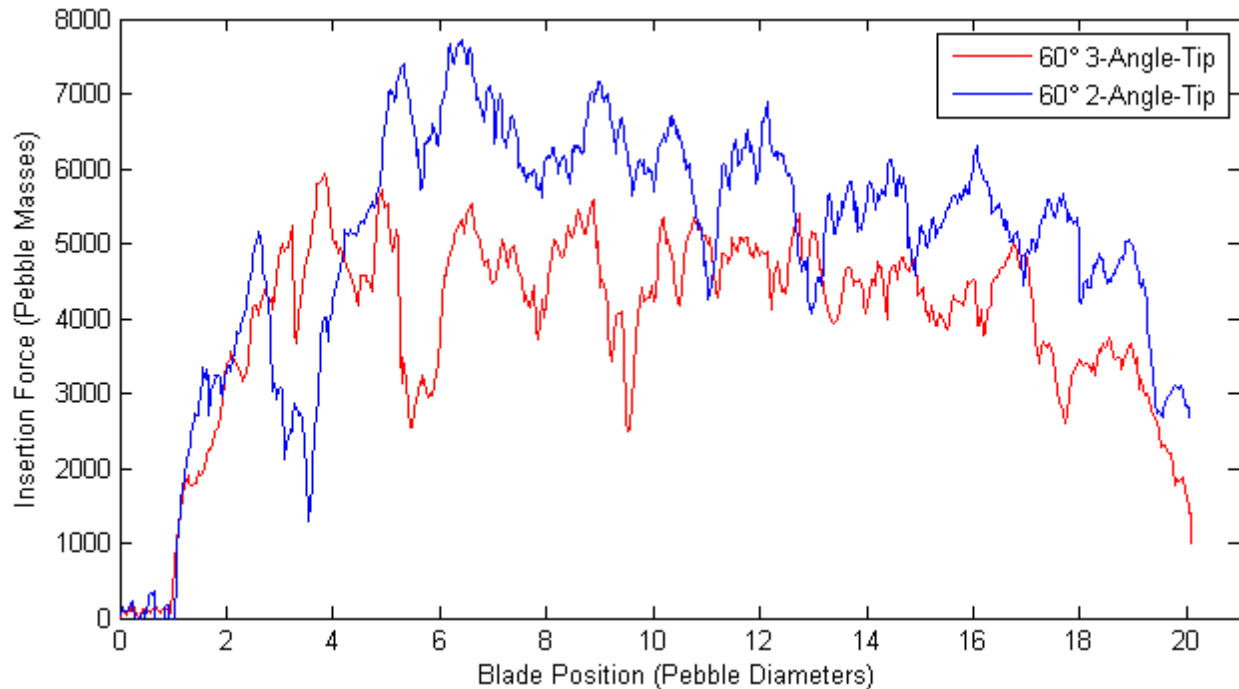


**Figure 2-29. Insertion force vs. blade position for 60-degree 2-angle and 3-angle tip blades with the 45-degree wedge insert and a pebble bed height of 36 pebble diameters above the point of entry.**

Figure 2-30 shows the result of repetitive blade insertions without the emptying/refilling of the test silo with pebbles. In this case, the packed pebble bed seems to undergo a re-ordering and decrease in density due to the first insertion. Subsequent blade insertions require many orders of magnitude less force at the entry region and converge to a similar force at the fully inserted region. The mechanisms by which this occurs will be particularly interesting to study with x-ray tomography.

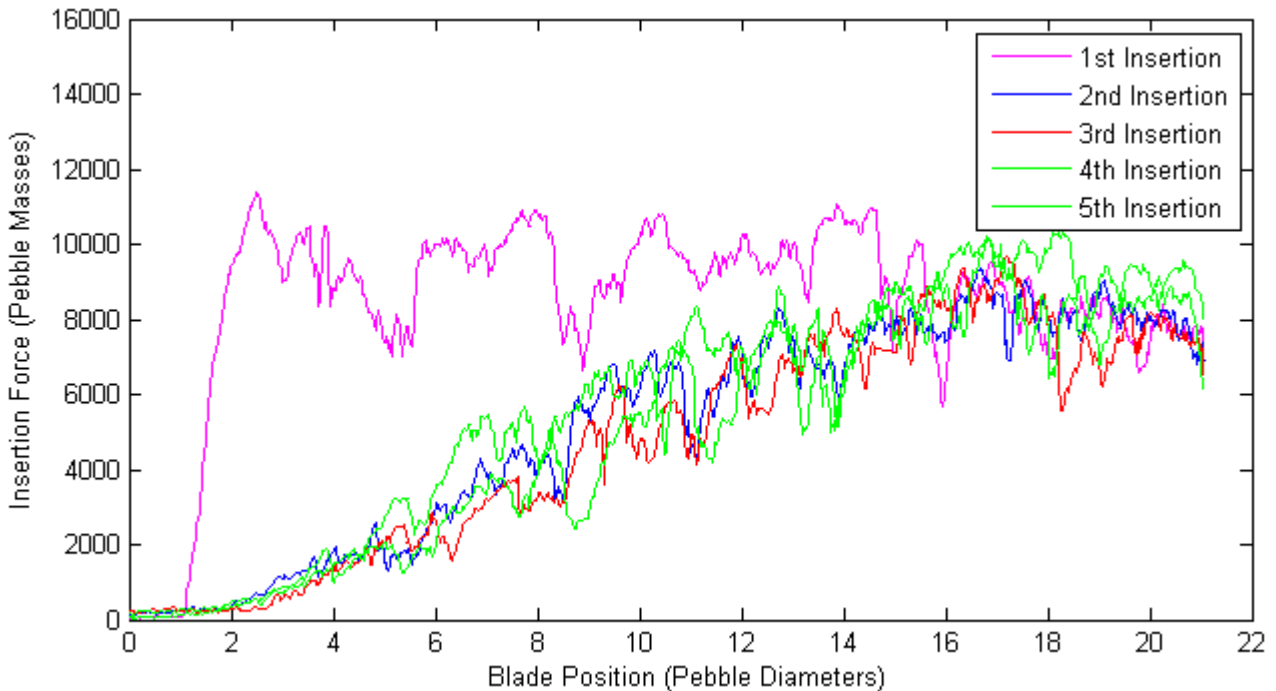


**Figure 2-30. Insertion force vs. blade position for five consecutive blade insertions without emptying or refilling the silo with pebbles. Configuration consists of 45-degree two-angle tip blade with 45-degree wedge insert and a pebble bed height of 49 pebble diameters above the point of entry.**

All experiments discussed in this report up to this point were conducted with a continuous, fixed speed blade insertion. While collecting x-ray images, the control blade will be inserted a fraction of a pebble diameter at a time, creating a stepwise motion profile.

Figure 2-31 aims to show that the distortion in measured forces during a continuous fixed speed insertion are negligible when compared to a stepwise insertion. The blue and green data points in Figure 2-31 were gathered with a  $\frac{1}{2}$  pebble diameter stepwise insertion motion. It can be seen that with small pebble beds, the stepwise motion results in a slightly larger force profile. With larger pebble beds, the two motion profiles result in very comparable forces. Furthermore, many of the same force peaks can be seen at the same location in the force profiles resulting from stepwise and continuous insertion motion.

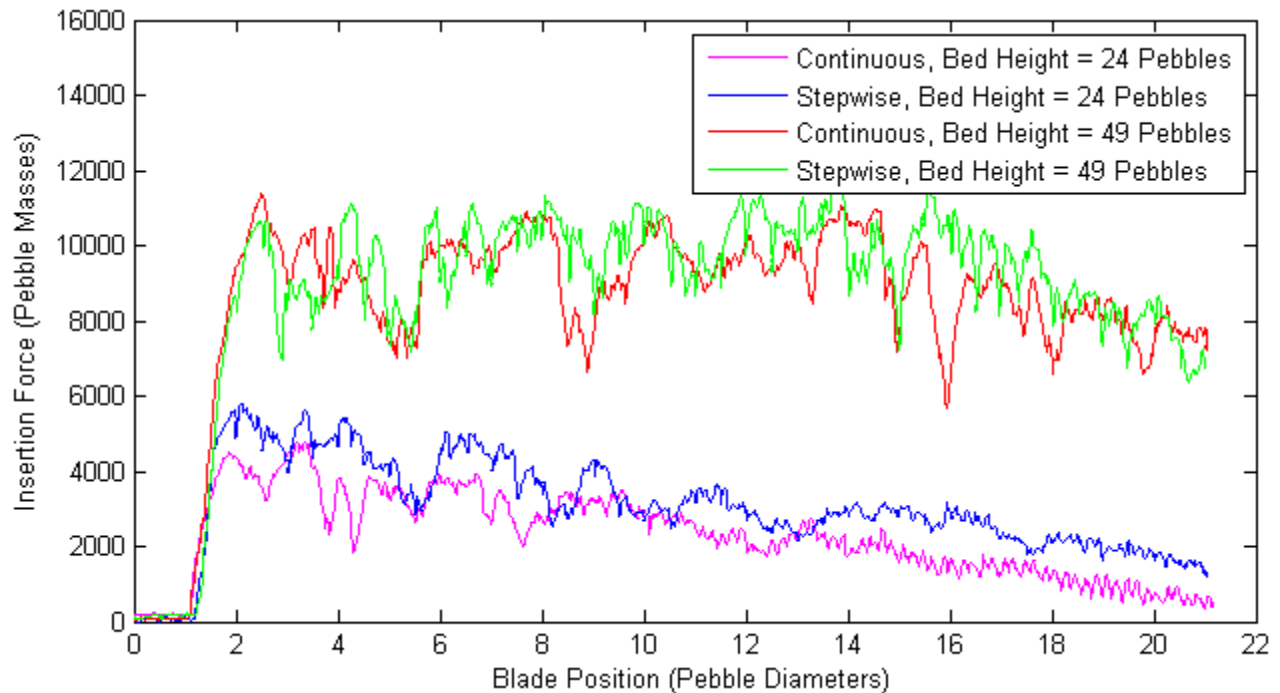


**Figure 2-31. Insertion force vs. blade position for two different pebble bed heights and two different insertion methods. Configuration consists of 45-degree two-angle tip blade with 45-degree wedge insert.**

#### 2.2.2.2 X-Ray Study

The x-ray pebble tomography software is still in development at UC Berkeley. As a result, the x-ray images cannot yet be fully processed to yield 3-dimensional pebble locations and displacements. Qualitative results can be seen in the images below for the 45-degree 3-angle tip blade with the 45-degree wedge insert.

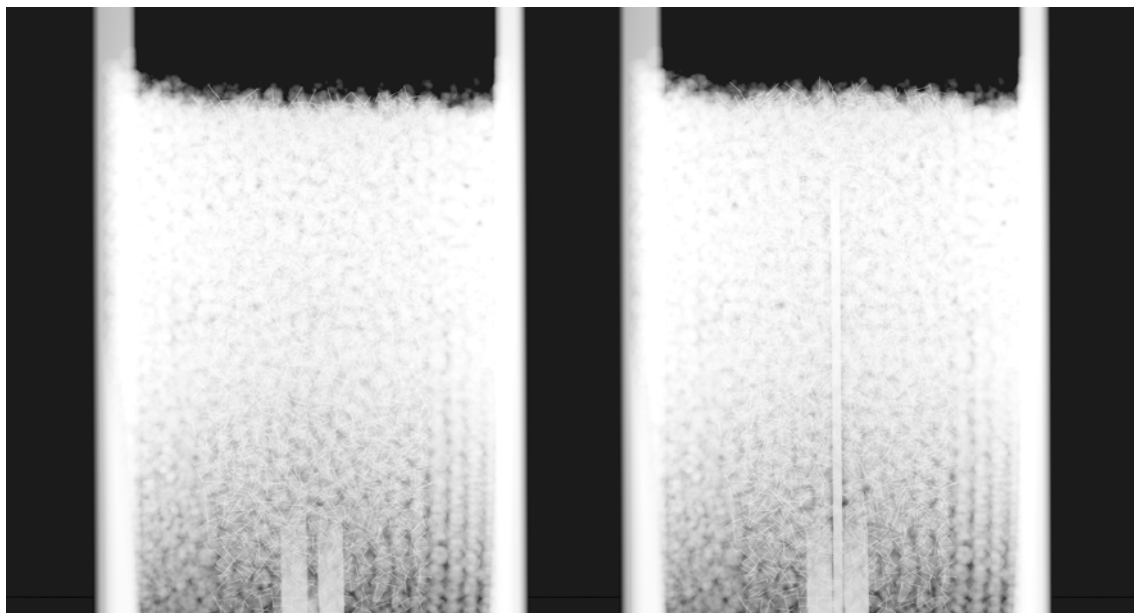


**Figure 2-32. 0-degree x-ray images showing the blade fully retracted (left) and fully extended (right).**

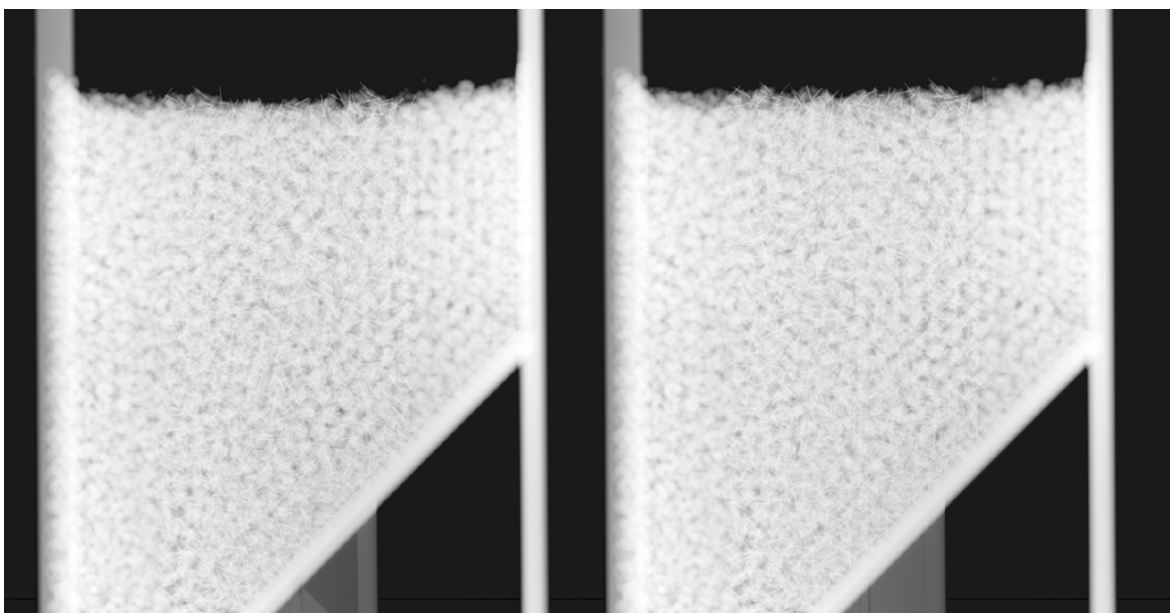


**Figure 2-33. 90-degree x-ray images showing the blade fully retracted (left) and fully extended (right).**

### 2.2.3 Conclusions

The results from the 2014 CoBIE experiments reveal a great deal about how to design a control blade for packed pebble bed insertion. Clearly, one of the major factors to consider is the maximum force required for control blade insertion. 10 CFR Appendix A includes General Design Criteria 26 and 29 that detail guidelines for preventing “stuck control rods” and assuring an “extremely high probability of accomplishing safety functions”<sup>4</sup>. Figure 2-28 suggests that given an infinitely tall bed, there will be a maximum force required for insertion. For large pebble bed reactors with tall pebble bed cores, this maximum force requirement for an infinitely tall bed could serve as a useful bounding case for pebble bed reactor shutdown systems. Furthermore, this infinite bed maximum force could serve as an NQA-1 standard for reactivity control system design requirements in pebble bed reactors.

Blade tip geometry including the bluntness of the blade could further reduce the maximum insertion forces required for blade insertion, as seen in Figure 2-25 and Figure 2-26. A sharper blade could decrease the maximum force necessary to drive the blade into the pebble bed, therefore improving the probability of successful safety-related shutdown functions. It is important to note that this would also affect the distribution of forces on the pebbles in direct contact with the blade tip, as a sharper blade exhibits a much smaller initial contact area with the pebble bed. Furthermore, the two-angle and three-angle tips show a discrepancy in force that favors the 3-angle tip for minimum required insertion force. However, the 3-angle tip exhibits approximately half of the initial pebble-bed contact area as the 2-angle tip, suggesting a larger initial contact force on individual pebbles by the 3-angle tip. Further work will have to be done to examine the tradeoff between maximum insertion force and maximum contact force on individual pebbles.

Figure 2-30 shows that additional variables must be considered after a control blade insertion event. The dramatic decrease in force for subsequent insertions seen in Figure 2-30 demonstrates a dramatic change in the porosity and randomly packed arrangement of the pebble bed. This rearrangement of the core geometry would have implications affecting many more parameters than just the subsequent blade insertion forces. A change in porosity of the packed pebble bed core after a shutdown event could affect the neutronics as well as the thermal hydraulics of the core. Specifically, this would affect a pebble bed reactor startup procedure directly following a shutdown event. Further work using x-ray tomography to analyze exactly how a blade insertion event rearranges the packed pebble bed can be used to help develop a safe reactor shutdown and restart procedure.

The results from the stepwise insertion experiment seen in Figure 2-31 support the notion that data collected during an x-ray image collection procedure using a stepwise blade insertion motion profile will be directly comparable to a continuous motion blade insertion. This will be significant for future CoBIE x-ray experiments that will associate the insertion force results presented in this report with individual pebble location and rotation measurements.

---

<sup>4</sup> Nuclear Regulatory Commission. “NRC Regulations Title 10, Code of Federal Regulations, Appendix A to Part 50 – General Design Criteria for Nuclear Power Plants”. Criterion 26 and 29. December 1, 2014.

## 2.3 Cylindrical Silo Experiment

Pebble drainage in a cylindrical silo (Figure 2-34) is a problem in granular flow that is directly relevant to pebble recirculation in nuclear reactor cores that can be studied in the X-PREX facility. The X-PREX facility can be used to track pebble motion in cylinders with an inner diameter to pebble diameter ratio ( $D/d$ ) up to 28, based on the size of the x-ray detector. This scale is comparable to that of small research and test pebble bed reactors such as the HTR-10 ( $D/d = 30$ )<sup>5</sup> and the TMSR-SF1 ( $D/d = 22.5$ )<sup>6</sup>. For reactors of this scale, the X-PREX facility can provide pebble packing configurations and residence time distributions that can be used to improve the physical accuracy of neutronics models and to study reactivity effects from stochastic pebble motion.



**Figure 2-34. Cylindrical silo test section installed in the X-PREX facility.**

---

<sup>5</sup> Z. Wu, L.-W. Hu, and D. Zhong, The Design Features of the HTR-10, Nuclear Engineering and Design, v218, p. 25, 2002.

<sup>6</sup> X. Yu, “Chinese TMSR-SF and TMSR-LF Development,” presented at the 5th FHR Workshop on Beyond Design Basis Events, Berkeley, CA, Jan. 2014.

### 2.3.1 Experimental Methods and Setup

#### 2.3.1.1 Physical Description

The baseline design for the cylindrical silo is based on the dimensions of a pebble bed FHR test reactor currently in planning by the Shanghai Institute of Applied Physics (SINAP). The proposed design would use 6 cm diameter pebbles and a container to pebble diameter ratio of 22.5, which can be studied in the X-PREX facility. This geometry provides an opportunity to complete experimental analysis that is directly applicable to a specific reactor design. Figure 2-35 shows a schematic view of the SINAP random bed test reactor design, as presented by Liu (2014)<sup>7</sup> and Table 2-2 gives the key scaling parameters for the test section in X-PREX relative to the TMSR-SF1 design. Based on the dimensions of the SINAP TMSR-SF1 design, U.C. Berkeley has selected an outer diameter of 28.6 cm for the test section.

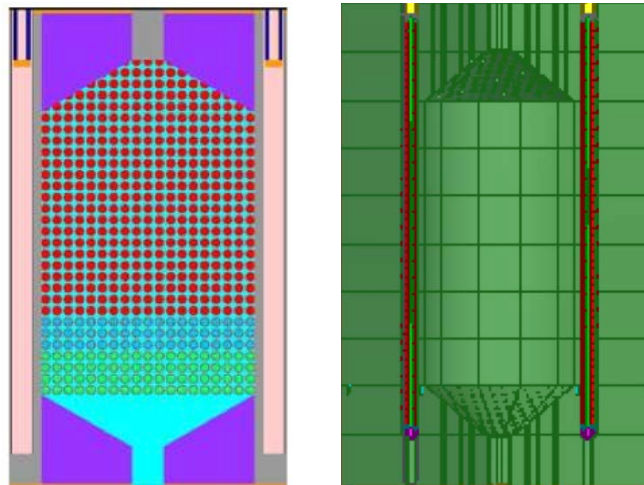


**Figure 2-35. Neutronics schematic (left) and CAD design model (right) for the random packed TMSR-SF1 reactor currently being considered by SINAP. The design uses 6 cm diameter pebbles and has a pebble to core diameter ratio of 22.5, which is within the imaging capabilities of the X-PREX facility.**

**Table 2-2. Key scaling parameters for TMSR-SF1 and the Cylindrical Silo Test Section in X-PREX.**

Parameter	TMSR-SF1	X-PREX
Power	10 MW	--
Pebble Diameter	6 cm	1.26 cm
Number of Pebbles	Start: 10,800 Full: 14,650	Start: 10,800 Full: 14,650
Core Outer Diameter	135 cm	28.6 cm
Core Height	180 cm	38.1 cm
Cone Angle	30 degrees	30 degrees

<sup>7</sup> Guimin Lui, “Design Considerations on Neutronics and Thermal-Hydraulics in TMSR-SF1,” presented at Berkeley, CA, October, 2014.

Figure 2-36 shows the final design for the cylindrical silo test section installed on the modular test base and Figure 2-37 shows the side cross-section views for the 30, 45, and 60-degree conical sections. These conical sections can be used for studies of both converging and diverging regions in the cylindrical silo. Each cone converges to a minimum diameter of 7.0 cm ( $5.5 d$ ) at the defueling chute, which is close to the minimum diameter commonly used in handling granular materials to avoid jamming. U.C. Berkeley completed the fabrication of these three conical sections in 2014. Figure 2-38 shows the machined cones for the 30 and 60-degree configurations and Figure 2-40 shows a sample x-ray image of the 45-degree cylindrical silo test section loaded with 8,000 pebbles instrumented with tungsten wires.

The wall of the cylindrical silo test section is made from cast acrylic tubing and the sourced tubing can be used to study packed beds up to heights of 126 cm ( $100 d$ ). Appropriate lengths of tubing are also able to accommodate packed beds with heights of 28.6 cm ( $22.5 d$ ), 57.2 cm ( $45 d$ ), and 113.4 cm ( $90 d$ ) if a second cone is installed at the top of the test section to simulate a diverging region at the core inlet.

Pebble motion for the Cylindrical Silo test section is controlled by two different configurations in the Modular Test Bay. For the converging studies, the area ratio of the constant area region to the defueling chute is too large to use the linear actuator. Therefore the continuous discharge device is used to unload pebbles. The counting scale in the base allows the facility operator to control the number of discharged pebbles in each motion step to within approximately 10 pebbles. For the diverging geometry studies, the packed bed motion will be controlled by the retraction of a random piston plate (Figure 2-39) while the continuous discharge device will be used to load additional pebbles into the narrow loading channel above the diverging conical region.

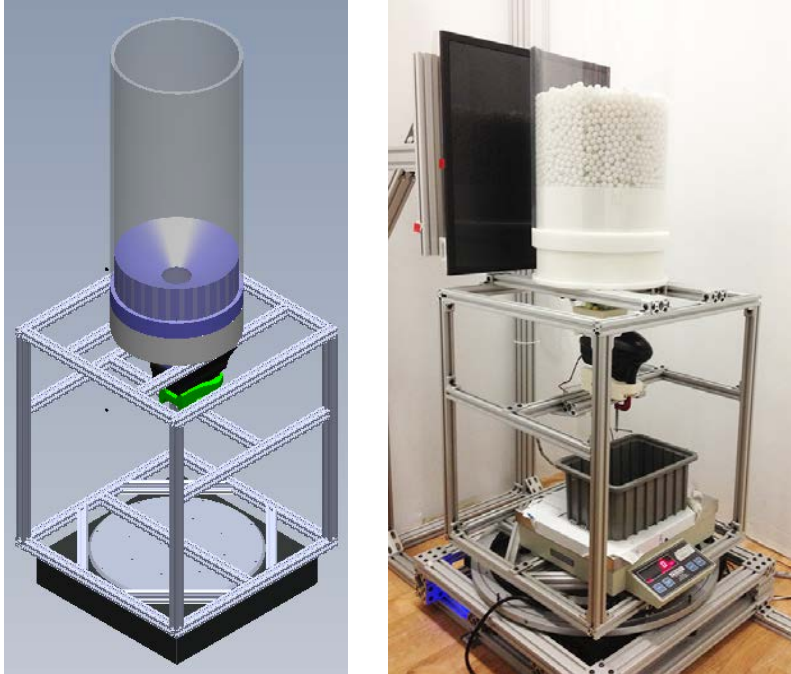


**Figure 2-36. CAD design (left) and installed test section (right) of the Cylindrical Silo test section mounted on the modular test base. The conical region is machined from a billet of acetal resin.**

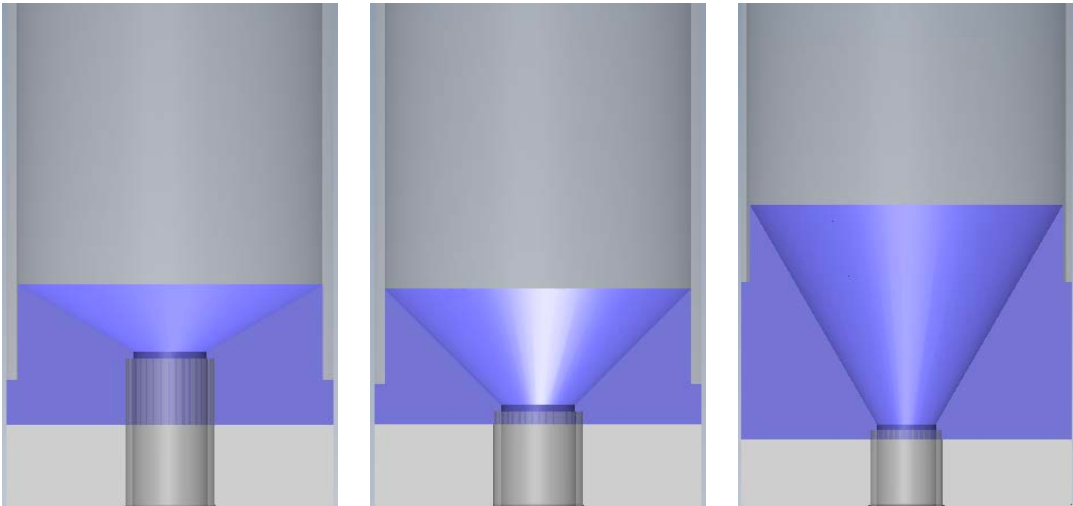


**Figure 2-37. Side cross-sectional views for the 30 (left), 45 (center), and 60-degree (right) configurations of the Cylindrical Silo test section.**



**Figure 2-38. Machined cones with 30 (left) and 60-degree (right) hopper angles.**



**Figure 2-39. Random packing piston plate for use in the Cylindrical Silo test section.**

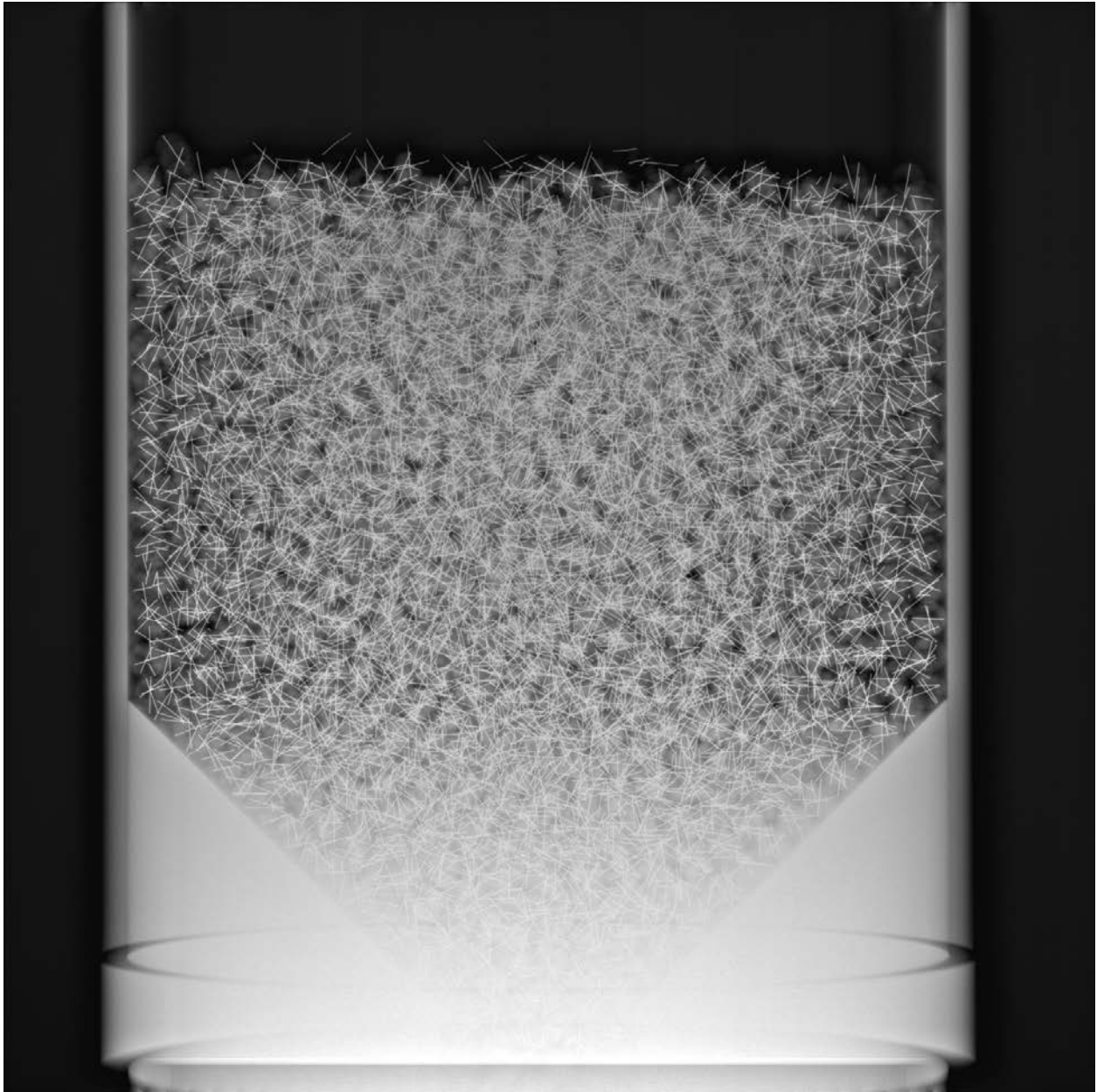


**Figure 2-40. X-ray image of the Cylindrical Silo Test Section with a 45-degree cone angle loaded with 8,000 pebbles instrumented with tungsten wire inserts.**

### 2.3.2 Results

The primary effort in 2014 was devoted to complete the design and fabrication of the Cylindrical Silo Test Section. U.C. Berkeley has completed an initial flow visualization test for the 45-degree converging silo loaded with layers of instrumented pebbles and unmodified high density polyethylene pebbles (Figure 2-41). For this test, each of the eight layers contains 1,000 pebbles. No additional pebbles were loaded onto the top of the bed during the data collection run. X-ray images were collected after the discharge of 200 pebbles until the test section was completely drained.

Figure 2-42-Figure 2-44 show sample results of this flow visualization study, including the initial packing configuration and images after the discharge of 2,000 (1/4) and 4,000 (1/2) of the pebbles. After the discharge of 2,000 pebbles (Figure 2-43), the top two layers are still clearly resolved indicating that there is not strong channeling effects in the region higher than approximately 10 pebble diameters above the top of the conical region. Some holdup can be observed in these layers at the left and right edge of the image where pebbles are in contact with the outer wall, however no stagnant pebble region is observed. The bottom two layers in Figure 2-43 show a significant amount of channeling in the region directly above the defueling chute. After the discharge of 4,000 pebbles (Figure 2-44), the bottom three layers are sufficiently mixed so that it is difficult to tell where their boundaries are. The top layer, however, is observed to have a small central region where the instrumented pebbles extend down to the next layer, while layer remains distinct at the left and right edge of the test section. These results are consistent with past observations of granular flow in conical hoppers.



**Figure 2-41. Cylindrical Silo Test Section loaded with alternating layers of instrumented (white) and unmodified (yellow and green) pebbles used for flow visualization tests. Each layer contains 1,000 pebbles and there are 8,000 pebbles in the test section.**

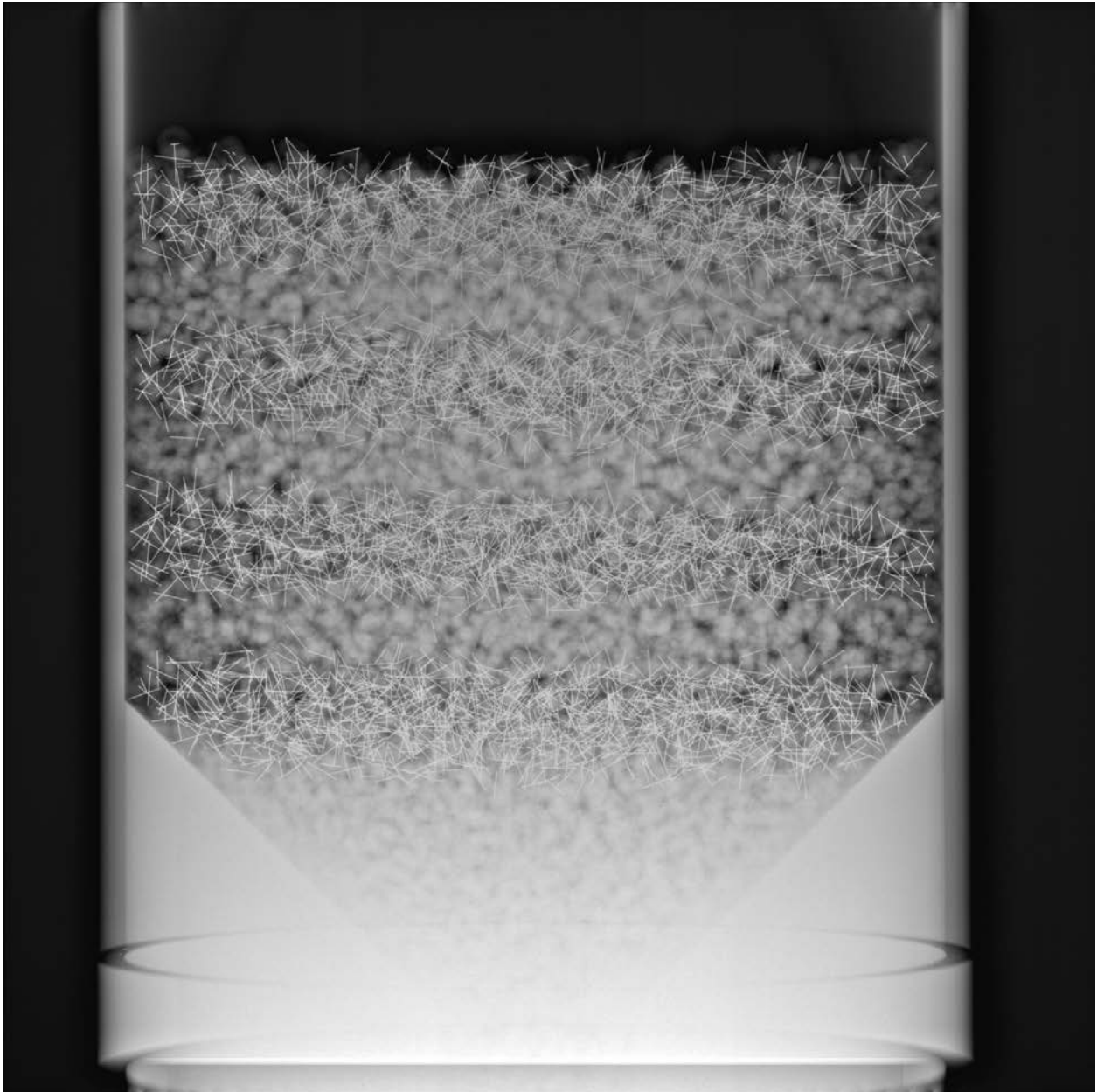


**Figure 2-42. Initial configuration of the cylindrical silo flow visualization data run.**

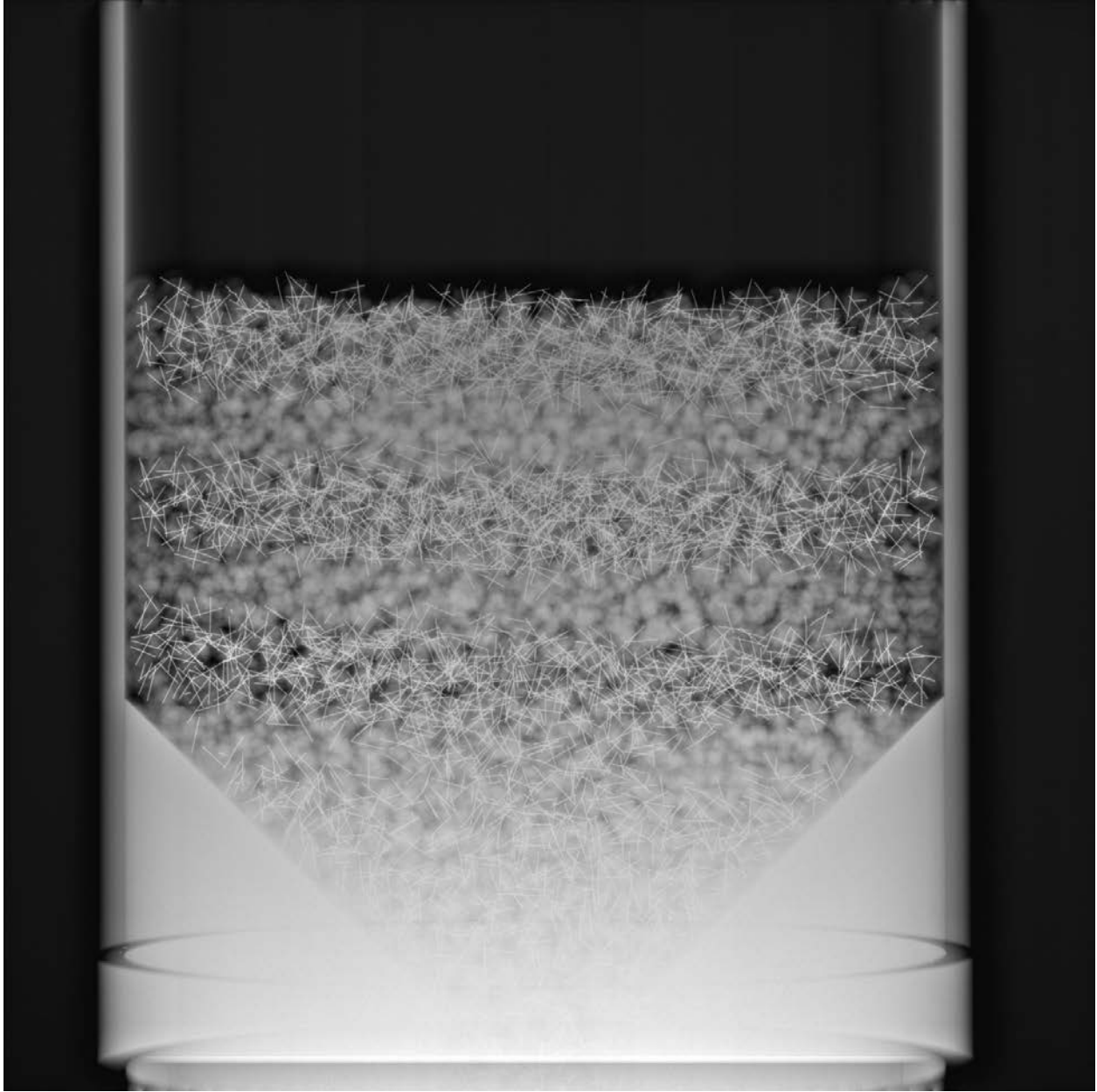


**Figure 2-43. Cylindrical silo flow visualization run after the discharge of 2,000 pebbles (one quarter of the pebbles in the original packed bed).**

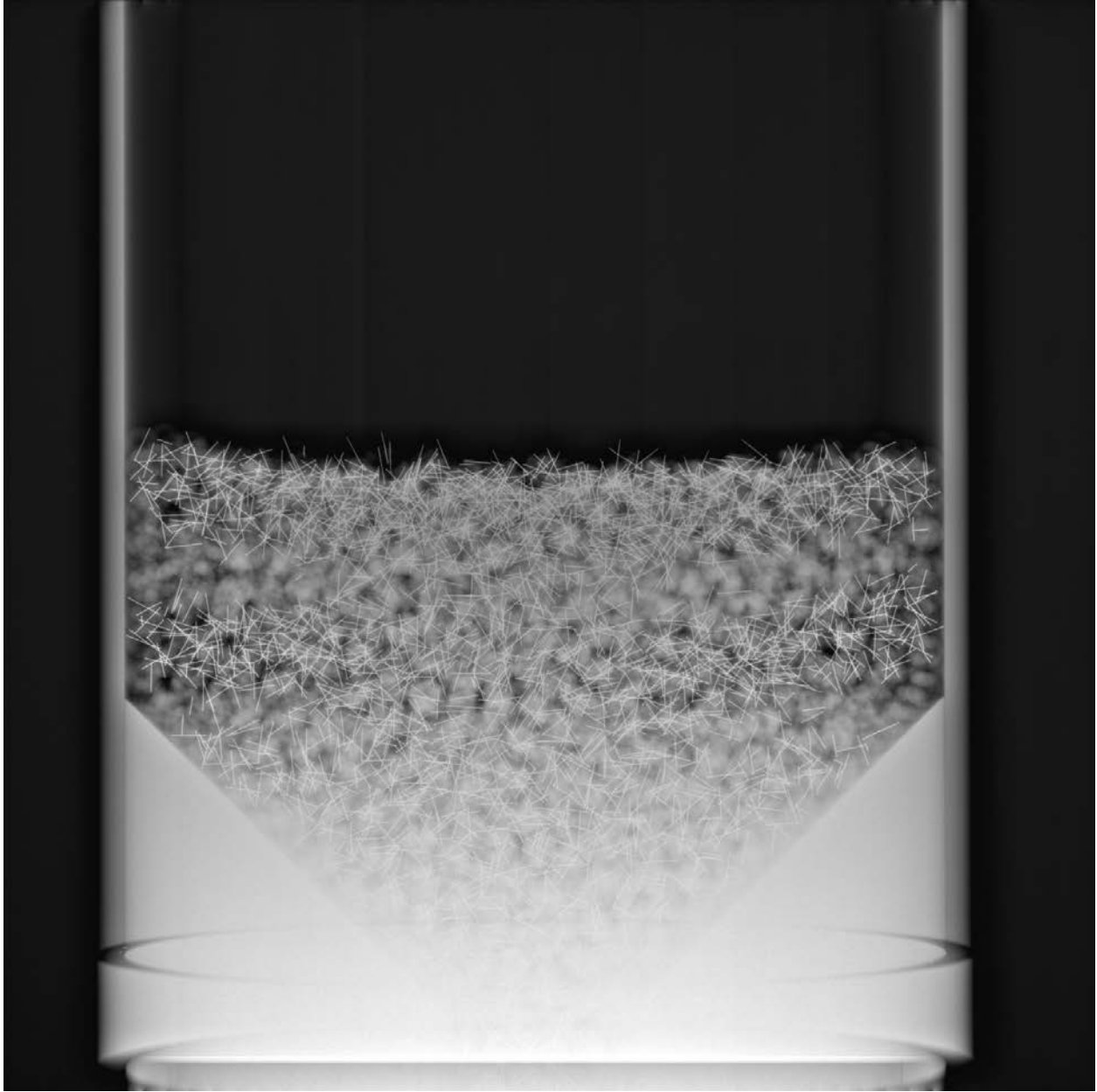


**Figure 2-44. Cylindrical silo flow visualization run after the discharge of 4,000 pebbles (half the pebbles in the original packed bed).**

### 2.3.3 Conclusions

This chapter describes the design and preliminary results from the Cylindrical Silo test section in the X-PREX Facility. This test section is representative of the geometry for a small pebble-bed test reactor and will provide valuable validation data that can inform neutronics models for these systems.

The fabricated test section is modular and can be adapted to study a wide variety of hopper angles in both converging and diverging geometries. The motion for the converging studies is achieved with the continuous discharge device in the Modular Test Bay and the motion for the diverging studies will be controlled by the retraction of a piston plate attached to the end of the linear actuator in the Modular Test Bay. These boundary conditions are well suited to what can be implemented in discrete element method simulations of granular flow.

The X-PREX image processing software will require further updates in order to reduce the number of false negatives (i.e. find more of the pins) to produce more useful data from the Cylindrical Silo test section. Qualitative results for the flow visualization with layers of instrumented pebbles are presented and are consistent with previously observed behavior for conical hopper drainage. After the necessary updates to the X-PREX imaging software, the results from the Cylindrical Silo test section will supplement this previous work with the capability to track rotational motion of the pebbles in the packed bed.

### 3 Simulation and Validation

This section describes the discrete element method (DEM) simulation methods and results for test section geometries studied to date in the X-Ray Pebble Recirculation Experiment (X-PREX). DEM simulations are based on molecular dynamics methods and are based on evaluating the contact forces between particles in a granular system to get the acceleration, then integrating in time to get the new position for all particles in the next time step. This is currently the best available simulation tool for modeling the complex behavior of granular flow. The X-PREX facility is uniquely suited to validate DEM simulation methods because it is the only experimental facility that has the capability to track the translational and rotational motion of all the pebbles in the packed bed.

The content of this chapter includes a description of the DEM simulation methods used, a qualitative validation study for the converging Quasi-2D Silo based on the pebble-packing configuration, and simulation results for the diverging Quasi-2D Silo and Cylindrical Silo Test Sections.

#### 3.1 Discrete Element Method Simulations

The DEM simulations for the Quasi-2D Silo and Cylindrical Silo test sections presented here are based on the friction model developed by Cundall and Strack.<sup>8</sup> The methodology adopted here has successfully been applied to the study of granular materials in a wide variety of container geometries and flow conditions, including the direct study of fuel pebble recirculation in reactor cores.<sup>9</sup> The simulations were completed using the LAMMPS code, which was originally developed by Sandia National Laboratory for molecular dynamics simulations and includes several models for the short-range interactions of granular particles.

In the DEM simulations,  $N$  pebbles of uniform diameter  $d$  interact with Hookean, history-dependent contact forces. Two pebbles at a distance  $r$  are in contact when  $\delta = d - |\mathbf{r}| < 0$  and the total force between the pebbles  $\mathbf{F} = \mathbf{F}_n + \mathbf{F}_t$  with the normal and tangential force components are

$$\mathbf{F}_n = \frac{\delta}{d} \left( k_n \delta \mathbf{n} - \frac{\gamma_n \mathbf{v}_n}{2} \right)$$

$$\mathbf{F}_t = \frac{\delta}{d} \left( -k_t \Delta s_t - \frac{\gamma_t \mathbf{v}_t}{2} \right)$$

---

<sup>8</sup> P. A. Cundall and O. D. L. Strack, A discrete numerical model for granular assemblies, *Géotechnique*, v29, p. 47, 1979.

<sup>9</sup> C. Rycroft, G. Grest, J. Landry, and M. Bazant, Analysis of granular flow in a pebble-bed nuclear reactor, *Phys. Rev. E*, v74, p. 021306, 2006.

where  $\mathbf{n} = \mathbf{r} / |\mathbf{r}|$ ,  $v_n$  and  $v_t$  are the normal and tangential components of the relative surface velocity at the point of contact,  $k_{n,t}$  are the elastic coefficients,  $\gamma_{n,t}$  are the viscoelastic damping constants, and  $\Delta s_t$  is the total tangential displacement over the lifetime of the contact. The tangential friction force is limited by the Coulomb yield criterion such that  $|\mathbf{F}_t| \leq \mu |\mathbf{F}_n|$ , where  $\mu$  is the static friction coefficient and can be set independently for pebble-pebble and pebble-wall interactions.

The simulation results here include a uniform pebbles of diameter  $d = 1.27$  cm, mass  $m = 1.00$  g, and friction coefficient  $\mu = 0.5$ . The value of the friction coefficient has been used successfully in the past, but is slightly higher than the true values in the Quasi-2D Silo. The elastic coefficients used are  $k_n = 2 \times 10^6$  gm/d and  $k_t = 2/7 k_n$  that were selected to provide stability with the time step  $\delta t = 2.5 \times 10^{-5} \tau$ , where  $\tau = (d/g)^{1/2} = 0.36$  s and is the time it takes for a pebble to fall a distance of one pebble radius from rest under acceleration  $g$ . The inelastic damping coefficients are set to  $\gamma_n = 50/\tau$  and  $\gamma_t = 0$ .

For each simulation run,  $N$  pebbles are loaded into the silo with the appropriate hopper configuration. For the converging Quasi-2D Silo, the pebbles are allowed to settle above a flat lower wall surface located  $2d$  below the orifice slit. The total number of pebbles used in the converging Quasi-2D Silo runs for the 0, 30, 45, and 60 degree simulations are  $N = 5,000, 4,700, 4,400,$  and  $4,000$ , respectively.

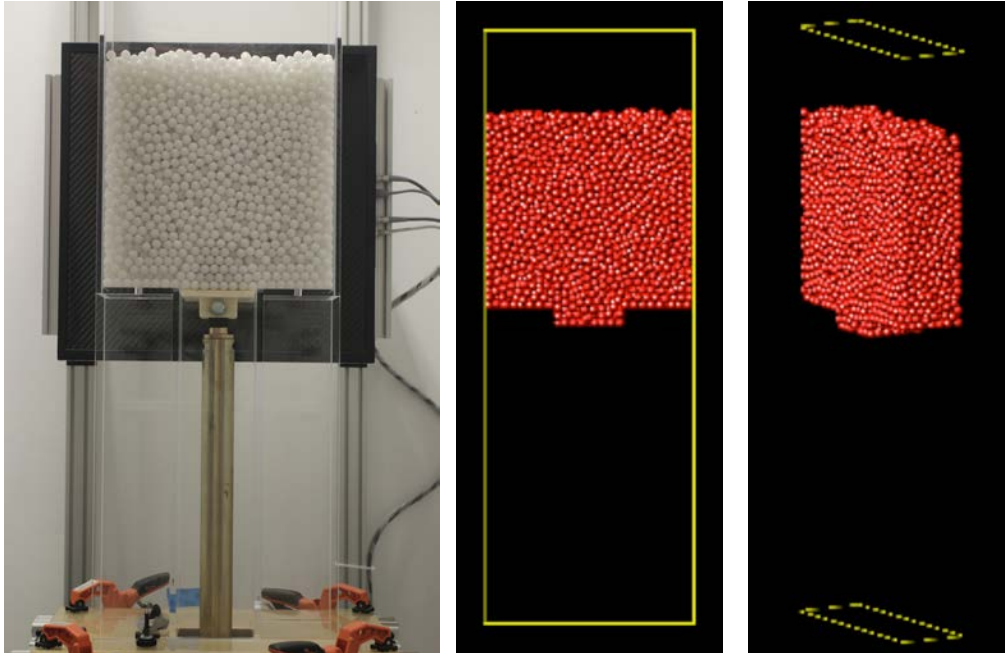
For the diverging Quasi-2D Silo, the pebbles settle above a flat lower wall surface located  $18d$  below the orifice slit. The total number of pebbles used in this geometry configuration are  $4,000, 4,500,$  and  $5,400$  for the 30, 45, and 60 degree simulations, respectively. Note that in this configuration, more pebbles are for the larger hopper angles due to the fact that they extend down lower and have more volume in the test section between the orifice slit and the lower boundary wall.

After the initial settling period, the pebbles in the Quasi-2D Silo simulations are divided into two groups, an upper mobile group and a lower group composed of pebbles in the lowest  $2d$  of the simulation domain with controlled motion. At the start of the motion simulation sequence, the pebbles in the upper region are allowed to flow while those below the orifice move with a fixed downward sinusoidal acceleration profile. This acceleration profile matches the step-wise increments of the linear actuator in the X-PREX facility. For each motion step, the pebbles at the bottom of the defueling chute move  $1d$  and  $0.3d$ , for the converging and diverging geometries, respectively, in a time of  $5\tau$ . This period ensures that the pebbles in the system remain densely packed to match the conditions in the Quasi-2D Silo test section. A total of 32 motion steps are used to match the final displacement of the linear actuator in the experiment. Figure 3-1 shows the initial and final pebble packing configurations for the zero-degree converging hopper geometry for the DEM simulations compared to the experimental setup for the Quasi-2D Silo

The boundary condition used here for the Quasi-2D Silo is different from the free discharge typically used in large-scale DEM simulations for computational efficiency. This assumption is generally acceptable when the bulk velocity distribution above the orifice is of primary interest because granular flow through an orifice will produce a constant discharge rate. However, in

this case the modified boundary condition is important in this case to match the experimental conditions in the X-PREX facility as closely as possible for the purposes of model validation. The slow dense flow in the defueling chute also more closely resembles the pebble packing and flow conditions in a reactor core.

Piston Displacement = 0 d



Piston Displacement = 32 d

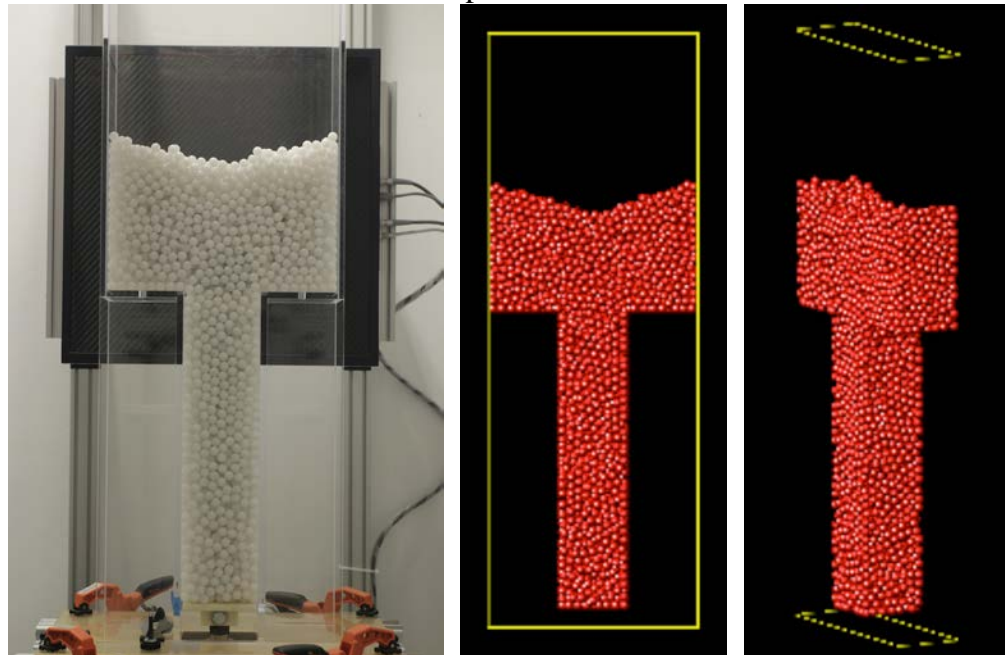


**Figure 3-1. Comparison of X-PREX front view (left) to DEM front view (right) for the step drainage of the Quasi-2D Silo test section at the initial and final time step.**

## 3.2 Quasi-2D Silo Validation Study

A qualitative comparison of the experimental and DEM simulation results is possible at the present time while the image processing and tomography software requires further development effort for large packed beds. This comparison is based on observations of the pebble flow and packing configuration in each data set as the piston moves downward in step-wise motion and serves as an initial test of how well the DEM results match the basic behavior observed in the experiment. This preliminary validation study will be supplanted by future quantitative comparison of the pebble packing and motion data from the experiment and simulations. These studies will serve as valuable validation tests for the DEM simulations and will provide initial pebble packing and boundary motion conditions that are closely matched between the two.

Figure 3-2 shows the front view of the x-ray images, visual images, and DEM simulation visualization for the zero-degree converging silo configuration at piston displacements of 0, 16 and 32*d*. The total number of pebbles in this system is 5,000. The initial pebble configurations at 2*d* shows that the total bed height *H* is matched between the two results at *H* = 24*d* above the orifice slit and that the packing fraction of the two systems will be comparable.

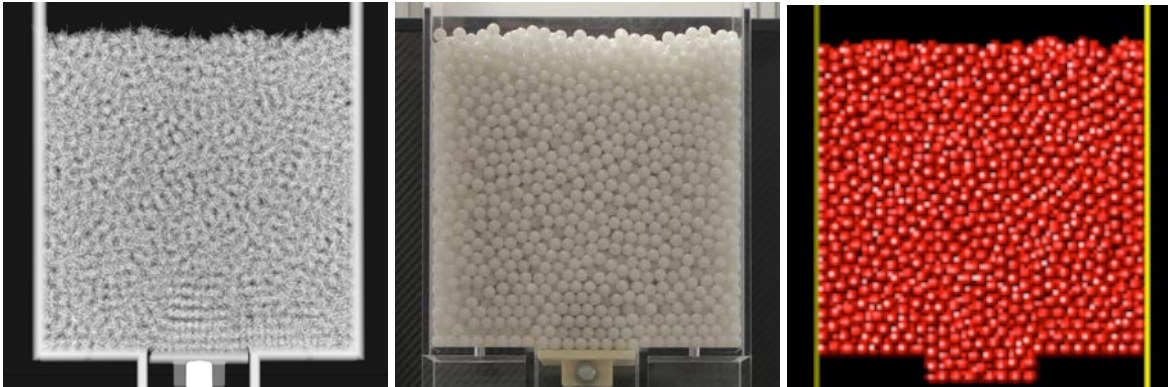
As the step-wise piston motion proceeds, stagnation regions were observed to the left and right of the orifice slit in both the experiment and DEM simulation. This is classical behavior for granular flow drainage and the angle of this stagnation region is based on the angle of repose and was previously demonstrated in DEM simulations for similar geometries.

While it is not possible to show the full visualization of these motion sequences in this report, it is possible to observe that the flows have similar velocity profiles. While this can be seen clearly in the animated image sequence, the packing configurations at piston displacements of 16*d* and 32*d* serve as a reasonable approximation of how the flow is structured here. Figure 3-2 shows these motion steps for the experiment and simulations for the zero-degree hopper angle. In both cases, the heap structure at the top of the bed is matched between the experiment and simulation, which is a direct result of flow channeling above the orifice where pebbles in this region flow more quickly into free space than pebbles located near the left and right walls.

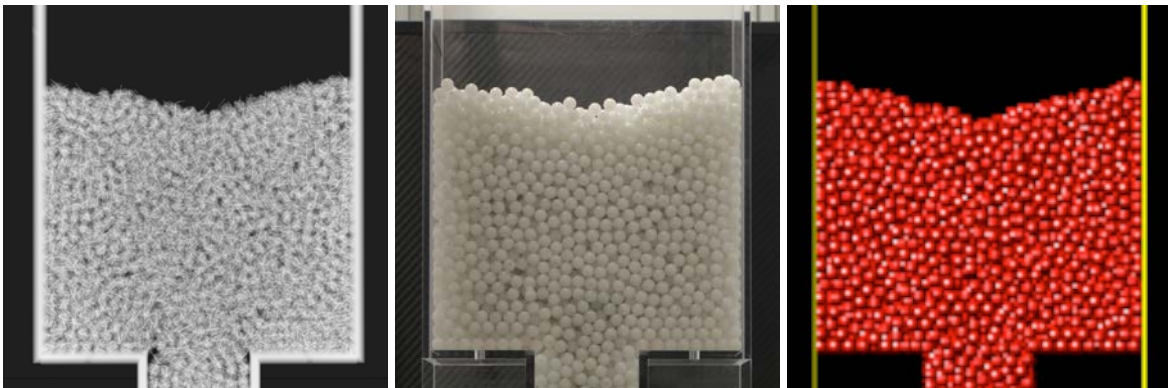
Figure 3-3 and Figure 3-4 show the packing configurations for the converging 30 and 60-degree hopper angles. Once again, the heap structure at the pebble free surface is closely matched. Differences can be observed, however, between the two geometries. In the 30-degree configuration, a deeper groove is observed in the heap structure as a result of longer pebble residence times along the sidewalls. In the 60-degree configuration, the free surface remains nearly flat, which indicates a more uniform velocity profile.

The flow patterns observed in these preliminary tests are consistent with previous studies of granular flow. However, the primary value for the X-PREX results will come with the ability to do direct quantitative comparison between the experiment and DEM simulations. The qualitative results shown here suggest great promise in this future validation effort that will increase confidence in the predictive use of DEM simulation results for larger systems, such as pebble bed reactor cores.

Piston Displacement = 0 d



Piston Displacement = 16 d



Piston Displacement = 32 d

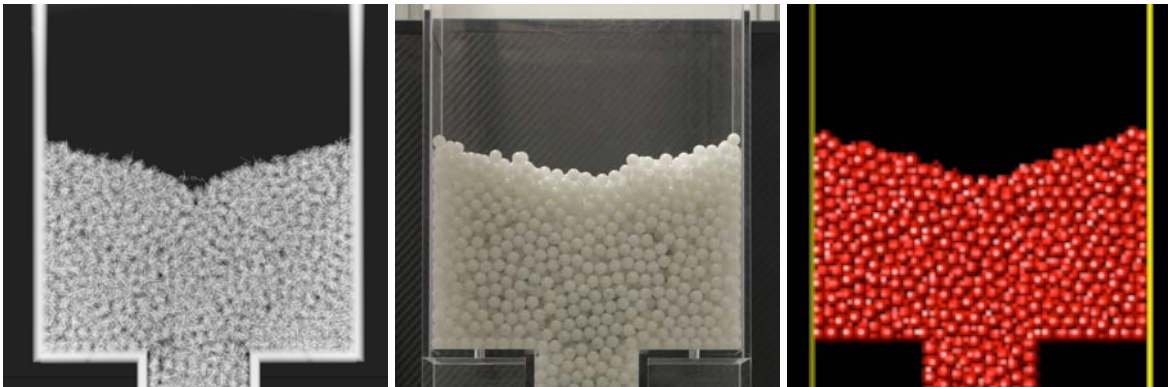
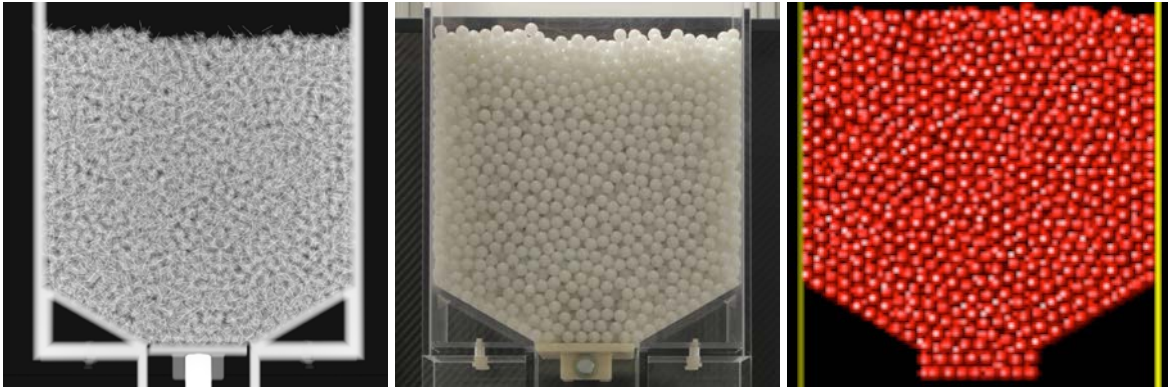
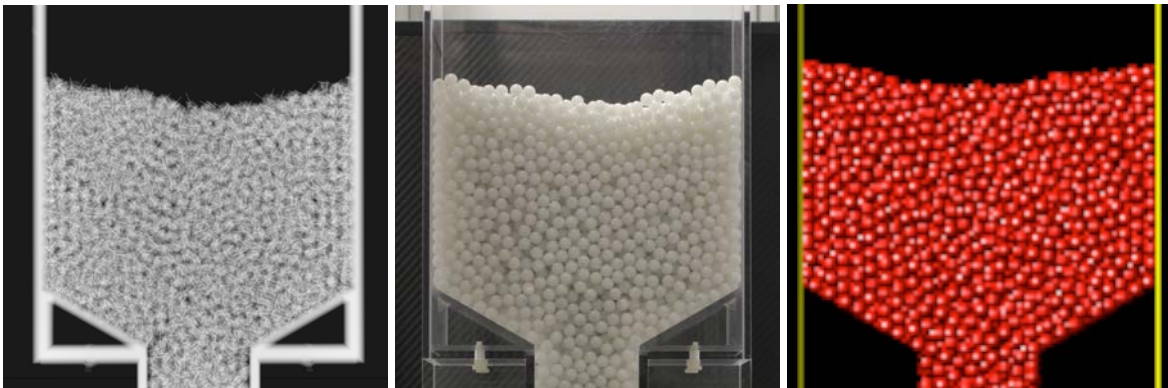


**Figure 3-2. Comparison of the front view for the x-ray image (left), photograph (center), and DEM simulation (right) for the step drainage of the Quasi-2D Silo test section without wedges for piston displacements of 0, 16, and 32 d.**

Piston Displacement = 0 d



Piston Displacement = 16 d



Piston Displacement = 32 d

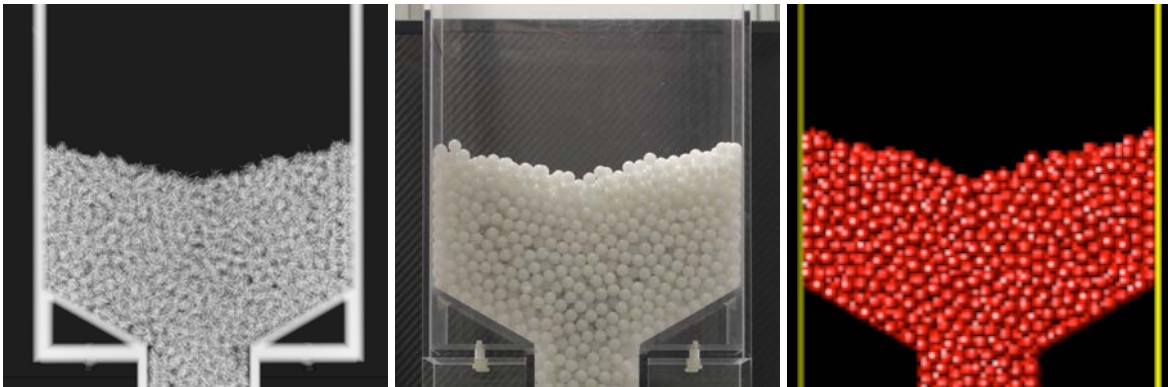
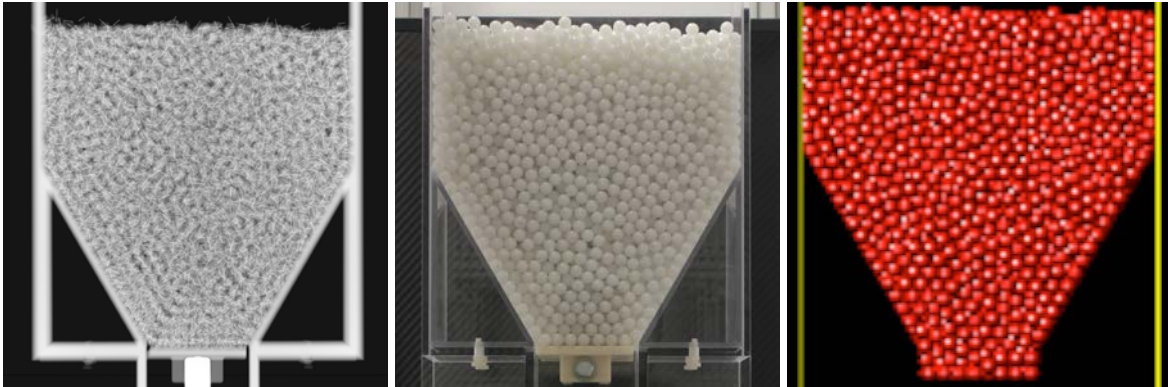
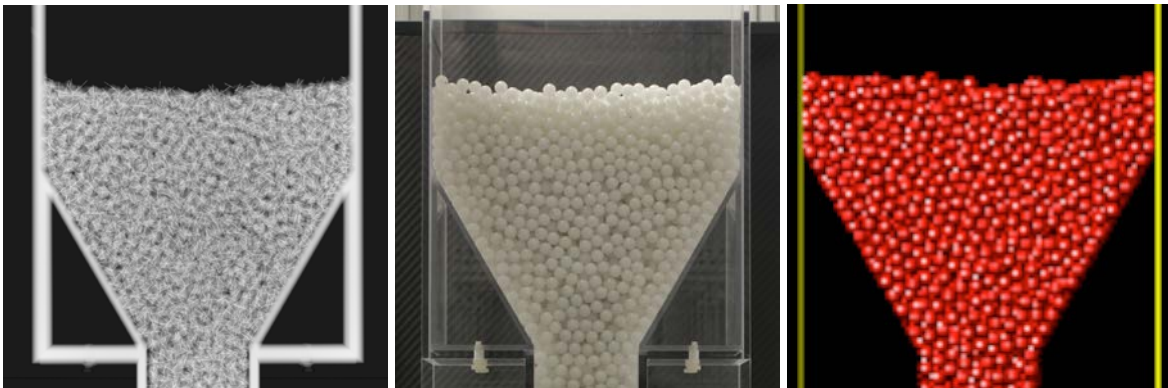


**Figure 3-3. Comparison of the front view for the x-ray image (left), photograph (center), and DEM simulation (right) for the step drainage of the Quasi-2D Silo test section with 30-degree angle for piston displacements of 0, 16, and 32 d.**

Piston Displacement = 0 d



Piston Displacement = 16 d



Piston Displacement = 32 d

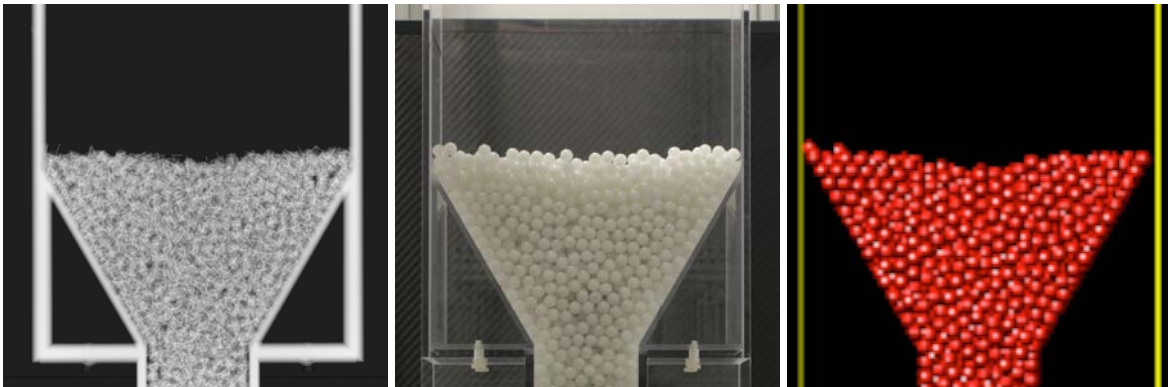


**Figure 3-4. Comparison of the front view for the x-ray image (left), photograph (center), and DEM simulation (right) for the step drainage of the Quasi-2D Silo test section with 60-degree angle for piston displacements of 0, 16, and 32 d.**

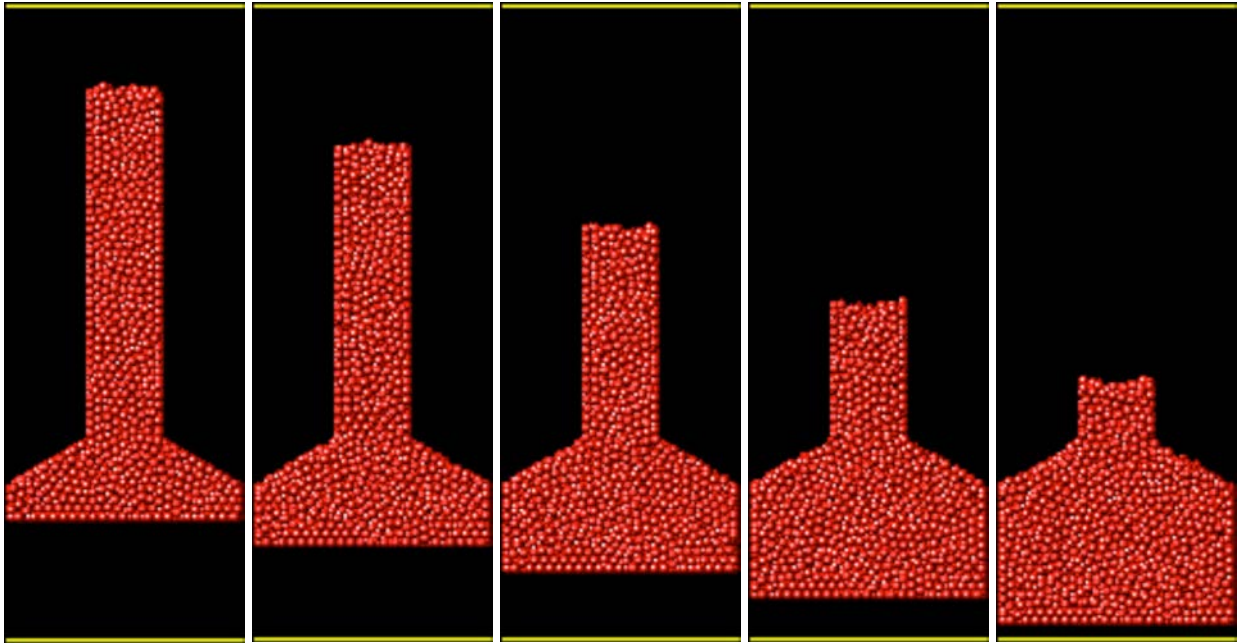
### 3.3 Simulation Results for Quasi-2D Diverging Geometry

Several DEM studies of the diverging Quasi-2D Silo geometry were completed that can be compared to the experimental data from the X-PREX facility. This diverging geometry case is a new problem with no previous study, but has important implications for the design options in pebble bed reactor cores. Figure 3-5 shows images of the sequence for the 30 and 60 degree diverging hopper geometries with piston displacements of 0, 2.67, 5.33, 8.00 and 10.67 d for the diverging geometry. In this case, the 30 degree hopper is close to the angle of repose and the bed does not remain densely packed at all time steps as it does in the 60 degree hopper. Gently sloping cone angles like this should be avoided in the design of pebble bed core geometries if a densely packed bed is desired is required in a diverging region. These simulations were performed without recirculation to match the conditions of the X-PREX data.

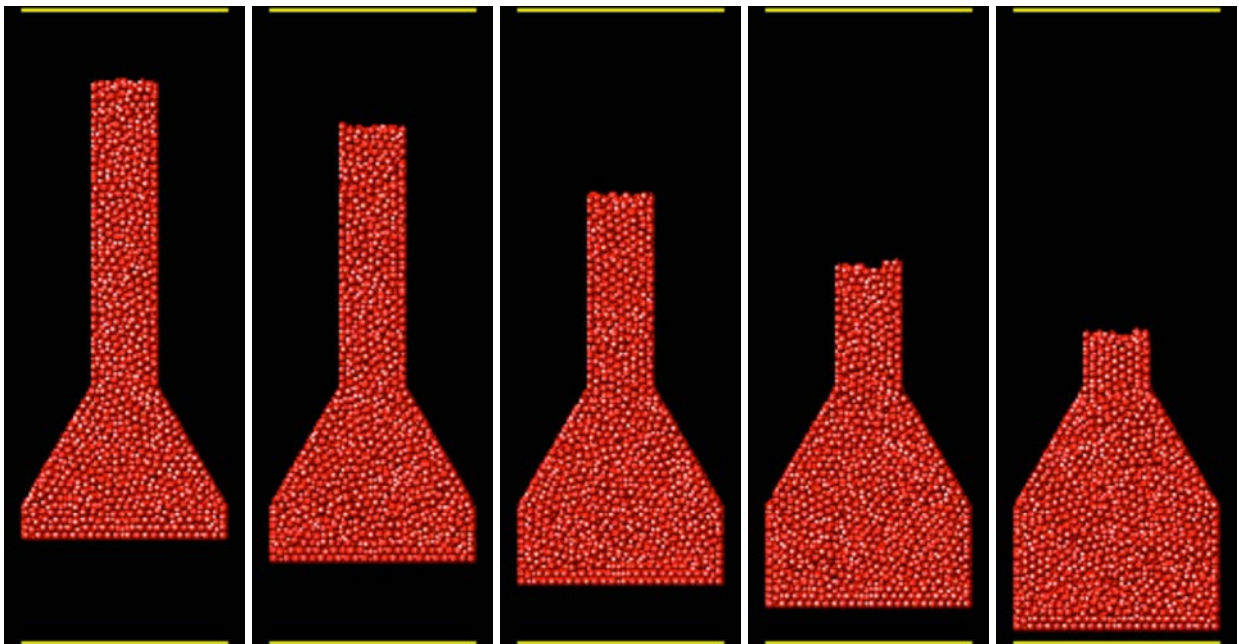
From the DEM simulation results, it is possible to extract a large amount of data and statistics on pebble motion in the test section. Figure 3-6 and Figure 3-7 show the average vertical and horizontal velocity components in the diverging region below the orifice slit for hopper angles of 45 and 60 degrees, respectively. In both cases, it is observed that plug flow conditions are established almost immediately below the diverging section where the horizontal velocity components are nearly zero. The vertical velocity data for the 60-degree hopper shows a smooth arc across the diverging region with a peak magnitude located at the centerline of the hopper. However, for the vertical velocity component, the 45-degree data shows two velocity peaks at the left and right sides in addition to the peak at the centerline of the hopper.

Figure 3-8 shows the average velocity vector field for the 45-degree diverging silo, which matches the component plots and shows the largest velocities at the center of the test section and along the diverging hopper walls. This flow pattern suggests that some shearing between the pebble layers may be happening near the wall surface. This result should be confirmed with data from the X-PREX facility and studied further in the future.

Diverging 30-Degree Hopper



Diverging 60-Degree Hopper



**Figure 3-5. Selected front view images from DEM simulations of the Quasi-2D Silo test section with 30 and 60-degree diverging hoppers.**

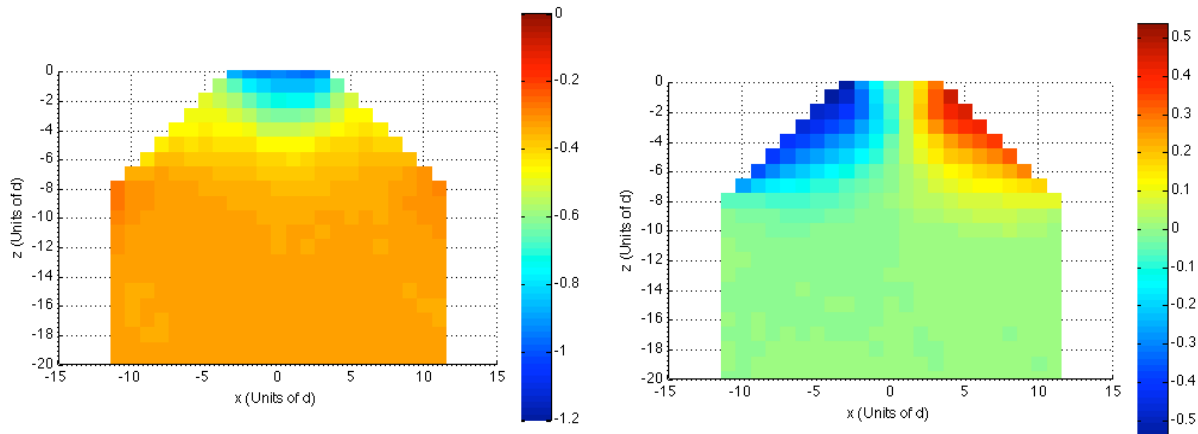


**Figure 3-6. Average vertical (left) and horizontal (right) velocity components below the orifice for the 45-degree diverging Quasi-2D Silo. The velocities are normalized by the displacement of pebbles in the narrow loading chute above the orifice.**

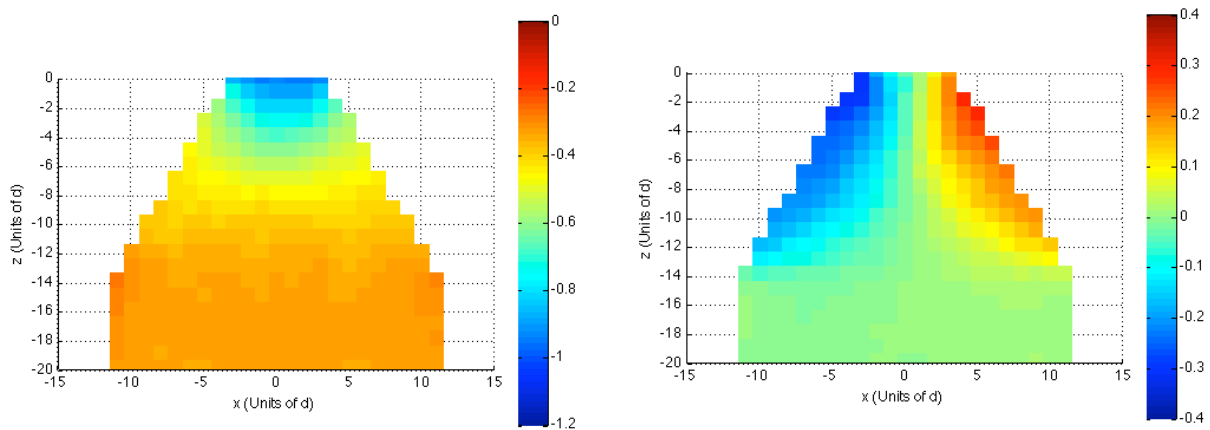


**Figure 3-7. Average vertical (left) and horizontal (right) velocity components below the orifice for the 60-degree diverging Quasi-2D Silo. The velocities are normalized by the displacement of pebbles in the narrow loading chute above the orifice.**

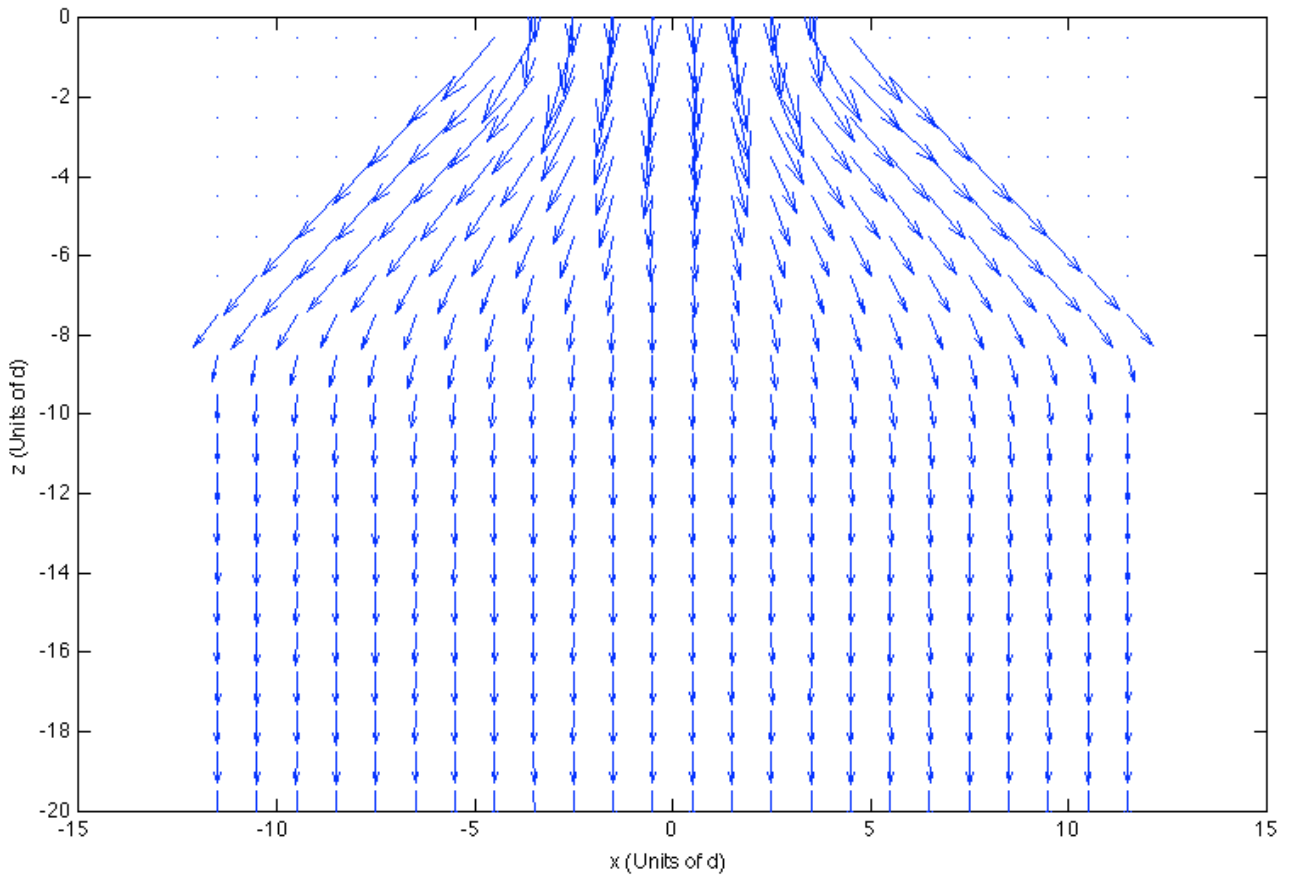


**Figure 3-8. Average velocity vectors below the orifice for the 45-degree diverging Quasi-2D Silo. The length of the arrows are proportional to the local velocity magnitude.**

### 3.4 Simulation Results for Cylindrical Silo

A series of DEM simulation runs was also completed for the cylindrical silo with an inner diameter of  $22.5 d$ , defueling chute diameter of  $5.5 d$ , and cone angles of 30, 45, and 60-degrees. These test sections were initially packed with 9,000, 8,000, and 6,500 pebbles for the three increasing hopper angles. These systems resemble the pebble packing that is expected for small test reactor geometries and will be studied in the X-PREX facility with additional improvements to the image processing software.

For these studies, the boundary condition for pebble motion was free drainage through the defueling chute located below the converging conical region, which results in a variation of choked flow that is commonly observed in granular flows for this hopper geometry, such as the flow of sand in an hourglass. These simulation runs include cases with and without pebble recirculation to the top of the packed bed. Figure 3-9, Figure 3-10, and Figure 3-11 show the initial packing configuration and two subsequent snapshots for each of the cone angles under free gravity drainage. Pebble motion data above the orifice and heap structure at the free surface from these simulations will be comparable to data collected in the X-PREX facility that can be used for validation of the DEM friction models.

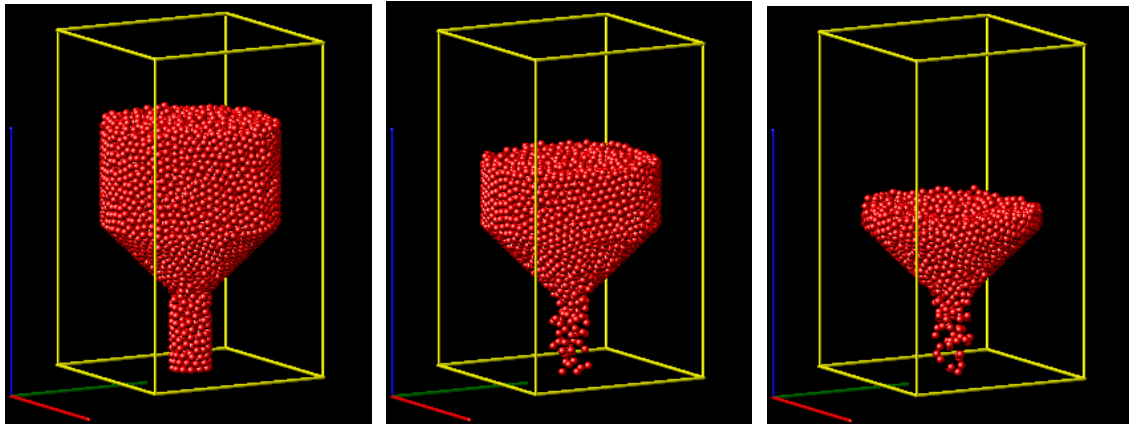


**Figure 3-9. DEM simulation screenshots with 8,000 pebbles in the 45-Degree Converging Cylindrical Silo test section geometry under gravity drainage with no pebble recirculation. The three steps show the initial configuration (left) and the packing after  $5 \times 10^6$  (center) and  $1 \times 10^7$  (right) time-steps.**

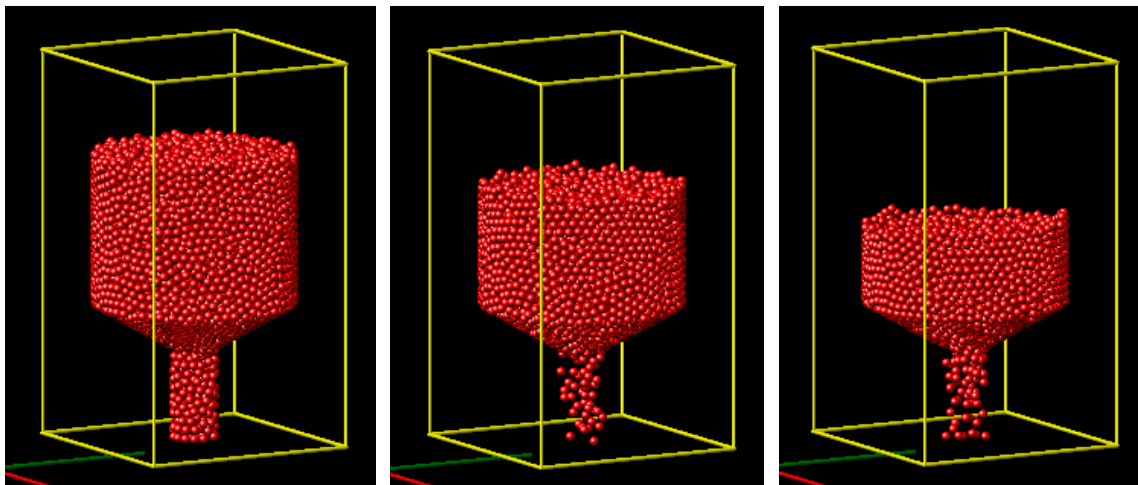


**Figure 3-10. DEM simulation screenshots with 9,000 pebbles in the 45-Degree Converging Cylindrical Silo test section geometry under gravity drainage with no pebble recirculation. The three steps show the initial configuration (left) and the packing after  $5 \times 10^6$  (center) and  $1 \times 10^7$  (right) time-steps.**

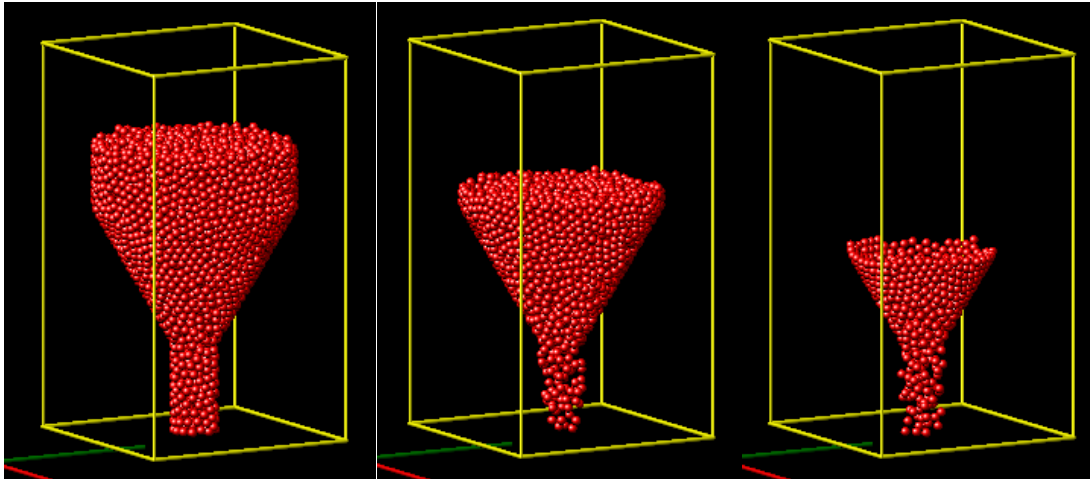


**Figure 3-11. DEM simulation screenshots with 6,500 pebbles in the 45-Degree Converging Cylindrical Silo test section geometry under gravity drainage with no pebble recirculation. The three steps show the initial configuration (left) and the packing after  $4 \times 10^6$  (center) and  $8 \times 10^6$  (right) time-steps.**

Figure 3-12 shows several DEM screenshots from the simulations in the cylindrical silos with pebble recirculation to the top of the test section. In these runs, the number of pebbles in the system is kept constant and the overall structure of the bed varies slightly with time. The heap structure at the top of the constant area region should match experiments from the X-PREX facility if the DEM friction models can accurately represent the challenging case of static friction at a free surface. However, the stochastic nature of pebble insertion and subsequent bounces with other pebbles implies that it is not feasible to precisely match the exact packing structure at the top of the bed.

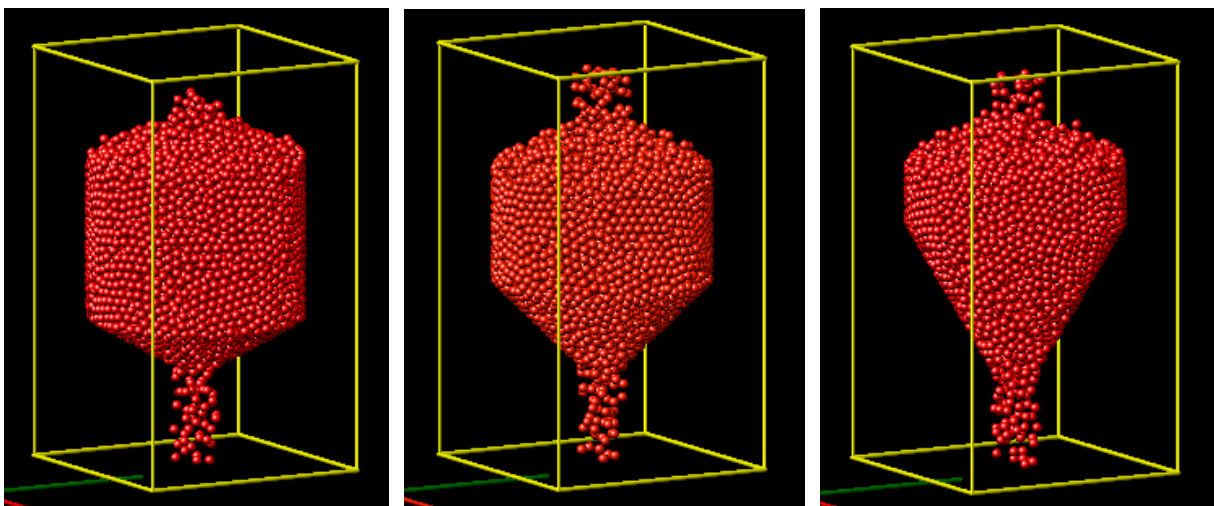


**Figure 3-12. DEM simulation screenshots for DEM runs under free gravity drainage in the Converging Cylindrical Silo test section with cone angles of 30 (left), 45 (middle), and 60-degrees (right). Each snapshot of the packed configuration is taken after  $5 \times 10^6$  time-steps.**

### 3.5 Conclusions

The report describes the DEM simulation methods and results that can be validated with data from the X-PREX facility. A preliminary qualitative validation study was completed for the Quasi-2D Silo test section that includes flow in converging hoppers of different geometries. Comparison to DEM simulations show similar pebble motion and final packing structures. Future quantitative studies will allow the initial packing configuration from the X-PREX facility to be used as the starting pebble coordinates for the DEM simulation and to closely match the step-wise motion in the defueling chute. The matched initial and boundary conditions for the experiment and simulation runs will provide a key separate effects test for DEM simulations that can be used to improve confidence in constitutive friction models and their predictive capabilities in the study of large-scale pebble systems. Additional studies were also described for the diverging geometry in the Quasi-2D Silo test section and converging geometries in the Cylindrical Silo test section with and without pebble recirculation.

## 4 References

- <sup>1</sup> U.C. Berkeley has performed a series of scaled experiments with positively buoyant pebbles based on the design parameters for the Pebble-Bed Fluoride Salt-Cooled High-Temperature Reactor (PB-FHR).
- <sup>2</sup> Jaehyuk Choi, Arshad Kudrolli, and Martin Z Bazant, “Velocity Profile of Granular Flows Inside Silos and Hoppers,” *J. Phys.: Condens. Matter*, (January 2005).
- <sup>3</sup> Chris Rycroft et al., “Dynamics of Random Packings in Granular Flow,” *Physical Review E* 73, no. 5 (May 2006).
- <sup>4</sup> Nuclear Regulatory Commission. “NRC Regulations Title 10, Code of Federal Regulations, Appendix A to Part 50 – General Design Criteria for Nuclear Power Plants”. Criterion 26 and 29. December 1, 2014.
- <sup>5</sup> Z. Wu, L.-W. Hu, and D. Zhong, The Design Features of the HTR-10, *Nuclear Engineering and Design*, v218, p. 25, 2002.
- <sup>6</sup> X. Yu, “Chinese TMSR-SF and TMSR-LF Development,” presented at the 5th FHR Workshop on Beyond Design Basis Events, Berkeley, CA, Jan. 2014.
- <sup>7</sup> Guimin Lui, “Design Considerations on Neutronics and Thermal-Hydraulics in TMSR-SF1,” presented at Berkeley, CA, October, 2014.
- <sup>8</sup> P. A. Cundall and O. D. L. Strack, A discrete numerical model for granular assemblies, *Géotechnique*, v29, p. 47, 1979.
- <sup>9</sup> C. Rycroft, G. Grest, J. Landry, and M. Bazant, Analysis of granular flow in a pebble-bed nuclear reactor, *Phys. Rev. E*, v74, p. 021306, 2006.